Università
Ca'Foscari
Venezia

Department of
Molecular Sciences and Nanosystems

Master's Degree in
Science and Technologies of Bio and Nanomaterials

Detection of different isotypes of anti-tissue transglutaminase by nanoelectrode ensemble biosensors for celiac disease diagnosis

Graduation Thesis of
Sara Longo
Matricola 820686

Supervisor: Prof. Paolo Ugo

Academic year: 2014/15

Table of contents

List of abbreviations

A_{act}	Active area [cm^2]
Ab	Antibody
Ab-Ag	Antibody-antigen complex
Ag	Antigen
A_{geom}	Geometric area [cm^2]
anti IgA-GOx	Anti IgA secondary antibody labelled with glucose oxidase
anti-IgG-HRP	Anti IgG secondary antibody labelled with horseradish peroxidase
anti-tTG	Anti-tissue transglutaminase
BQ	Benzoquinone
BSA	Bovine serum albumin
C	Concentration [mol cm^{-3}]
CD	Celiac disease
C_{dl}	Double-layer capacitance [µF cm^{-2}]
C_H	Heavy chain constant domain
C_L	Light chain constant domain
CV	Cyclic voltammogram
D	Diffusion coefficient [cm^2 s^{-1}]
DAGA	Deamidated gliadin
DL	Detection limit
e^-	Electron
E	Enzyme
$E_{1/2}$	Half-peak potential
ELISA	Enzyme-linked immunosorbent assay
ES	Enzyme-substrate complex
f	Fractional electrode area
FA^+	(ferrocenylmethyl)trimethylammonium cation
F_{ab}	Fragment antigen binding
$FAPF_6$	(ferrocenylmethyl)-trimethylammonium hexafluorophosphate
F_c	Constant region
FEIA	Fluoroenzyme immunoassay

GFD	Gluten-free diet
Gln	Glutamine
Glu	Glutamic acid
GOx	Glucose oxidase
GTP	Guanosine triphosphate
HER	Human epidermal growth factor receptor 2
H_2Q	Hydroquinone
HLA	Human leukocyte antigen
HRP	Horseradish peroxidise
h-tTG	Human tissue transglutaminase
i_c	Double-layer charging current [A]
i_f	Faradaic current [A]
Ig	Immunoglobulin
IgA	Immunoglobulin A
IgA-NEE	NEE-based immunosensor for the detection of IgA anti-tTG
IgG	Immunoglobulin G
IgG-NEE	NEE-based immunosensor for the detection of IgG anti-tTG
i_{max}	Maximum electrocatalytic current increment [A]
i_{net}	Electrocatalytic current increment [A]
i_p	Peak current [A]
IUPAC	International union of pure and applied chemistry
k^0	Standard charge transfer rate constant
k^0_{app}	Apparent rate constant
kDa	Kilo Dalton
K_{eq}	Equilibrium constant
K_m	Michaelis-Menten constant
k_2	Turnover
Lys	Lysine
m	Slope
n	Number of transferred electrons
NEEs	Nanoelectrode ensembles
NPs	Nanoparticles
$\boldsymbol{\nu}$	Scan rate [V s^{-1}]

p	Pore density
P	Product
PB	Phosphate buffer
PBE	Partially blocked electrode
PBS	Phosphate buffer saline
PC	Polycarbonate
PVP	Polyvynilpyrrolidone
QL	Quantification limit
r	Radius
RDS	Relative standard deviation
S	Enzyme substrate
SD	Standard deviation
Sec-Ab	Secondary antibody
SEM	Scanning electron microscopy
SIgAD	Selective immunoglobulin A deficiency
tTG	Tissue transglutaminase
tTG-NEE	Nanoelectrode ensemble functionalized with tissue transglutaminase
U	Unit
V	Rate of the enzymatic reaction
V_H	Heavy chain variable domain
V_L	Light chain variable domain
V_m	Maximum rate of the enzymatic reaction

Summary

Celiac disease (CD) is a chronic autoimmune disease with a prevalence of 1% in the general population, characterized by an immunologically mediated inflammatory damage of the small bowel as consequence of the ingestion of gluten in genetically predisposed people. In order to reduce the morbidity and the mortality associated to CD, it is important to develop simple and effective methods that allow to perform screening tests in the general population for an early diagnosis of the disease and follow-up tests to manage the regression of the disease while the patient is on a gluten-free diet (GFD).

It has been demonstrated that the blood levels of anti-tissue transglutaminase (anti-tTG) correlate with the degree of the mucosal intestinal damage and that levels of this antibody decrease when the celiac patient does not assume gluten. Although definitive diagnosis of CD is still based on biopsy, since anti-tTG can be considered an effective biomarker of CD, it would be important to develop a useful analytical method for the detection of this antibody in the blood.

In this thesis we study and develop selective and sensitive electrochemical immunosensors based on nanoelectrode ensembles (NEEs) to examine the possibility to detect selectively both the IgG and IgA isotypes of anti-tTG.

NEEs are prepared in our laboratory by electroless deposition of gold in track-etch polycarbonate (PC) membranes. The polycarbonate of the NEEs is functionalized with tissue transglutaminase (tTG) as capture antigen. The obtained immunosensor shows to be able to capture both the isotypes of anti-tTG in serum samples. The selective detection of isotype IgG is possible by using an anti-IgG secondary antibody (Sec-Ab) labelled with horseradish peroxidase (HRP): in the presence of the target analyte (IgG anti-tTG), the addition of HRP substrate (hydrogen peroxide) and hydroquinone as redox mediator generates an electrocatalytic increase of the cathodic current which scales with the IgG antibody concentration. For the detection of IgA isotype, a different secondary antibody is employed, that is anti-IgA Sec-Ab labelled with glucose oxidase (GOx). In the case of positive response, with the

addition of glucose (the substrate) and (ferrocenylmethyl)trimethylammonium (FA^+, i.e. the redox mediator), an electrocatalytic increase of the anodic current is observed, which scales with IgA anti-tTG concentration.

Analytical performances of the two biosensors are presented and discussed together with applicative prospects for molecular diagnosis of the celiac disease.

Chapter 1
Introduction

1. 1. Celiac disease

The celiac disease (CD) is an autoimmune chronic inflammatory disorder characterized by damage of the small intestinal mucosa that occurs in adults and children, with a prevalence approaching 1% of the population [1-5], that results from the interaction between an environmental trigger (gluten) and immune factors, genetic factors and environmental cofactors [6-9].

1. 1. 1. Pathogenesis

1. 1. 1. 1. Environmental trigger: gluten

Gluten is the major storage protein of wheat, rye and barley that remains after starch is washed from wheat-flour dough [6,7]. Gluten is made up of proteins that can be divided into two different fractions according to their different solubility in alcohol-water solution: gliadins and glutenins [7]. It has been demonstrated that the toxic and immunogenic component is gliadin, the alcohol soluble fraction of gluten, that is enriched in proline and glutamine [6,10] (**Figure 1.1**). Proline residues make these peptides resistant to gastrointestinal proteolysis, so that they are poorly digested in the human upper gastrointestinal tract [6,7], whereas glutamine residues enhance their immunogenicity, because they are the substrate for the deamidation mediated by the tissue transglutaminase (as explained in Paragraph 1. 1. 8) [7,11]

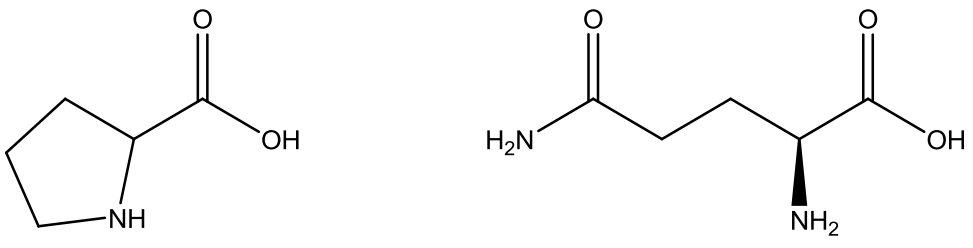

Proline Glutamine

Figure 1.1. Chemical structure of proline and glutamine.

1. 1. 1. 2. Genetic factors

The celiac disease occurs only in genetically predisposed people, bearing the human leukocyte antigen (HLA) alleles that encodes for HLA-DQ2 or HLA-DQ8 glycoproteins, involved in the mechanism responsible for the intestinal damage [6-8]. Not all individuals that carry these alleles are affect by the disease: studies demonstrated that the genetic component attributable to HLA genes is about 50%, so the presence of these genes is necessary but not sufficient for the development of the celiac disease [6-8]. Indeed, the absence of these alleles has a high predictive value (almost 100%) [12], because it allows to rule out the celiac disease in patients in whom the diagnosis in unclear [6].

1. 1. 1. 3. Immune factor

The celiac disease is the result of an inappropriate immune response against the indigested gliadin fractions, that promote an inflammatory reaction in the small intestine mediated by both the innate (in the intestinal epithelium) and the adaptive (in the lamina propria) immune system [6]. The adaptive response is mediated by the CD4+ T cells in the lamina propria that, after recognizing the deamidated gliadin (DAGA), produce proinflammatory cytokines [13], responsible for the villous atrophy and crypt hyperplasia [14]. On the other hand, the epithelial damage by gliadin activates an innate immune response, characterized by an increased expression of interleukin-15 that in turn activates intraepithelial lymphocytes, which become cytotoxic so killing enterocytes (the epithelial cells that constitute the intestinal villi) [6].

1. 1. 1. 4. Environmental cofactors

Epidemiologic studies have suggested that there are different environmental cofactors that play an important role in the development of the celiac disease, such as dietary cofactors and gastrointestinal infections [6,7]. In genetically predisposed children, the risk of the raise of the disease is enhanced if gluten has been introduced in the diet before 4 months of age, whereas it is minimized if gluten has

been administrated after 7 months of age, and during the breast-feeding [6,7,15]. The risk of this disease in infancy increases also in the case of frequent gastrointestinal infections due to rotavirus, that enhance the permeability of the small bowel [6,7].

1. 1. 2. Pathophysiology

After gluten ingestion, undigested molecules of gliadin that are resistant to degradation by gastric, pancreatic and intestinal proteases, remain in the intestinal lumen, passing through the epithelial barrier of the intestine when there is an increase in intestinal permeability (for example during intestinal infections), activating an immune response [6]. In the lamina propria, once gliadin peptides are deamidated by the tissue transglutaminase (an enzyme in the intestine), they are bound by the antigen presenting cells, so exposing them to the pathogenic CD4+ T cells, thanks to the HLA-DQ2 and HLA-DQ8 proteins. Once activated by the deamidated gliadin, the CD4+ T cells, on one side produce the cytokine responsible for the intestinal lesion (villous atrophy, crypt hyperplasia, intraepithelial lymphocytosis), on the other side present the DAGA to the B cells, that release antibodies, in particular antigliadin, connective tissue antibodies (antireticulin and antiendomysial) and anti-tissue transglutaminase. **Figure 1.2** shows the mechanism of the pathophisiology of the celiac disease.

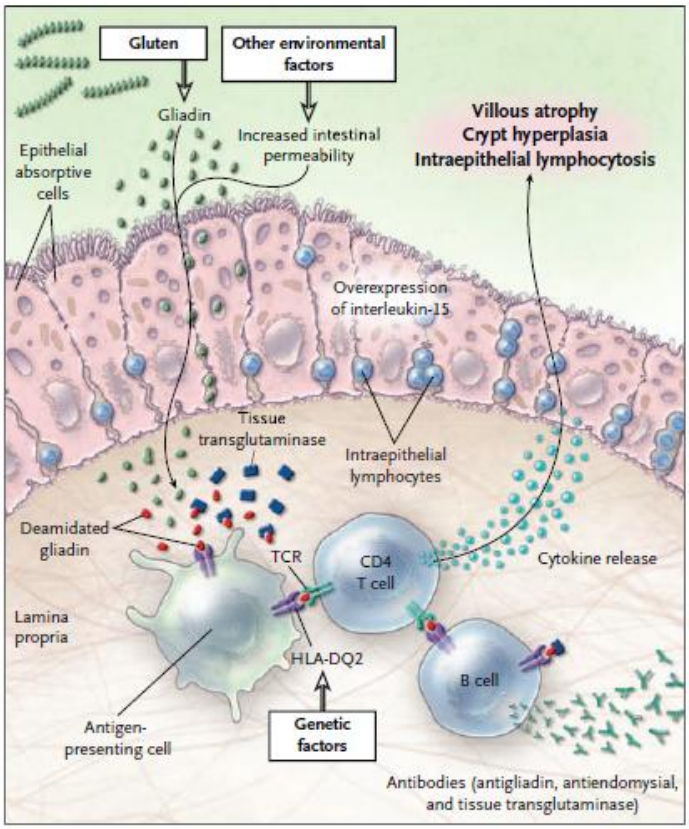

Figure 1.2. Interaction of gluten with environmental, immune and genetic factors in CD [6].

1. 1. 3. Epidemiology: the iceberg model

In order to identify the areas "at risk" for celiac disease, it would be important to evaluate the world distribution of the genetic (HLA genes) factors and the level of wheat consumption (**Figure 1.3**): on this basis, Europe is a region at risk for CD, but also Middle East, Asia, South America and North Africa [3,6,8,16-19].

Epidemiological studies, conducted in the last decades, suggest that the celiac disease affect 1% of the population, although this percentage is expected to increase due to the fact that in some regions such as North Africa, Middle east and India the disease remains still underdiagnosed. Indeed, in these areas, the diagnosis of the CD is not possible due to the lack of diagnostic facilities [8].

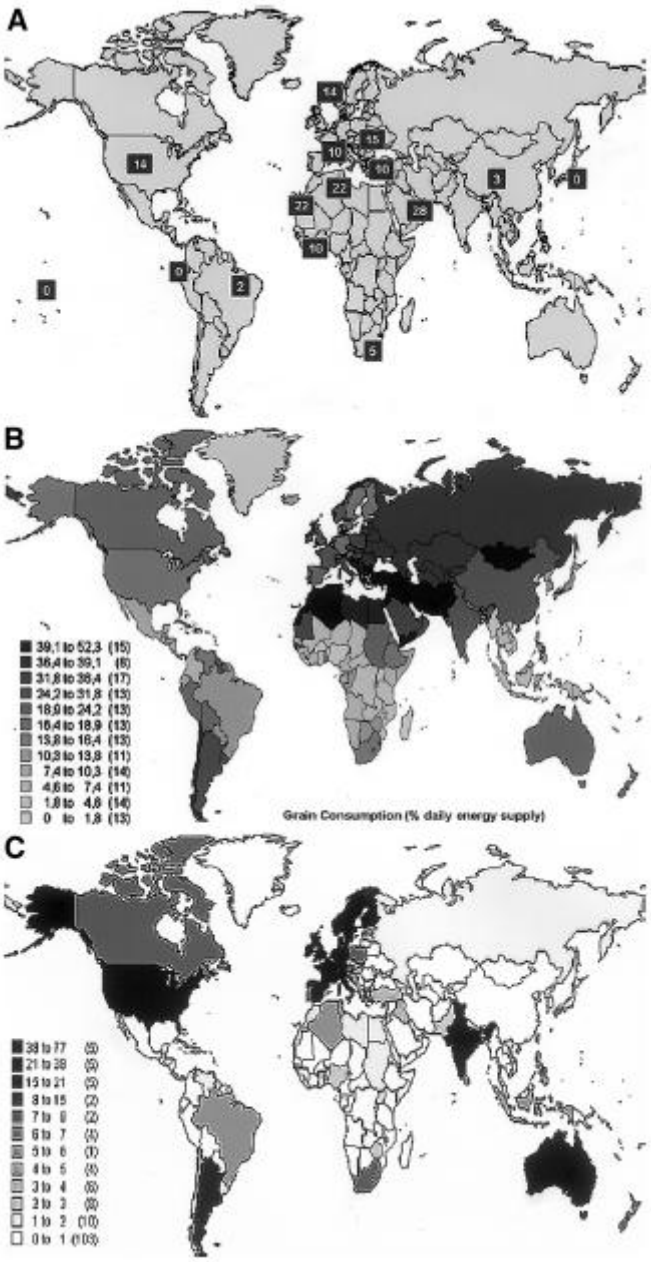

Figure 1.3. A. Percentage of genetic frequency of HLA genes in the world. B. World distribution of grain consumption. The intensity of colour is directly related to the amount of wheat products consumed (expressed as percent of daily energy supply). Numbers in parentheses represent the number of countries that have the wheat consumption shown on the left. C. Scientific production on CD worldwide during the period from 1966 to 2001. The intensity of colour is directly related to the number of articles found in a MEDLINE search for CD and the name of the country. Numbers in parentheses represent the number of countries that have published within the range of manuscripts shown on the left [8].

Moreover, the diagnosis of the CD is extremely challenging since the symptoms associated to the disease are more frequently extraintestinal than intestinal. For this reason, in order to have a correct idea of the epidemiological change of the CD, it is useful to consider the iceberg model (**Figure 1.4**), introduced in 1991 by Richard Logan [8]: the overall size of the iceberg represents the prevalence of the CD that in several cases is not diagnosed. The "water line" is the ratio of diagnosed to undiagnosed cases, that have fluctuation from a country to another: the emerged part of the iceberg increases in the region where there is a greater awareness of the disease, where there is the availability of diagnostic laboratory equipment and where there is a higher amount of ingested gluten, that increases the intensity of the CD clinical manifestation.

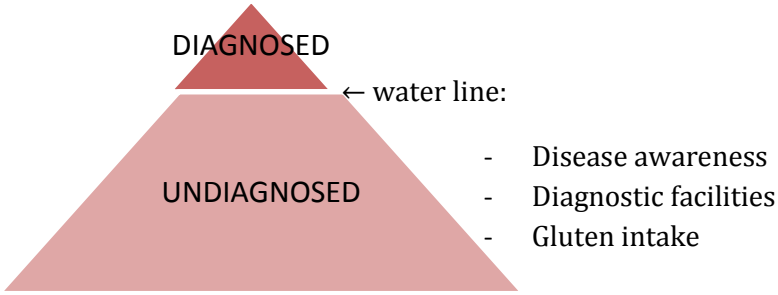

Figure 1.4. The CD iceberg model.

1. 1. 4. Clinical presentations

There are different forms of clinical manifestation of celiac disease, according to the age of the patient, duration and extension of the disease and presence of extraintestinal manifestations. Patients can be from asymptomatic to severely symptomatic [7,8].

In children affected by celiac disease, growth is usually normal in the first months of life, and symptoms begins a few months after the introduction of gluten in their diet. The more common symptoms in infants and young children are abdominal pain, chronic diarrhea, failure to thrive, anorexia, muscle wasting. Manifestations in older children and adolescents can include anemia, neurologic symptoms and short stature. As a consequence of malabsorption, they can also present vitamin

deficiencies, iron deficiency anemia, hypocalcemia and hypoalbuminemia [8]. In adults the more common symptoms are chronic unexplained diarrhea, abdominal pain, iron-deficiency anemia, bloating, irritable bowel syndrome, chronic fatigue, and, less commonly, weight loss, neurologic symptoms, constipation [6].

The celiac disease is often associated with other diseases, such as osteoporosis [20,21] (loss of bone mass with consequent higher risk of fracture), autoimmune and immune mediate diseases (type 1 diabetes, IgA deficiency, neurological abnormalities, autoimmune thyroiditis) [22-24], mild liver abnormalities, neurological and psychiatric disorders (headache, epilepsy, depression, ataxia, autism, schizophrenia) [6].

The severity of clinical presentation does not correlate with the degree and the extent of the mucosal intestinal damage assessed by endoscopy and biopsy [25,26].

1. 1. 5. Diagnosis of the celiac disease

Due to its wide clinical symptomatology, the diagnosis of celiac disease is difficult. From the moment that CD can be also asymptomatic, in order to reduce the morbidity and the mortality associated with this disease, it would be important to perform a mass screening of the general population. For this reason, the developing of a simple and sufficiently accurate method that allows to discriminate between healthy and CD affected people has acquired even more interest between researchers in the last decades.

One of the approach for the diagnosis of the celiac disease is to determine the level of the antibodies that are overproduced in the case of the disease, such as antiendomysial antibodies and anti-tissue transglutaminase antibodies [27,28] and then perform a duodenal biopsy to have a histological confirmation.

For a simpler diagnosis of CD, it is useful to consider the family history of the CD. In order to determine which family members should be screened with serologic testing, it is important to assess the presence or the absence of the alleles HLA-DQ2 and HLA-DQ8: only individuals in whom these alleles are identified should be

screened for CD, since their absence has a negative predictive value [12]. These genetic test should be performed to rule out the CD diagnosis in dubious cases [6].

Nowadays the gold standard for the diagnosis of the celiac disease is the intestinal biopsy in serologically positive individuals, that is aimed to assess the presence of lesions in small-intestine, especially in the distal duodenum [7]. In order to establish the severity of these lesions, the Marsh classification as modified by Oberhuber and colleagues is used [29]. A simpler classification is the one proposed by Corazza and colleagues based on the morphologies of the small intestine [7,30] (**Figure 1.5**):

- infiltrative non-atrophic lesions (grade A);
- atrophic lesions with shortened but still detectable villi (grade B1);
- atrophic lesions with undetectable villi (grade B2).

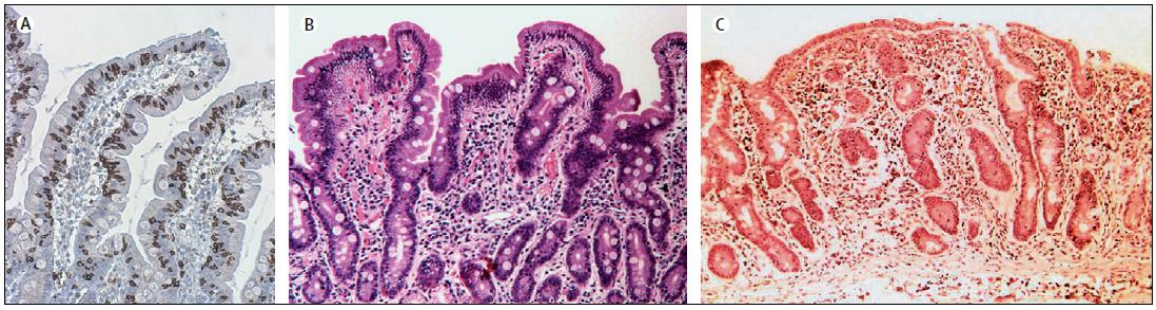

Figure 1.5. Representative pictures of celiac disease grades. A. Grade A (infiltrative non-atrophic lesions). B. Grade B1 (atrophic with shortened but still detectable villi). C. Grade B2 (atrophic with no longer detectable villi) [7].

Villous atrophy is also characteristic of other disorders (such as autoimmune enteropathy, bacterial overgrowth, cow's milk enteropathy, eosinophilic gastroenteries, protein energy malnutrition), so the diagnosis of celiac disease can be only confirmed by clinical symptoms, a positive serology and a positive response with histological improvement to a gluten-free diet [6,7].

The most sensitive antibody serological tests for the diagnosis of celiac disease are of IgA class: antigliadin antibodies, connective tissue antibodies (antireticulin and antiendomysial antibodies) and anti-tissue transglutaminase antibodies [6].

Antigliadin and antireticulin antibodies are rarely detected because they are not considered enough sensitive and specific for the diagnosis of the disease [6]. The highly specific biomarkers for the celiac disease are the IgA antiendomysial antibodies and the anti-tissue transglutaminase antibodies [31-33], whose concentration in the serum correlates with the degree of the mucosal damage [34,35]. For this reason, the diagnostic standard serological tests for the screening of the CD are aimed to determine these antibodies. Different assays for anti-tissue transglutaminase antibodies are available, that have different sensitivities and specificities [36]. The most used is the enzyme-linked immunoassay for the detection of anti-tTG that is less expensive and has a sensitivity greater than 90% [37].

It is worth to note that celiac people are more commonly affected by the selective IgA immunodeficiency, with respect to the general population (1 case in 40 as compared with 1 in 400). From a diagnostic viewpoint, in the case when the level of IgA antiendomysial antibodies and IgA anti-tTG antibodies is within the normal range but there is a high suspicion of CD, a test to determine the IgG isotype of these antibodies should be performed [38].

Diagnosis of the celiac disease made on the bases of clinical manifestation, serological tests and intestinal biopsy is finally confirmed when there is a favourable response to a gluten-free diet [6,7].

1. 1. 6. Treatment and follow-up

The only accepted treatment for celiac disease is a strict and lifelong adherence to a gluten-free diet (GFD), which involves the elimination of wheat, rye and barley from the diet [6,7]. Even if the initiation of a gluten-free diet induces a clinical improvement within days or weeks, the mucosal recovery requires months or years [39]. During this nutritional treatment, the level of antiendomysial and anti-tissue transglutaminase antibodies usually decreases, but the determination of their blood level is not sufficient to assess if the mucosal recovery is going on. On the other side, high levels of celiac antibodies suggest a poor adherence to a GFD

[40]. The best way to control the disease is the assessment of the dietary compliance of the patient, that correlates to the intestinal recovery [41] and, at the same time, has the advantages to be low cost and non-invasive [7]. During the follow-up, it is important to monitor the patient's nutritional status and the growth and development of children. When dietary treatment is not followed by clinical improvement, the initial diagnosis should be evaluated since the villous atrophy is not characteristic only of the celiac disease [6].

The limit of the nutritional therapy is that not all the patients follow a strict GFD, especially teenagers and adults [42,43], whereas there is a high rate of adherence among children and in patients with severe symptoms [6]. To improve the nutritional content of the gluten-free diet, oats, according to some clinical studies, seems to be tolerated, even if in some cases the patient could become oat-sensitive [44,45]. Another limit of this therapy is that the gluten-free products are usually expensive, especially in developing countries, so making the dietary treatment problematic for people with limited financial resources [6].

One of the alternative to the dietary treatment are therapies aimed to interfere with the abnormal mucosal immune response that induces tissue damage (by blocking the mechanism that involves tissue transglutaminase and the HLA-DQ2 and HLA-DQ8 glycoproteins), but this solution can have collateral effects [6]. A more attractive alternative is the use of recombinant enzymes that digest the toxic components of gluten (the gliadin fraction) in the stomach or in the upper small intestine [46,47].

1. 1. 7. Complications

Compared to the general population, people affected by celiac disease have a twofold risk of death [48,49], which increases in patients with poor dietary compliance and in patients with late diagnosis. Celiac people may have serious complications: in fact they have a twice risk of intestinal adenocarcinoma of the small intestine (more often located in the jejunum) that in the general population [50], they can develop enteropathy-associated T-cell lymphoma (a tumour that

derives from a clonal proliferation of intraephitelial lymphocytes) [6] or refractory celiac disease [51,52]: the last is a syndrome that is characterized by the persistence of clinical symptoms and villous atrophy although the patient is following a strict GDF [53]. Refractory disease can be treated adhering to a strict gluten-free diet, together with nutritional repletion of vitamins and minerals. Autologous hematopoietic stem-cell transplantation is an efficient therapeutic strategy for the treatment of the refractory sprue [54].

1. 1. 8. The role of tissue transglutaminase in the celiac disease

Transglutaminases are a widely distributed group of enzymes that, once activated by the binding of calcium, catalyse the post-translational modification of proteins by the formation of isopeptide bonds [55], generating high molecular mass products that are resistant to mechanical stress and proteolytic degradation, and accumulate in tissues (such as skin, hair) where these properties are crucial (for example in the processes of cornification of the epidermis, fibrin-clotting cascade, seminal vesicle coagulation, and wound healing) [56].

There are different human transglutaminases families, encoded by separates genes: even if they have a common sequence in the catalytic site, they are characterized by different substrate specificities, expression patterns and functions [57].

1. 1. 8. 1. Function of tissue transglutaminase

Tissue transglutaminase (tTG) or transglutaminase 2 is a calcium dependent ubiquitous enzyme made up of 686 amino acids, which has different cell localizations, each one characterized by different tTG physiological functions [58-60].

The main biochemical function of tTG (at pH >7) at intracellular level is the catalysis of the covalent and irreversible Ca^{2+} dependent crosslinking between a protein with a glutamine (Gln) residue (glutamine donor) to another protein with a lysine (Lys) residue (glutamine acceptor), resulting in the formation of an ε-(γ-

glutamyl)–lysine (isopeptidyl) bond, with the release of a NH_3 molecule (**Figure 1.6 A**). In particular, tTG shows a high specificity for the substrates in which the lysine-containing glutamine acceptor are numerous [61,62], such as wheat gliadin (its preferred substrate): up to 36% of its glutamine residues are accessible to modification by tTG. Intracellular tTG activation and subsequent crosslinking can also occur when cellular integrity is lost, as found in apoptosis or inflammation [11].

Intracellularly, tTG catalyses also the Ca^{2+}-dependent incorporation of primary amines (such as polyamines and histamine) into proteins (transamidation, **Figure 1.6 B**) and the deamidation of glutamine (Gln) to glutamic acid (Glu) in the absence of suitable amines or at relatively low pH (<7), when water can replace amine donor substrates (**Figure 1.6 C**). tTG seems also involved in the regulation of cellular proliferation, differentiation and apoptosis [63].

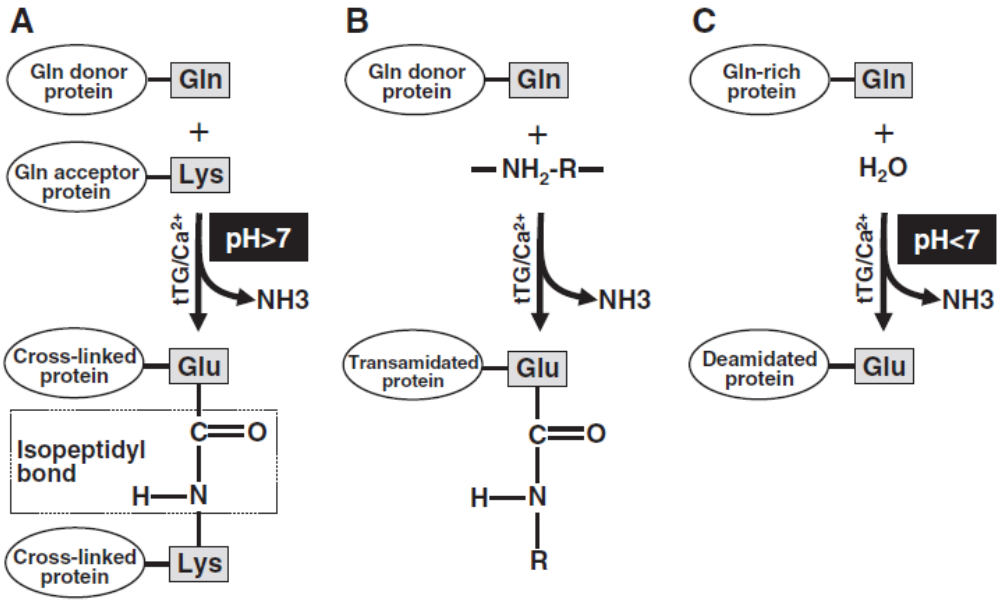

Figure 1.6. Main biochemical functions of tissue transglutaminase (tTG). A. Crosslinking between Gln donor and Gln acceptor proteins. B. Transamidation. C. Deamidation of glutamine to glutamic acid [11].

Another feature of tTG is the ability to bind and hydrolyse guanosine triphosphate (GTP): the binding of GTP excludes the binding of the substrate to the catalytic site, so inhibiting its crosslinking activity [64].

Besides intracellular activities, tTG, always in the presence of high concentration of Ca^{2+}, plays an important role in the extracellular space, in the stabilization and remodelling of the extracellular matrix [65]. Indeed, tTG has an immunological function, activating the growth factor (TGF-β) [66], a cytokine that exert anti-inflammatory properties and prevents autoimmunity [67].

Dysregulation of tissue transglutaminase activity, generally associated with major disruptions in cellular homeostatic mechanisms, makes this enzyme acquiring a pathogenic role in different pathological condition, such as chronic degenerative disorders (Alzheimer's disease, atherosclerosis, arthritis), autoimmune diseases (celiac disease, insulin-dependent diabetes mellitus, autoimmune thyroiditis), chronic inflammatory disorders (rheumatoid arthritis, inflammatory bowel disease, liver cirrhosis), infectious and neoplastic diseases [11].

tTG has been widely investigated in chronic neurodegenerative disorders (such as Huntington's and Alzheimer's disease), neoplastic diseases (the lower enzyme expression and activity tTG activity is related to tumour metastasis [68]) and celiac disease [11].

1. 1. 8. 2. Tissue transglutaminase as the autoantigen of celiac disease

During the last two decades, the role of tTG in the pathogenesis of celiac disease has been widely studied. For the first time, Bruce et al [69] observed in 1985 that tTG activity was increased in celiac patients in comparison to healthy people, and that the enzyme acts preferentially on glutamine-rich gliadin peptides that, among dietary proteins, are effective acyl donor substrates for tTG. These observations were confirmed in later studies [70,71]. In 1997 a single protein band of 85 kDa was immunoprecipitated from celiac sera, that after sequence analysis was identified as tTG [72]. The researchers hypothesized and later demonstrated that

the formation of the tTG-gliadin complex (that can occur in the lamina propria but also inside enterocytes) originated an immune response directed against gliadin and tTG: such immune response is involved in the pathogenesis of CD. This allowed to implement anti-tTG antibody ELISA test based on tTG (initially guinea pig tTG and then human tTG) for the diagnosis of celiac disease [73].

Immunohistochemical studies pointed out that the tTG expression is slightly increased in untreated celiac small intestinal mucosa in comparison to the normal small intestine [11]. Summarizing, tTG plays a double role in the development of the intestinal damage characteristic of the celiac disease: it enhances the immunostimulatory role of gluten thanks to its deamidation activity toward the gliadin peptides, and it is a target for CD-specific antibodies.

1. 1. 8. 3. Tissue transglutaminase modification of gliadin peptides

The gliadin residues that constitute the 30-40% of gluten are the preferential target sites for the deamidation by tTG (**Figure 1.7**): the deamidated gliadin (DAGA) peptides (containing glutamate residues) acquire a higher affinity for HLA-DQ2 and HLA-DQ8 molecules, accommodating in their pockets which have a preference for glutamate peptides, characterized by negatively charged side chains [11].

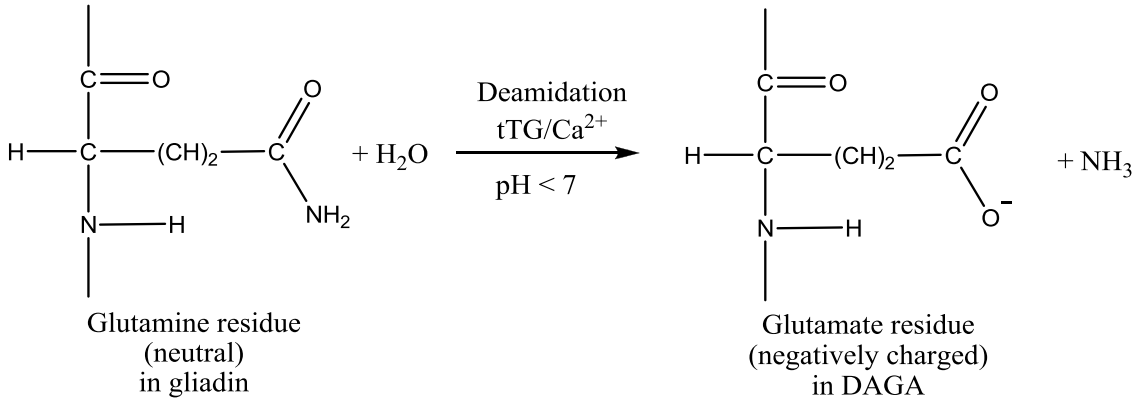

Figure 1.7. Deamidation of gliadin by tTG (pH<7).

Once the T-cells are activated by the binding of the DAGA peptides [74-76], they produce proinflammatory cytokines that initiate a series of inflammatory

reactions, that are responsible for the intestinal lesions characteristic of CD. It has been hypothesized that, in celiac disease, the gliadin and glutenin peptides activate an early immune response, whereas the immunogenic deamidated gliadin fragments, thanks to their increased affinity for the antigen presenting T-cell, are responsible for the longstanding intestinal damage [77,78].

1. 1. 8. 4. Immune response against tissue transglutaminase

Tissue transglutaminase is the autoantigen in celiac disease, since it stimulates the generation of autoantibodies against itself [11]. Anti-tTG antibodies are present in the 98% of the celiac patients on a gluten-containing diet [79], therefore they have been identified as effective biomarkers of CD. The formation of gliadin-tTG immunogenic complexes as a consequence of the tTG crosslinking activity, brings to an overproduction of anti-tTG antibodies both in the IgA and IgG isotypes, that, by interaction with tTG, contribute in the progression and maintenance of the intestinal mucosa damage, by inducing cytoskeleton changes [80].

Since tTG plays a crucial role in the pathogenesis of celiac disease, an attractive therapeutic strategy for CD is the use of inhibitors of intestinal tTG, aimed to inhibit its deamidation activity toward gliadin peptides, in order to prevent the pathogenic activation of T-cells [81-88].

1. 1. 9. Anti-tissue transglutaminase isotypes: IgG and IgA

1. 1. 9. 1. Immunoglobulin and isotype classes

As said in Paragraph 1. 1. 8, in celiac patients, anti-tissue transglutaminase is overproduced, both in the IgA and IgG isotypes.

Immunoglobulins (Ig) (**Figure 1.8**), are glycoproteins produced by white blood cells, which play an important role in the complex and specific immune response: they specifically recognize and bind particular antigens (such as bacteria or viruses), helping to eliminate the foreign substance from the body [89,90].

Figure 1.8. Typical antibody molecules [89].

All immunoglobulins have a common structure made up of four polypeptide chains [89,90] (**Figure 1.9**):

- two identical heavy (H) chains (molecular weight of about 50 kDa) with covalently attached oligosaccharide groups), which are joined each other through disulphide bonds located in a flexible region (called "hinge region");
- two identical light (L) chains (molecular weight 25 kDa, non-glycosylated), each bound to a heavy chain through a disulphide bond.

The constant region of the heavy chain determines the effector functions of the antibody (such as antigen-dependent cellular toxicity or placental transport).

The antibodies recognize and bind specifically an antigen thanks to the two fragment antigen binding (F_{ab}) regions, that have the highest degree of variability between different antibodies. The F_{ab} regions are the two identical "arms" (each of them can bind the antigen) composed by a portion of light chain and a portion of heavy chain: in particular, they are composed by four domains, two variable domains (light chain variable domain, V_L, and heavy chain variable domain, V_H) and two constant domains (light chain constant domain, C_L, and heavy chain constant domain, C_H) [89,90].

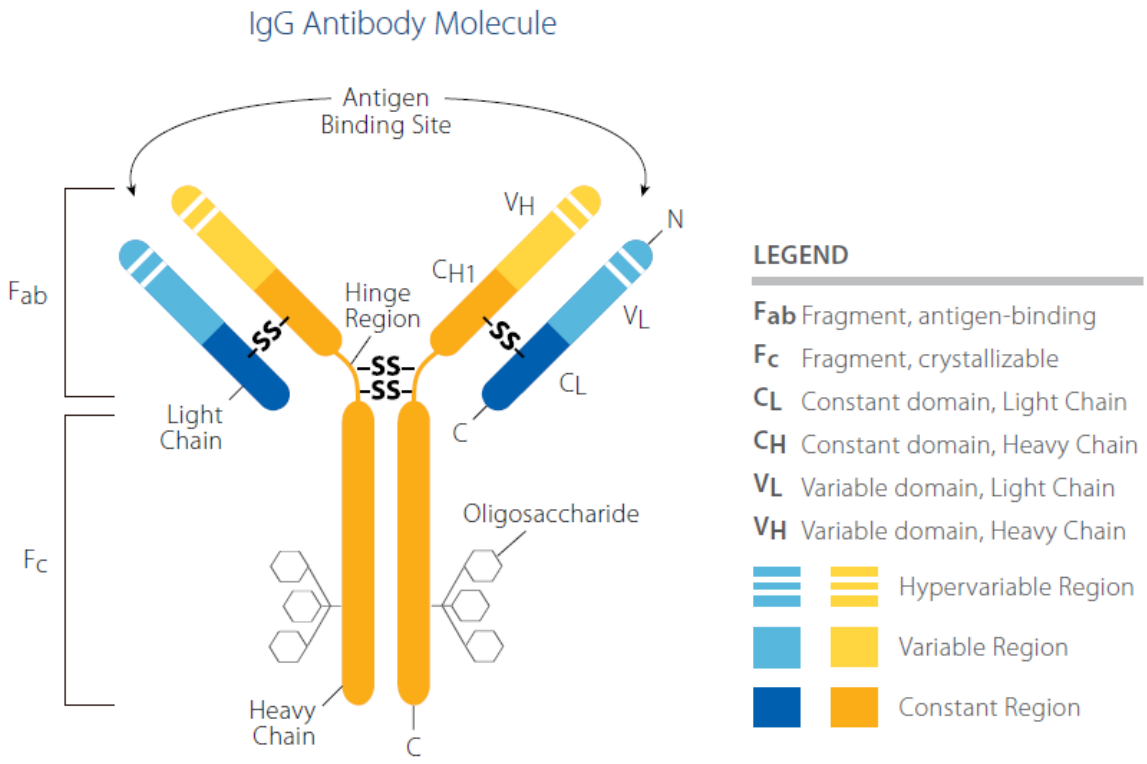

Figure 1.9. Immunoglobulin structure [89].

The specificity towards an antigen of the different antibodies depends on the aminoacidic sequence of the variable domain, that changes from an antibody to another: this allows to have a complex an efficient immune response. The formation of the antigen binding site occurs when a heavy chain variable domain come close to a light chain variable domain [89].

Antibodies produced by plasma cells exist in various isoforms (immunoglobulin isotypes) that have proper biological features, structure and distribution, and consequently different function and target specificity, that is at the base of the complexity of the humoral immune response.

Antibodies isotypes are classified according to differences in their aminoacid sequence in the constant region (F_c) of the antibody heavy chain; in the placental mammals five major antibody isotypes have been identified: IgA, IgD, IgE, IgG and IgM. These different isotypes have the same antigen's specificity, from the moment that they have the same variable regions of heavy chain and light chain, but each class can execute different effector functions.

1. 1. 9. 2. Properties of IgG and IgA isotypes

IgG immunoglobulins (structure in **Figure 1.10**) are the major immunoglobulin in blood, lymph fluid, cerebrospinal fluid, and peritoneal fluid: they are produced in a delayed response to an infection and can be retained in the body for a long time. IgG immunoglobulins play a fundamental role in the humoral immune response, in the activation of the immune system's complement system and in the phagocytosis of microorganisms (thanks to the binding of the F_c portion of the antibody to a receptor present on a phagocyte). In healthy humans, immunoglobulin IgG represents approximately 15% of the total content of proteins in serum. Detection of IgG in serum usually indicates a prior infection or vaccination [89].

Figure 1.10. IgG immunoglobulin structure [89].

Also IgA immunoglobulins (structure in **Figure 1.11**) are present in serum (in healthy individuals represent approximately 15% of all immunoglobulins in serum), but they are mostly present in secreted form (in saliva, tears, colostrum, mucus, sweat and gastric fluid). IgA acts as a neutralizing antibody, by attaching and penetrating epithelial surfaces of the invading pathogens, thus enabling the attachment of the phagocyting cells to clear the infection [89].

People who do not have sufficient quantities of IgA are affected by selective immunoglobulin A deficiency (SIgAD), that is the most prevalent antibody defect. These patients can more easily develop autoimmune disorders (like allergies, asthma and rheumatoid arthritis).

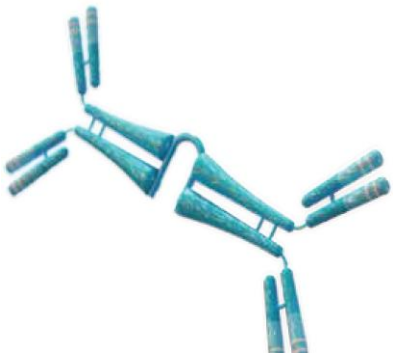

Figure 1.11. IgA immunoglobulin structure [89].

1. 2. Electrochemical biosensors

1. 2. 1. Definition of electrochemical biosensor

According to the IUPAC definition (1996), a chemical biosensor is a "self-contained integrated device that is capable of providing specific quantitative or semi-quantitative analytical information using a biological recognition element (biochemical receptor) which is in direct spatial contact with a transduction element" [91].

In other words, in order to have a biosensing response, the chemical recognition and the energy transduction processes must be coupled, and this is possible if the molecularly selective chemical component and the transducer are intimately associated.

The chemically selective component of a biosensor is a component selective for the analyte, which can be of biological origin, such as tissues, cells, immunochemical species (antibodies or antigens) or enzymes, or abiotic, such as the synthetically produced host-guest molecules and molecularly imprinted polymers.

The transducer is the detector of the biosensor, that responds to the molecular recognition event and converts this response to an output that can be amplified, stored or displayed [90]. In practice, the analytical function of a biosensor is a

combination of chemical transduction and energy transduction. The chemical transduction is due to the biorecognition process that occurs on the reaction layer that enhances the chemical selectivity toward analytes, producing an input signal to the transducer. The energy transduction is typical of any instrumental method, and it consists in processing chemical information about the analyte as an electrical signal which can be acquired by a recorder, meter or computer, in order to be subsequently interpreted.

Figure 1.12 shows a schematic representation of the main components of a biosensor and its operating principle.

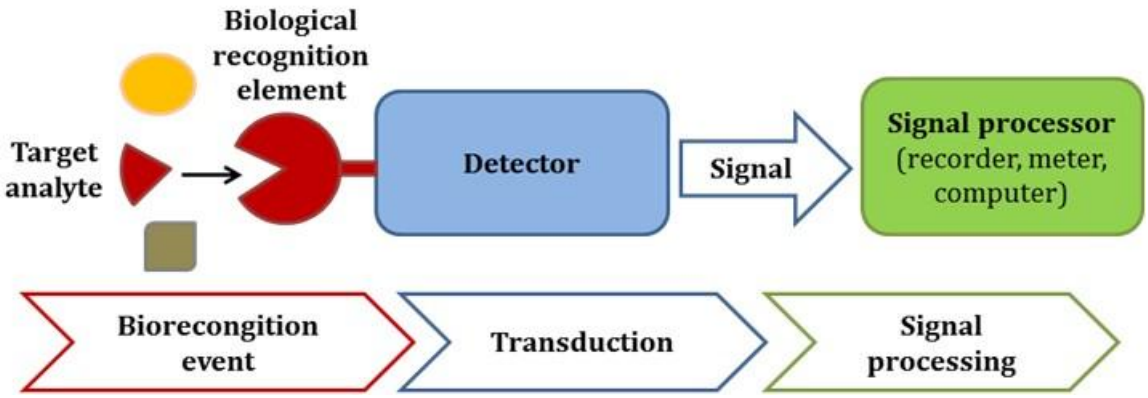

Figure 1.12. Operating principle of a biosensor: the analyte is specifically recognized by the bioreceptor that is in close proximity to the detector. The biorecognition event is transduced by the detector into a signal which can be amplified or displayed.

In many cases, it is difficult to produce biosensors with adequate selectivity, in spite of some very clever molecular recognition schemes developed over the years [91].

Biosensors can be classified in terms of the energy transduction mode (amperometric, potentiometric, chemiluminescent, thermal or piezoelectric), in terms of the biological recognition element (enzymatically based, immunosensor) or in terms of the analyte (e. g. glucose sensor).

Electrochemical sensors represent an important subclass of chemical sensors in which an electrode is used as the transduction element. These devices are

presently the most widely commercialized sensors. They have different important applications in clinical, industrial, environmental and agricultural analysis, as well as for safety and military use [92]. Electrochemical biosensors combine the analytical power of electrochemical technique with the specificity of biological recognition process. They are designed in order to convert a biological recognition process into an electrical signal representative of the concentration of the analyte. They are easy-to-use, compact and inexpensive [92].

According to the classification of Arnold and Meyerhoff, there are two general categories of electrochemical biosensors: biocatalytic and bioaffinity types, depending on the nature of the biological recognition process, that in the first case utilizes enzyme, cells or tissues as immobilized biocomponents with biocatalytic activity, in the second case antibody-antigen interactions, nucleic acids interactions or membrane receptors [91,92].

There are different methods to immobilize the chemically selective biomolecules on the transducer surface, depending on the properties of the immobilized species and nature of the surface of the transducer. The most common techniques of immobilization are based on absorption, entrapment, cross-linking and covalent bonding. These techniques can be applied to the development of different type of biosensors, simply adapting the basic chemistry of the immobilization method [91].

1. 2. 2. Enzyme-based electrodes

Enzymes are proteins that catalyse chemical reaction in living systems in an extremely efficient and selective way, remaining unchanged after the reaction: the coupling of an enzymatic layer with an appropriate electrode allows one to develop enzyme electrodes, that combine the specificity of the enzyme for its substrate with the analytical power of electrochemical devices. Moreover, by exploiting the electrochemical regeneration of the enzyme substrate or of a suitable redox mediator, it is possible to take advantage of the electrocatalytic

amplification of signals [92]. Enzyme biosensors can be used for monitoring many biomolecules in the clinical, environmental and food fields.

In an enzyme electrode, the immobilized enzyme layer is chosen to catalyse a reaction, which generates or consumes detectable species: the enzyme catalyses the conversion of its substrate in a product, with the contemporary transformation of a co-reactant.

In order to have a good enzyme electrode, it is important that the enzyme layer is immobilized on the sensing surface while keeping the enzyme stability and activity [92]. There are different methods of immobilization of enzymes onto electrodes, that can be divided into physical (for example entrapment of an enzyme solution between the electrode and a dialysis membrane, in polymeric films via casting or electropolymerization, in a thick gel layer, absorption onto a graphite surface) or chemical; in the latter case, the enzyme is attached by means of covalent coupling through a cross-linking agent such as glutaraldehyde, via amide bonding, or biotin-avidin interactions or ion-exchange [93,94].

The behaviour of an immobilized enzyme can be different from that in homogenous solution: in fact, an enzyme unfolding could be associated to the immobilization step, that can affect the kinetics of an enzyme-catalysed reaction. On the other side, a careful engineering of the microenvironment on the sensing surface can improve the enzyme electrode performance [92].

In a simple enzymatic reaction that involves a single substrate, the enzyme (E) combines the substrate (S) to form an intermediate enzyme-substrate complex (ES) which subsequently converts to product (P) and liberates the enzyme (**Equation 1.1**) [90-92].

$$E + S \underset{k_{-1}}{\overset{k_1}{\rightleftarrows}} ES \xrightarrow{k_2} E + P \qquad (\mathbf{1.1})$$

At a fixed enzyme concentration, the rate of the enzyme-catalysed reaction V is given by the Michaelis-Menten equation (**Equation 1.2**) [90-92].

$$V = \frac{k_2\,[E]\,[S]}{K_m + [S]} \qquad (\mathbf{1.2})$$

where:

- k_2 is the turnover of the enzyme, that represent the number of molecules of substrate that can be converted to the product within a period of time;
- [E] is the enzyme concentration;
- [S] is the substrate concentration;
- K_m is the Michaelis-Menten constant that quantifies the enzyme's affinity for its substrate.

The product of the turnover of the enzyme k_2 and the enzyme concentration is often indicated as V_m (**Equation 1.3**), that is the maximum rate of the enzymatic reaction [90].

$$V_m = k_2[E] \qquad (\mathbf{1.3})$$

By substituting Equation 1.3 in Equation 1.2, **Equation 1.4** is obtained.

$$V = \frac{V_m\,[S]}{K_m + [S]} \qquad (\mathbf{1.4})$$

The Michaelis-Menten constant K_m corresponds to the substrate concentration for which the rate is equal to half V_m. In the construction of enzyme electrodes, it is preferable to obtain the highest V_m and the lowest K_m. A suitable enzyme for labelling must be stable under the reaction conditions and it must have a high turnover rate [90].

In an enzyme electrode the most important challenge is to establish electron transfer between the active site of the enzyme and the electrode surface: this can be achieved using natural secondary substrates (first generation biosensors), artificial redox mediators (second generation biosensors) or direct electron transfer (third generation biosensors), as shown in **Figure 1.13** [92].

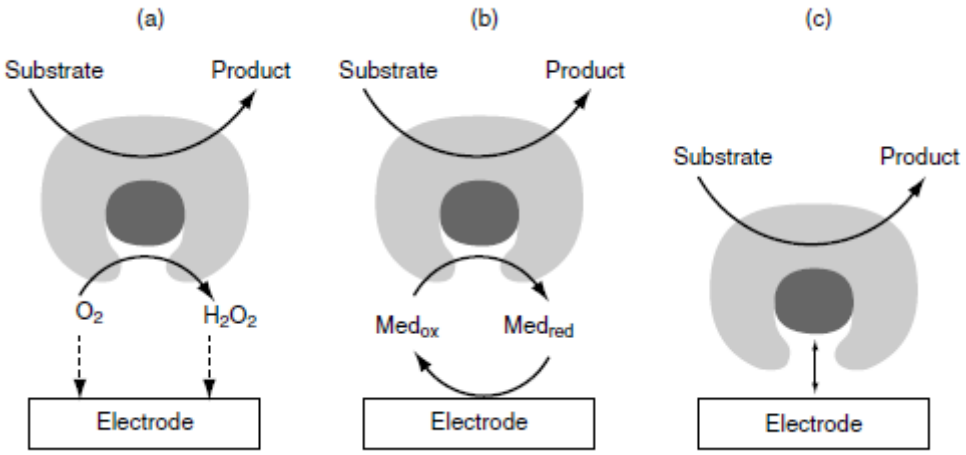

Figure 1.13. Three generations of amperometric enzyme electrodes based on the use of natural secondary substrate (a), artificial redox mediators (b), or direct electron transfer between the enzyme and the electrode (c) [92].

1. 2. 3. Affinity biosensors

Certain biomolecules, such as antibodies, receptors, oligonucleotides, which are characterized by selective binding toward specific target species, can be used to develop affinity electrochemical biosensors. The biomolecular recognition process is an associative process characterized by the high specificity and affinity between the receptor and the ligand of interest. It is a thermodynamically controlled process, that depends, among other parameters (e. g. chemical functionalities, ionic charge, hydrogen bonding), on the size and shape of the receptor pocket and the nature of the ligand [92].

Affinity electrochemical biosensors exploit the suitability of electrochemical transducer for detecting the molecular recognition event and the selectivity and sensibility of the binding process. There are different types of affinity biosensors: immunosensors (based on the antibody-antigen complexation), DNA hybridization biosensors, receptor-based sensors and electrochemical sensors based on molecularly imprinted polymers.

Immunosensors can be used to identify and quantify a wide range of substances, providing very low detection limits [90].

As explained in Paragraph 1. 1. 9, antibodies are globular proteins produced by an organism to bind foreign molecules, the antigens, and mark them for elimination from the organism: antibodies are characterized by a very high selectivity for their antigen, thanks to the stereospecificity of the binding site for the antigen [92]. The biorecognition event between antibody and antigen occurs via suitable recognition sites that are a fundamental feature of both of them: in particular, the recognition site on the antibody is called paratope whereas the one on the antigen is the epitope (usually made up of no more than 18 aminoacids) [90]. The paratope specifically recognizes and matches the epitope of a specific antigen (shape recognition), so forming the antibody-antigen complex that is characterized by large binding constants (K_{eq}, usually ranging from 10^6 to 10^{12} L mol^{-1}), expressed by the **Equation 1.5** [90,92].

$$K_{eq} = \frac{[Ab - Ag]}{[Ab][Ag]} \qquad (\mathbf{1.5})$$

where:

- K_{eq} is the equilibrium constant for the immune-complex formation;
- [Ab-Ag] is the concentration of the antibody-antigen complex;
- [Ab] is the antibody concentration;
- [Ag] is the antigen concentration.

Two different types of antibodies can be distinguished: monoclonal and polyclonal. Monoclonal antibodies are produced by a single clone of antibody-producing cells and they have affinity only for one particular epitope on an antigen. On the other hand, polyclonal antibodies, produced by a host upon injection of an antigen, can bind several epitopes on the antigen. Since monoclonal antibodies are more specific and reproducible, they are usually preferred for analytical assays [90].

Thanks to the high affinity between antibodies and antigen, the recognition event can be exploited for the direct detection of these biomolecules in complex samples (e. g. untreated blood or urine) even at very low concentration [90]. In the more "classical" immunotest approach, for the detection of the analyte it is necessary

that the antibody (or antigen) is labelled with a fluorescent, luminescent, radioactive molecule, an enzyme or an electrochemically active group [90].

Electrochemical immunosensors combine the specificity of immunoreactions for the recognition of the biochemical analyte and the electrochemical transduction [95-100]. In such biosensors usually the label is a redox enzyme: when its substrate is added, an electroactive species is generated (or consumed), that can be detected so producing an electrochemical signal.

Affinity immunosensors have been developed also using a label-free detection strategy; for instance, the antigen-antibody interaction can cause changes in resistance or in capacitance of the electrode-solution interface, which can be monitored by electrochemical impedance spectroscopy [91].

1. 3. Nanoelectrode ensembles

The application of nanotechnology in the engineering of biosensing devices has recently acquired great interest, since the clever use of nanomaterials allows to improve the analytical performances of biosensors, in terms of selectivity, sensitivity, detection limit and response time [101]. A particular class of nanodevices, attractive for developing improved electrochemical biosensors, are the so called nanoelectrode ensembles (NEEs).

NEEs were introduced in the mid-nineties by Chuck Martin's group and developed and applied by Prof. Ugo's research group in Ca' Foscari. They are made by a very large number of nanodisk electrodes (diameter of 30-50 nm) confined in a small space [102]. They have many advantages from the electrochemical point of view, that are: highly improved signal-to-background current ratios, very low detection limits [103-106], high miniaturization [105], without requiring high signal amplification nor shielding from external electric field in a Faraday cage. Moreover, they can be turned into 3-D nanoelectrode systems [107-110] or can be developed in groups of singly addressable arrays for multianalyte detection [111,112].

Ensembles of gold nanodisk electrodes are prepared using the pores of microporous filtration membranes as templates: they can be prepared by an electrochemical method to fill the pores with metal nanowires [113] or by means of electroless deposition. With the latter method, gold nanodisk electrodes with a diameter as small as 10 nm have been prepared [103].

1. 3. 1. Electroless deposition and NEEs fabrication

The electroless deposition method can be used for the template fabrication of gold nanowires, nanotubes and other shaped gold nanomaterials [103,114]. The objective is to make the process compatible with the membrane chemistry, to plate gold uniformly in nanoscopic pores, using a chemical reducing agent to deposit the metal from a solution onto a surface [103].

The electroless deposition process developed is for the gold deposition on track-etch polycarbonate (PC) membrane filters, that are preferred with respect to alumina membranes because the PC membrane are not brittle and have a smaller pore density, that is a convenient feature from an electroanalytical point of view because there is reduced interaction between the nanoelectrodes [115].

The electroless deposition involves different steps (a detailed description of the procedure is reported in the Experimental Section) [103]:

- **sensitization of the membrane**: the surfaces of the polycarbonate membrane are sensitized by absorption of Sn^{2+} ions;
- **activation of the membrane**: metallic nanoparticles, typically Ag^0, are deposited onto the walls of the pores and onto the membrane faces. Typically, Ag^0 nanoparticles (NPs) are produced by reaction between the sensitizer Sn^{2+} and an Ag^+ solution;
- **galvanic displacement**: catalytic particles, typically Au nanoparticles, are deposited by galvanic reaction between Au^+ solution and the activator (Ag NPs);

- **catalytic reduction**: the AuNPs act as catalytic and preferential sites for the massive deposition of Au^0 by reacting Au^+ solution with a reducing agent (formaldehyde). In practice, the AuNPs grow up to completely fill the pores with metallic gold.

After removing the gold layer from one side of the membrane, using a suitable microfabrication procedure (see Experimental Section), a handy array of gold nanodisk electrodes embedded in PC is obtained (namely, NEE).

It is important to underline that, when connected to a potentiostat, all the nanoelectrodes in the NEE will experience the same applied potential, since they are all connected each other [115].

1. 3. 2. Current signals of NEEs

From an electrochemical point of view, NEEs can be considered as a large assembly of very small ultramicroelectrodes confined in a small space [115].

Depending on the scan rate or the distance between the nanoelectrodes [115-117] or the viscosity [118], three different diffusional regimes determine the voltammetric responses at NEEs (**Figure 1.14**):

A. **Total overlap regime**: radial diffusion boundary layers overlap totally (slow scan rate, short inter-electrode distance, low viscosity);
B. **Pure radial regime**: radial diffusion layers are separated, nanoelectrodes behave individually (intermediate scan rate, inter-electrode distance or viscosity);
C. **Linear active regime**: nanoelectrodes behave as isolated planar electrodes (very high scan rate, inter-electrode distance or viscosity).

For electroanalytical applications, total overlap and pure radial regimes are the most convenient ones because they are characterized by high faradaic-to-capacitive current ratios.

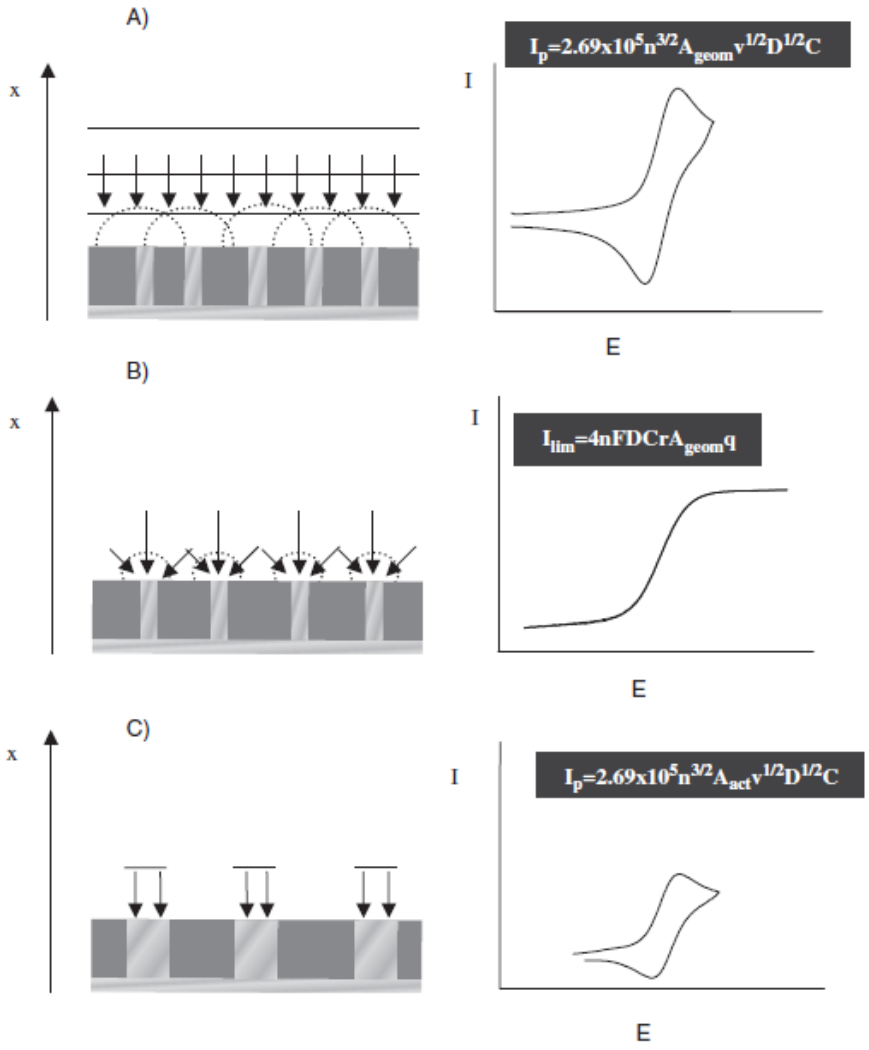

Figure 1.14. Schematic representation of different voltammetric responses at NEE. A: Total overlap. B: Pure radial. C: Linear active. Relevant equations for peak currents (A e C) and plateau current (B) refer to reversible redox systems [115].

The signal-to-noise ratio of NEEs depends on the relative weight of two geometric parameters:

- **geometric area** (A_{geom}): it is the area determined by the dimension of the hole punched into the insulator, that is the overall area of the active nanoelectrode elements and the polycarbonate between them;
- **active area** (A_{act}): it is the electroactive area, that is the area of the gold nanoelectrodes (**Equation 1.6**).

$$A_{act} = \pi r^2 \mathrm{p}\, A_{geom} \quad (\mathbf{1.6})$$

where:

- p is the pores density;
- r is the mean pore radius.

Fractional electrode area (f) is defined as the ratio between active area and geometric area (**Equation 1.7**).

$$f = \frac{A_{act}}{A_{geom}} \quad (\mathbf{1.7})$$

Under total overlap diffusion conditions [103]:

- double-layer charging current, i. e. capacitive current (i_c), scales with the active area of the gold nanodisks;
- faradaic current (i_f) scales with the overall geometric area of the ensemble.

The faradaic current at a NEE operating in total overlap regime for a reversible redox system obeys the Randles-Sevcik equation (**Equation 1.8**) [103].

$$i_p = 2.69 \cdot 10^5 \cdot n^{3/2} \cdot A_{geom} \cdot D^{1/2} \cdot C^* \cdot \nu^{1/2} \quad (\mathbf{1.8})$$

where:

- i_p is the peak current [A];
- n is the number of transferred electrons;
- A_{geom} is the geometric area [cm^2];
- D is the diffusion coefficient of the reversible redox probe [$cm^2\ s^{-1}$];
- C^* is the redox species bulk concentration [mol cm^{-3}];
- $\boldsymbol{\nu}$ is the scan rate [V s^{-1}].

At the same NEE, the capacitive current is proportional only to the area of the nanoelectrode elements, according to **Equation 1.9** [119,120].

$$i_c = \nu \cdot C_{dl} \cdot A_{act} \quad (\mathbf{1.9})$$

where:

- $\boldsymbol{\nu}$ is the scan rate [V s^{-1}];

- C_{dl} is the double layer capacitance of the gold nanodisks of the NEE, that is 21 μF cm^{-2};
- A_{act} is the active area [cm^2].

At a NEE, typical double-layer charging currents values are in the range between 1 and 2 nA (based on a C_{dl} value between 20 and 40 μF cm^{-2} [120] for a NEE with A_{geom} 0.079 cm^2, average pore radius $1.5 \cdot 10^{-6}$ cm and scan rate 0.1 V s^{-1}) [115], that are orders of magnitude lower than at a macro-electrode of equivalent geometric area. So, since at a NEE the faradaic currents are equal to those at a macro-electrode of the same area [103], NEEs are characterized by a signal-to-background ratio that is orders of magnitude greater than at a macro-electrode [117,121] that allows to use low electroactive species concentrations (even three order magnitude lower).

Since the voltammetric detection limit for a redox species at a NEE is obtained by multiplying the detection limit for the same species at the corresponding macro-electrode by the fractional area [117], the detection limit at a NEE results even three orders magnitude lower than the limit achievable at a conventional macro-electrode [103].

NEEs behave as partially blocked electrodes (PBE) [122-125], since the nanodisk electrodes are the unblocked surface whereas the template polycarbonate membrane is the blocking material. Their current response is very sensitive to electron-transfer kinetics [103], being identical to that of a naked electrode with the same overall geometric area, however, undergoing a heterogeneous electron transfer process characterized by a smaller apparent rate constant ($k°_{app}$), related to the true standard rate constant (k^0) by the **Equation 1.10**:

$$k°_{app} = k°f \qquad (\mathbf{1.10})$$

where f is the fractional electrode area.

1. 4. Immunosensors for the detection of anti-tTG

1. 4. 1. Most common serological methods for CD diagnosis

Even if intestinal biopsy still remains the gold standard for the diagnosis of the celiac disease, in the last decades many researchers have focused their efforts in the development of serological methods for the detection of the specific biomarkers of the celiac disease, namely antiendomysial antibodies and anti-tissue transglutaminase antibodies [9,31,32,33], whose concentration in the serum correlates with the degree of the intestinal damage [34,35].

It is important to develop such diagnostic tests since they are fundamental both for the diagnostic screening of CD in the general population (since an early diagnosis of the disease should minimize the risk of complications) and for the follow-up of the disease while the celiac patient is following a strict gluten-free diet, so avoiding invasive intestinal biopsy.

The most used diagnostic tests are the enzyme-linked immunosorbent assay (ELISA) for the identification of anti-tissue transglutaminase antibodies, that are the antibodies against tissue transglutaminase, the enzyme responsible for the deamidation of gliadin in the lamina propria (in both IgA and IgG isotypes) [126,127] and the indirect immunofluorescence for the determination of anti-antiendomysial antibodies [128-133].

Different studies using ELISA method were aimed to evaluate and compare the sensitivity and specificity of the serologic marker anti-tTG antibodies with those of the antiendomysial antibodies, establishing that the presence of high levels anti-tTG in the serum is a reliable indicator for the diagnosis and follow-up of CD [9, 128,131].

With an automatic chemiluminescent immunoassay, F. Panetta et al. determined the values of anti-tTG in healthy people and celiac patients, confirming a

satisfactory correlation between the amount of the detected anti-tTG and the expression of mucosal damages, established via bowel biopsy [9]. These data confirm that serological tests for the detection of tTG are suitable for the first-line screening of celiac disease [9].

In following studies, it was reported that sensitivity and specificity for both the IgA and IgG isotypes of anti-tTG exceed 95% [134,135].

1. 4. 2. Electrochemical immunosensors for CD diagnosis

Electrochemical biosensors have gained great attention in recent years in the field of clinical diagnostic [136-138] from the moment they present a lot of advantages: they allow to reach low detection limits, high sensitivity and specificity, being at the same time cost-effective, user-friendly, simple and speedy. Moreover, they can be miniaturized, so they are portable, important feature since it is important to bring these facilities also in developing countries. Recently, due to these advantages, different electrochemical biosensors for the detection of the biomarkers for the celiac disease (in particular anti-tTG) have been produced [139-147].

Different substrates were used as electrochemical transducer surface: screen-printed electrodes [142,146], gold based self-assembled monolayers of a carboxylic group terminated bipodal alkanethiol [143], graphite-ephoxy composite electrodes [145], glassy carbon electrodes functionalized with gold nanoparticles [147]. All the methods mentioned used the antigen tissue transglutaminase as recognition element for the anti-tTG and a secondary antibody against the IgA or IgG immunoglobulin isotype labelled with an enzyme, typically alkaline phosphatase [142] or horseradish peroxidase [143,144,145,147]. In the presence of the enzyme substrate and a suitable redox mediator, an electrocatalytic signal is generated. In particular, different electrochemical methods have been used: cyclic voltammetry [142], electrochemical impedance spectroscopy [143,146], amperometry [145,147]. **Figure 1.15** shows a schematic representation of a

typical immunosensor used for the electrochemical detection of anti-tissue transglutaminase.

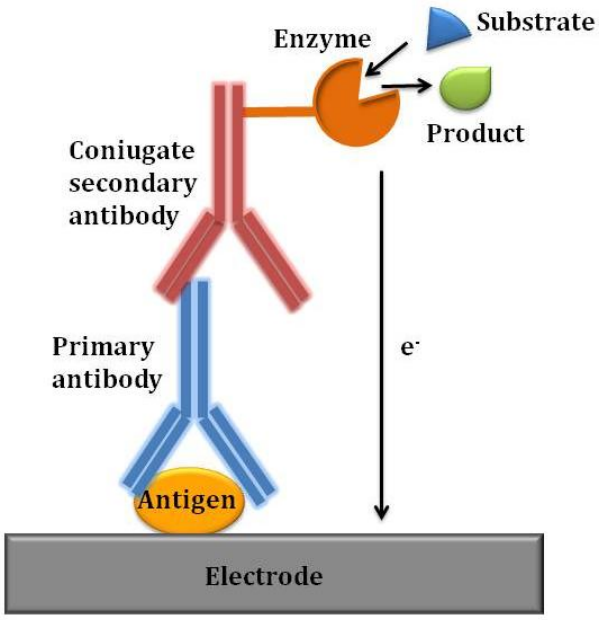

Figure 1.15. Schematic architecture and functionality of electrochemical immunosensor. After immobilization of the capture antigen (tissue transglutaminase) onto the electrode surface, the obtained sensor is incubated with anti-tissue transglutaminase (antibodies for calibration and antibodies in serum samples). The detection of the antigen-antibody complex is achieved incubating the sensor with secondary antibodies labelled with an enzyme. After adding the corresponding substrate, an enzymatic reaction occurs, enabling the detection and quantification of the analyte by electrochemical measurements.

The majority of the existing methods for the detection of anti-tTG are aimed to the detect and quantify the IgA isotype, but in patient with the immunoglubulin IgA deficiency [38] or in children under 2 years of age (who may not produce some of the auto-antibodies since their immune system is not well matured) [37], it is important to determine the serological value of the IgG isotype. For this reason, it would be important to develop a highly specific and sensitive electrochemical method that allows to determine both the anti-tissue transglutaminase isotypes (IgA and IgG) in the serum.

1. 4. 3. NEE-based immunosensor for IgG and IgA anti-tTG

Nanoelectrode ensembles have been recently used for interesting bioanalytical application since they allow to reach low detection limits, and the biorecognition element can be immobilized on the polycarbonate membrane without any modification of the electrode surface, without hindering the electron transfer.

For the first time, NEEs have been used in diagnostics by Pozzi Mucelli et al. in 2008, to detect the human epidermal growth factor receptor 2 (HER2) that is overexpressed in some breast cancer, immobilizing on the NEEs surface the monoclonal anti-HER2 antibody trastuzumab [102]: the interaction between the capture antibody and the analyte was detected by a suitable secondary antibody labelled with horseradish peroxidase. In the presence of the enzyme substrate (hydrogen peroxide) and of a suitable redox mediator (methylene blue) that shuttles electrons from the nanoelectrodes to the biorecognition layer, an electrocatalytic signal was generated. The obtained results proved that the biorecognition element is immobilized mainly on the PC template membrane and not on the nanoelectrodes, since the electron transfer between the redox mediator and the nanoelectrodes is not hinder after the whole immobilization procedure. Polycarbonate is employed in the biorecognition process since its carbonyl groups can react with the amine group of proteins [148], while the gold nanoelectrodes remain free to play in the transduction process. Similar approaches were used to detect DNA probes [149], and IgY immunoglobulin in hen's egg yolk in tempera paintings [150].

Established that NEEs are an attractive tool for the development of electrochemical immunosensors, for the first time, in our research group, H. B. Habtamu developed a novel immunosensor based on NEEs for the detection of anti-tissue transglutaminase, a reliable biomarker of the CD [151]. In particular, a specific and sensitive NEE-based immunosensor for the detection of the IgG anti-tTG isotype in the serum of celiac paediatric patients was developed.

To this aim, NEEs present many advantages, that are now discussed. Since blood is a complex matrix containing a large number of biomolecules, for the detection of the anti-tTG it is important to dilute the serum sample in order to minimize the possible interference of these biomolecules with the antigen-antibody binding process that occurs on the electrode surface. It is fundamental to use sensitive tools such as NEEs that allow to reach very low detection limit in order to detect small amounts of analyte in diluted matrix. Indeed, the use of NEEs for diagnostic purposes avoid time-wasting procedures for the immobilization of the biorecognition element, since the polycarbonate membrane of the NEE has strong affinity for proteins, allowing to immobilize the capture biomolecules without requiring any preliminary modification of the electrode surface. Moreover, since the polycarbonate area available for the immobilization of biomolecules is more than 100 times larger than the area of the nanoelectrodes elements, by this strategy a large number of biorecognition molecules can be immobilized (in the case of the proposed immunosensor, the capture antigen tissue transglutaminase). Furthermore, it was noted that after using NEEs for the preparation of the immunosensors, they still maintain unchanged their electrochemical properties.

In this work we develop electrochemical immunosensors based on NEEs for the detection of both IgG and IgA isotypes of anti-tissue transglutaminase.

Both the devices for the detection of IgG and IgA anti-tTG are based on a scheme similar to the one reported in **Figure 1.15**. In the proposed immunosensor, the capture antigen tissue transglutaminase is immobilized on the polycarbonate of the NEEs. After a blocking step with BSA to minimize aspecific absorptions, the obtained immunosensor can be used for the specific detection of anti-tTG in serum samples. It is worth stressing that the capture antigen binds both the IgA and the IgG anti-tissue transglutaminase: the selective detection of the IgG or IgA isotype is possible thanks to a clever choice of the secondary antibody, that in the first case is against immunoglobulin IgG and in the second case against IgA. In particular, the selectivity towards IgG is gained using a secondary Ab labelled with horseradish peroxidase (HRP) whereas the selectivity towards IgA is achieved using a

secondary Ab labelled with glucose oxidase (GOx). In the case the antibody-antigen complex is formed, adding the enzyme substrate and a suitable redox mediator to shuttle electrons between the enzyme active site and the gold nanoelectrodes, an electrocatalytic signal is generated, which can be detected by means of cyclic voltammetry.

1. 5. Aim of the thesis

In this work we aim to develop a simple, cost-effective, user-friendly, specific and sensitive immunosensor for the detection and quantification of both IgA and IgG isotypes of anti-tissue transglutaminase in the serum using electrochemical immunosensors based on NEEs (nanoelectrode ensembles) prepared in our laboratory by electroless deposition of gold in track-etch polycarbonate membranes, that present different advantages. Thanks to their structure made up of a great number of gold nanoelectrodes grown in the nanopores of the PC membrane, NEEs are characterized by a high signal-to-background ratio, that allows to achieve very low detection limits. Indeed, since polycarbonate is affine to biomolecules, it is possible to immobilize a huge number of proteins directly on the template membrane without any preliminary modification of the electrode surface. We wish to study the possibility of functionalizing the PC membrane of NEEs with tissue-transglutaminase as capture antigen to obtain an immunosensor able to capture both the IgG and IgA isotypes of anti-tTG in serum samples. The selective detection of isotype IgG is possible by using a secondary anti-IgG antibody labelled with horseradish peroxidase (HRP): in the presence of the target analyte (IgG anti-tTG), the addition of HRP substrate (hydrogen peroxide) and a suitable redox mediator (hydroquinone) should generate an electrocatalytic increase of the cathodic current. For the detection of IgA isotype, a different secondary antibody will be employed, that is an anti-IgA Sec-Ab labelled with glucose oxidase (GOx). In this case, in the presence of the target analyte (IgA anti-tTG), with the addition of glucose (the substrate) and (ferrocenylmethyl)trimethylammonium (the redox mediator), an electrocatalytic increase of the anodic current is expected.

Chapter 2
Experimental Section

2. 1. Materials and instrumentation

2. 1. 1. Reagents and immunochemicals

Track-etch polycarbonate filtration membranes coated by the producer with wetting agent polyvinylpyrrolidone in order to make them hydrophilic (47 mm diameter, 6 μm thickness, $6 \cdot 10^8$ pores per cm^2, 30 nm nominal pore diameter and 200 nm average center-to-center pore distance) used as template to preparing NEEs, were purchased from SPI-pore.

For the synthesis of the gold nanodisks, a commercial gold electroless plating solution (Oromerse Part B, Technic Inc.) was used.

$FAPF_6$ was prepared by metathesis of the (ferrocenylmethyl)trimethylammonium iodide (Alfa aesar) with potassium hexafluorophosphate 99% (Alfa Aesar).

Carbonate-bicarbonate buffer (pH 9.2), 0.01 M phosphate buffer saline (PBS, pH 7.4) and 0.1 M sodium phosphate buffer (PB, pH 7.4) were prepared according to the Cold Spring Harbor Protocols, using distilled water.

Human recombinant tissue transglutaminase (h-tTG), HRP-labelled goat anti-human IgG, standardized serum samples and patient serum samples were kindly supplied by IRCCS Materno Infantile Burlo Garofolo (Trieste, Italy), and stored in the freezer until use. Bovine serum albumin (BSA), Tween 20, hydrogen peroxide, hydroquinone (H_2Q) 99% and β-D-glucose were purchased from Sigma Aldrich. GOx labelled goat anti-human IgA (1 mg mL^{-1}) was purchased from Abcam (stored in the fridge until use). All the biochemical reagents were diluted using 10 mM phosphate buffer saline (PBS, pH 7.4), except the h-tTG that was diluted in carbonate-bicarbonate buffer (pH 9.2).

All other reagents were of analytical grade and used as received.

Purified water was obtained using a Milli-Ro plus Milli-Q (Millipore) water purification system.

2. 1. 2. Instrumentation

The scanning electron microscopy (SEM) analysis of the track-etch PC membrane and of the Au-NEEs were performed with a Hitachi TM3000 Tabletop Microscope.

Voltammetric measurements with NEEs were carried out at room temperature (20 ± 1°C), using a CH-660B potentiostat (CHIIJ Cambria Scientific, UK) controlled via personal computer by its own software, using a three electrodes single compartment cell equipped with NEE as working electrode, platinum spiral counter electrode and an Ag/AgCl in saturated KCl as reference electrode, to which all the potential values are referred.

To stir the biological solutions, an Advanced Vortex Mixer (Velp Scientifica 2x3, Vetrotecnica) was used.

2. 2. Methods

2. 2. 1. Electroless deposition

NEEs were prepared by electroless deposition of gold in track-etch polycarbonate membrane (30 nm pore diameter, SEM image in **Figure 2.1**) according to the procedure described by Menon and Martin, slightly modified by Ugo's group [103,106,115,152,153,154].

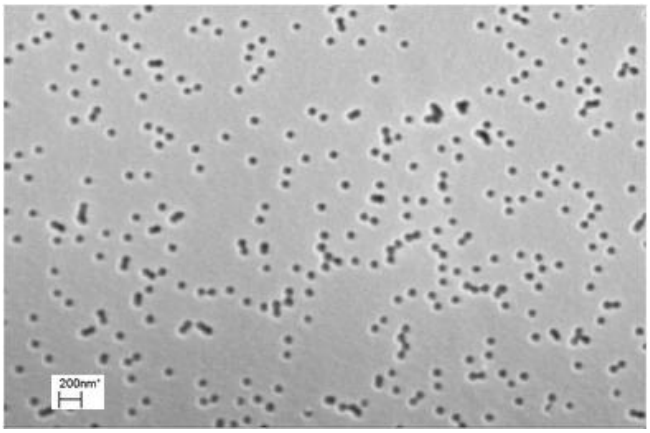

Figure 2.1. SEM image of a commercial track-etch polycarbonate membrane.

Track-etch PC membranes impregnated by the manufacturer with polyvinylpyrrolidone (PVP) were used, since this hydrophilic polymer gives to the membranes a better wettability and suitability for sensitizing with $SnCl_2$ [155].

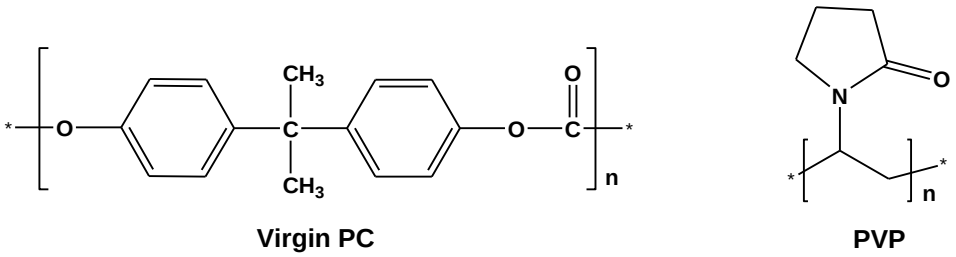

Figure 2. 2. Chemical structure of polycarbonate (on the left) and of PVP (on the right).

The electroless deposition was performed according to the following steps:

1. **Sensitization of the membrane**: after wetting the PC membrane in methanol for 2 hours, Sn^{2+} was applied as sensitizer, immersing the membrane in 0.026 M in $SnCl_2$ and 0.07 M trifluoroacetic acid in 1/1 methanol/water for 45 minutes. Sn^{2+} ions are complexed by the amine and carbonyl groups of the layer of PVP, so binding to the surfaces of the membrane;

2. **Activation of the membrane**: after rinsing three times for one minute in methanol, the sensitized membrane was activated immersing for 10 minutes in a 0.029 M ammoniacal-$AgNO_3$ solution ($Ag[(NH_3)_2]NO_3$). The

surface-bound Sn^{2+} ions reduce the Ag^{+} to elemental Ag. In this way the pore walls and membrane faces become coated with nanoscopic Ag particles:

$$Sn^{2+} + 2\,Ag^{+} \rightarrow Sn^{4+} + 2\,Ag^{0}$$

3. **Galvanic displacement**: after rinsing the Ag activated membrane two times in methanol and one time in water, the membrane was immersed in a diluted form of the commercial gold plating solution ($7.9 \cdot 10^{-3}$ M in $Na_3Au(SO_3)_2$ and 0.127 M in Na_2SO_3) for 24 hours maintaining the temperature between 0 and 2°C, in order to obtain the slow formation of the first gold nuclei on the pore walls and faces by galvanic displacement of the Ag particles by the more noble Au:

$$Au^{+} + Ag^{0} \rightarrow Au^{0} + Ag^{+}$$

4. **Catalytic reduction**: after 30 and 90 minutes, the slow addition of 1 mL of 0.625 M formaldehyde (a reducing agent) in the plating bath allowed a catalytic growth of the gold nuclei thanks to further gold deposition due to the reduction of Au(I) to Au(0):

$$2\,Au^{+} + HCOH + 3\,OH^{-} \rightarrow 2\,Au^{0} + HCOO^{-} + 2\,H_2O$$

The gold deposition was left to proceed for 23 hours at 4°C: as a result, the gold deposition continued into the membrane pores, and also on the outer surfaces of the membrane, that result covered by a thin Au film (Au/Au-PC-Au membrane, where Au-PC is the polycarbonate containing the gold nanowires).

The Au/Au-PC-Au membrane was then taken out from the bath, thoroughly rinsed with water and immersed in 25% nitric acid solution for 6 hours (in order to dissolve any residual Sn or Ag that might be left in the membrane), then rinsed thoroughly in water for 3 hours and again in water for 12 hours. The membrane was finally dried with clean air.

2. 2. 2. Fabrication of handy NEEs

To assemble the electrodes easy to handle to be used for the electrochemical measurements, the procedure described below was used [103,115,118].

The outer gold layer was removed from the smooth side of the Au/Au-PC/Au membrane by peeling it off by simply applying and then removing adhesive tape (Magic™ 3M) in order to expose the tips of the nanowires. A piece of copper adhesive tape (5 mm x 40 mm) with conductive glue (containing Ni particles) that acts as a current collector for the NEE was attached on a small non-conducting aluminium square (**Figure 2.4**). The lower Au-coated surface of a 5 x 6 mm piece of peeled membrane was placed partly on the copper tape, partly on the aluminium foil tape, so that only a small part was in contact with the copper tape (in fact the nichel particles can puncture the membrane, damaging the gold nanowires [103]).

Strips of non-conductive tape (heat-shrinkable adhesive polymer film, Topflite Monokote) were applied to the lower and upper sides of the assembly to insulate the aluminium and copper foil tapes. Before the attachment on the assembly, on the upper piece of Monokote a circular hole was punched with a diameter of 3 mm that defines the geometric area of the NEE. The hole should be carefully positioned on the part of membrane attached onto the aluminium tape: this prevents punctures in the region of the membrane that is exposed to the solution [103].

Once assembled, NEEs were heat-treated for 30 minutes at 153°C, that is slightly above the glass-transition temperature of the polycarbonate, in order to promote the tight sealing between the gold nanowires and the pore walls of polycarbonate.

Figure 2.3 shows the main steps of the fabrication of Au-NEEs using track-etch PC membrane as template.

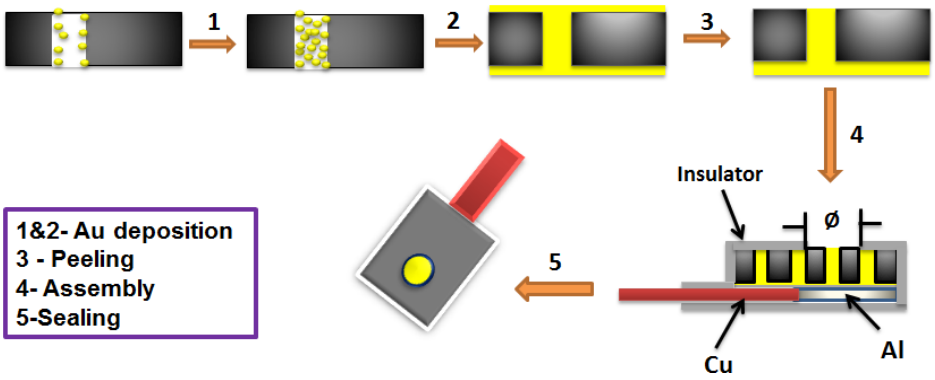

Figure 2.3. Main steps (gold deposition, peeling, assembly and sealing) of manufacturing Au-NEEs using track-etch PC membrane as template [151].

From each membrane about 50 Au-NEEs were prepared, 70% of which showed to have electrochemical properties suitable for the development of biosensors.

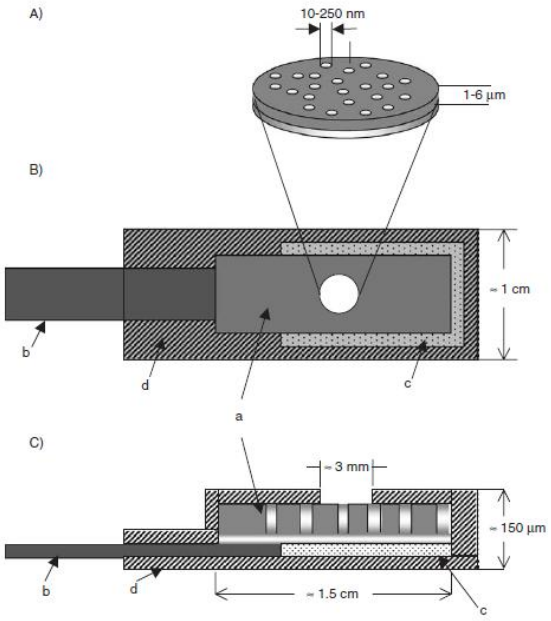

Figure 2.4. Scheme of an Au-NEE prepared using a track-etch polycarbonate membrane as template. A. Particular of the section of the active area. B. Top view. C. Section of the all NEE ready for use as working electrode. (a) track-etch golden membrane; (b) copper adhesive tape with conductive glue to connect to instrumentation; (c) aluminium adhesive foil with non-conductive glue; (d) insulating tape. *Note*: Some dimensions are only indicative and not in scale [115].

2. 2. 3. Preparation of NEE-based anti-tTG immunosensors

The procedure used for the preparation of the immunosensor for the detection of IgG and IgA isotypes of anti-tTG is similar to the one used by Habtamu [151]. The immobilization of the human tissue transglutaminase (h-tTG) was performed adapting the procedure described by Pozzi Mucelli et al. for Trastuzumab [102,155]. In particular, after washing the NEE with distilled water and drying with air, a microvolume of 20 µL of the capture antigen, namely, recombinant tTG solution diluted in carbonate-bicarbonate buffer pH 9.2 (final concentration 20 µg mL^{-1}) was put on the geometric area of the NEE, and incubated for 2 hours. Hereafter, the NEE functionalized with tTG will be named tTG-NEE.

After washing with 10 mM PBS and drying, the tTG-NEE was incubated with bovine serum albumin (BSA) solution (1% or 3%) in 10 mM PBS for 30 minutes, putting a drop of 20 µL of solution on the geometric area to block the empty sites still present on the electrode surface, in order to minimize non-specific adsorptions. The BSA solution was stored in a refrigerator for three days and then discarded.

After washing with 10 mM PBS and drying, the blocked tTG-NEE was incubated for 1 hour with the standardized serum sample, dropping 20 µL of serum sample properly diluted in 10 mM PBS.

After washing with 0.05% Tween 20, then with 10 mM PBS and drying gently with air, the NEE was finally incubated with a drop of 20 µL of the anti-human enzyme-labelled secondary antibody (Sec-Ab). Note that in the case of the detection of the IgG isotype, a goat anti-human HRP-labelled Sec-Ab against immunoglobulin IgG (anti IgG-HRP) solution was used (10 µg mL^{-1}); incubation was carried out for one hour. For simplicity, hereafter we will call the obtained immunosensor IgG-NEE. Instead, in the case of the detection of the IgA isotype, a goat anti-human GOx-labelled Sec-Ab against immunoglobulin IgA (anti IgA-GOx) was used (20 µg mL^{-1}), and the incubation was carried out for 30 minutes. For simplicity, hereafter we will call the obtained immunosensor IgA-NEE.

All the instrumentation used to carry out the biological experiments was previously cleaned with ethanol, and all the biological solutions were stirred for one minute before dilution and before incubation. All the incubation steps were carried out at room temperature (20 ± 1°C) placing the NEE into a covered Petri dish together with a piece of filter paper moistured with 10 mM PBS in order to saturate the environment, avoiding the evaporation of the biological solution drop.

2. 2. 4. Electrochemical detection

After washing with 10 mM PBS, the IgG-NEE or IgA-NEE was dipped in an electrochemical cell containing the redox mediator: cyclic voltammograms were recorded before and after the addition of the enzyme substrate.

In particular, for the detection of the IgG anti-tTG isotype, the immunosensor incubated with the anti IgG-HRP was used. In the cell 1 mM H_2Q was added as redox mediator and hydrogen peroxide as substrate for HRP. In order to avoid oxidation to benzoquinone by light and atmospheric oxygen, the hydroquinone solution was prepared in 50 mM sodium phosphate buffer (pH 7.4) in an amber glass bottle under nitrogen, and the electrochemical measurements were performed after de-aerating the electrolyte solution with nitrogen. Cyclic voltammograms were recorded at room temperature (20 ± 1°C) before and after addition of 1.5 mM H_2O_2 between -0.65 and +0.85 V at 50 mV s^{-1}. The measurements were carried out by three segment cyclic voltammetry with an initial scan from 0 to +0.85 V, reversed to -0.65 V and finally back to 0, at a scan rate of 50 mV s^{-1}.

For the detection of the IgA anti-tTG isotype, the immunosensor incubated with anti IgA-GOx was used; in this case, in 10 mM PBS solution, 0.1 mM $FAPF_6$ was used as redox mediator, and glucose as substrate for glucose oxidase. Cyclic voltammograms were recorded at room temperature (20 ± 1°C) before and after addition of 0.1 M glucose, between 0.1 and 0.8 V at 50 mV s^{-1}. The glucose solution was prepared freshly and stored overnight before use.

Negative controls were performed in the absence of anti-tissue transglutaminase, that is performing the all procedure as described above, apart the incubation step with the serum sample.

2. 2. 5. FEIA analysis

Fluoroenzyme immunoassay (FEIA) for anti-tTG antibodies was performed by the group of Prof. Tarcisio Not, IRCCS Burlo Garofolo, using the Elia™ Celikey, Phadia 250 kit (Thermo Scientific) following the provider instructions. Since there are no international standards for anti-tTG antibodies, results are given in arbitrary EliA Units mL^{-1}. These values were obtained using suitable calibration standards. The ranges both for the IgG and IgA isotype of anti-tTG are given in the Table below, expressed as range for negative, equivocal and positive.

Test	Unit	negative	equivocal	positive
EliA Celikey	EliA U mL^{-1}	< 7	7 - 10	> 10

The IgG and IgA anti-tTG concentration determined with the proposed NEE-based immunosensors is expressed using the same units, since data obtained with the electrochemical immunosensor were calibrated on the basis of FEIA standardized serum samples.

Chapter 3
Results and discussion

3. 1. NEEs characterization

3. 1. 1. Experimental measurement of the active area

In order to measure experimentally the active area of the prepared NEEs, cyclic voltammograms were recorded at different scan rates in a blank solution containing pure supporting electrolyte (**Figure 3.1**).

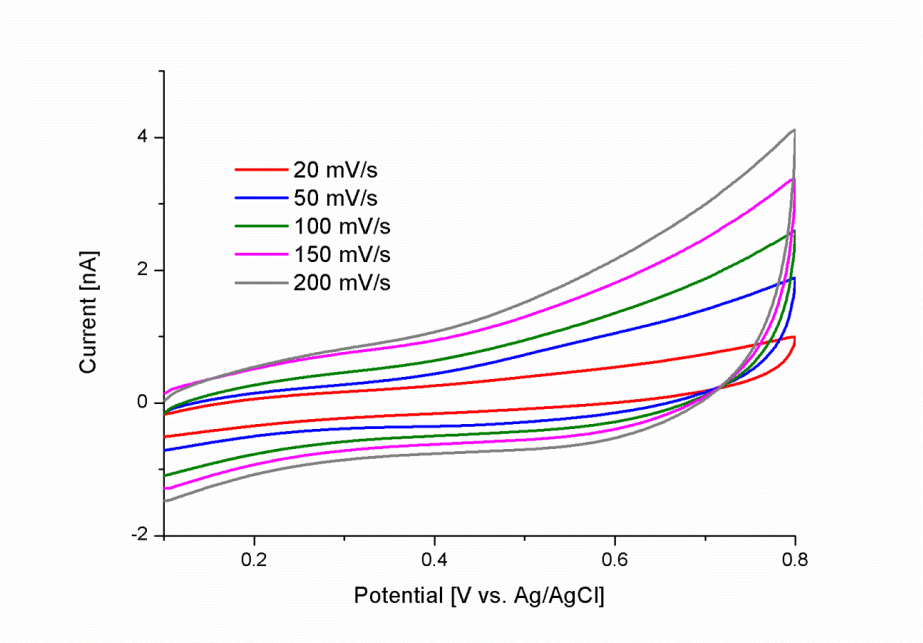

Figure 3.1. Cyclic voltammograms recorded at a bare Au-NEE in 5 mM KNO_3 at different scan rates (20, 50, 100, 150 and 200 mV s^{-1}).

The capacitive current was calculated as half the sum of the forward and the backward background current (see **Figure 3.2** for measurement scheme), measured from the CVs in **Figure 3. 1** at the potential of 0.4 V, according to **Equation 3.1**.

$$i_c = \frac{i_{forward} + i_{backward}}{2} \qquad (3.1)$$

where:

- $i_{forward}$ is the current measured in the forward scan at 0.4 V;

- $i_{backward}$ is the current measured in the reverse scan at 0.4 V.

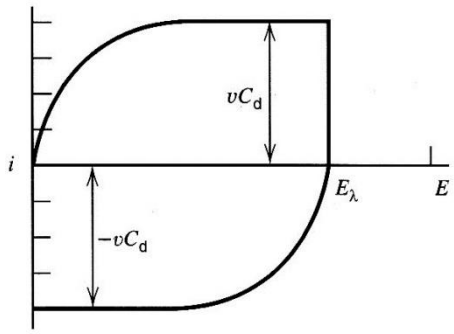

Figure 3.2. Schematic representation of the capacitive current [156].

As shown in **Figure 3.3**, at our NEEs the capacitive current increases linearly with the scan rate.

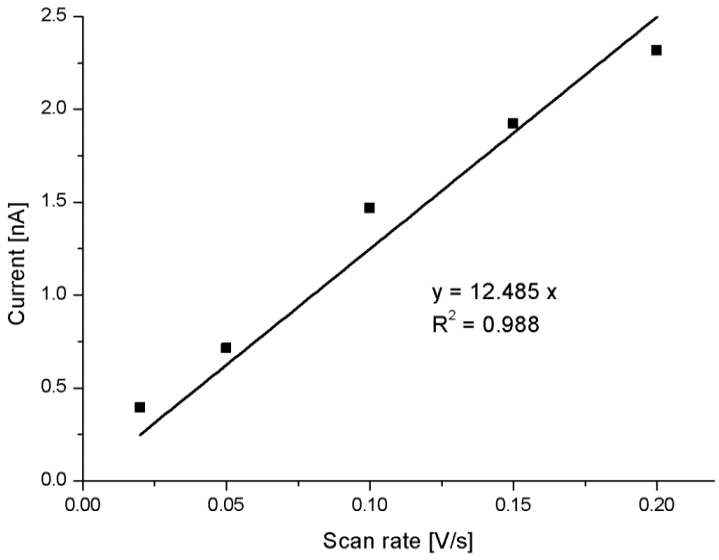

Figure 3.3. Plot of the dependence of capacitive current, measured at 0.4 V, on scan rate.

This agrees with **Equation 3.2**.

$$i_c = \nu \cdot C_{dl} \cdot A_{act} \qquad \textbf{(3.2)}$$

where:

- $\boldsymbol{\nu}$ is the scan rate [V s^{-1}];
- C_{dl} is the double layer capacitance of the gold nanodisks of the NEE, that is 21 µF cm^{-2} [103];
- A_{act} is the active area [cm^2].

Therefore, the value of the experimental active area can be calculated dividing the slope value by the double layer capacitance of the gold nanodisks (**Equation 3.3**).

$$A_{act} = \frac{slope}{C_{dl}} = \frac{12.485 \cdot 10^{-9} A\ V^{-1}\ s}{21 \cdot 10^{-6}\ F\ cm^{-2}} = 5.945 \cdot 10^{-4}\ cm^{-2} \qquad \textbf{(3.3)}$$

The theoretical active area (area of the gold nanodisk electrodes) can be calculated according to **Equation 3.4**:

$$A_{act} = \pi r^2 \cdot \mathrm{p} \cdot \mathrm{A_{geom}} = \pi(15 \cdot 10^{-7}\mathrm{cm})^2 \cdot 6 \cdot 10^8 \mathrm{cm}^{-2} \cdot 0.07\ \mathrm{cm}^2 = 2.97 \cdot 10^{-4}\ \mathrm{cm}^2 \qquad \textbf{(3.4)}$$

where:

- πr^2 is the area of one track-etch pore in the polycarbonate membrane (radius of 15 nm);
- p is the pore density, that is $6 \cdot 10^8$ nanodisks cm^{-2};
- A_{geom} is the geometric area, that is 0.07 cm^2.

Both r and p are the values for the pores reported by the provider of the track-etch PC membranes (SPI-pore), that we assume to correspond to r and p values for the gold nanodisk electrodes.

The value of the experimental active area is indeed close to the theoretical value calculated for the pores, so confirming that the gold deposition occurred successfully and in a controlled way.

3. 1. 2. Evaluation of electrochemical parameters

The electrochemical reversibility was evaluated by calculating voltammetric parameters such as peak-to-peak separation, current ratio and half-peak potential ($E_{1/2}$) testing each NEE in an electrolyte solution containing (ferrocenylmethyl)trimethylammonium hexafluorophosphate ($FAPF_6$) as electroactive probe (chemical structure in **Figure 3.4**).

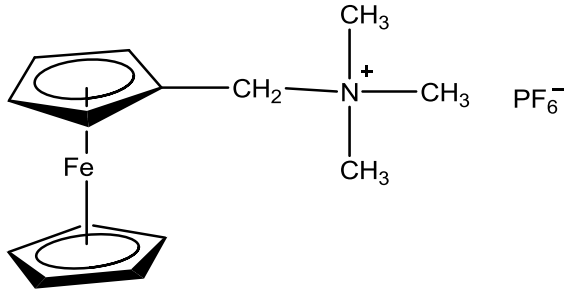

Figure 3.4: Chemical structure of $FAPF_6$.

This redox probe undergoes a well-known one electron reversible oxidation at electrode surfaces which corresponds to the oxidation of the Fe(II) to Fe(III) [103,105,115,121].

$$FA^{+} \rightleftarrows FA^{2+} + e^{-} \qquad E_{\frac{1}{2}} = 0.44 \text{ [103]} \quad (\mathbf{3.5})$$

Figure 3.5 reports a typical cyclic voltammogram recorded at a bare NEE in a solution containing 0.1 mM FA^{+}. As shown by data reported **in Figure 3.6** and **Figure 3.7** (see Paragraph 3. 1. 3), faradaic peak currents scale linearly with the square root of the scan rate. This evidence confirms that our NEEs operate in the "total-overlap" response regime, giving well resolved shaped patterns.

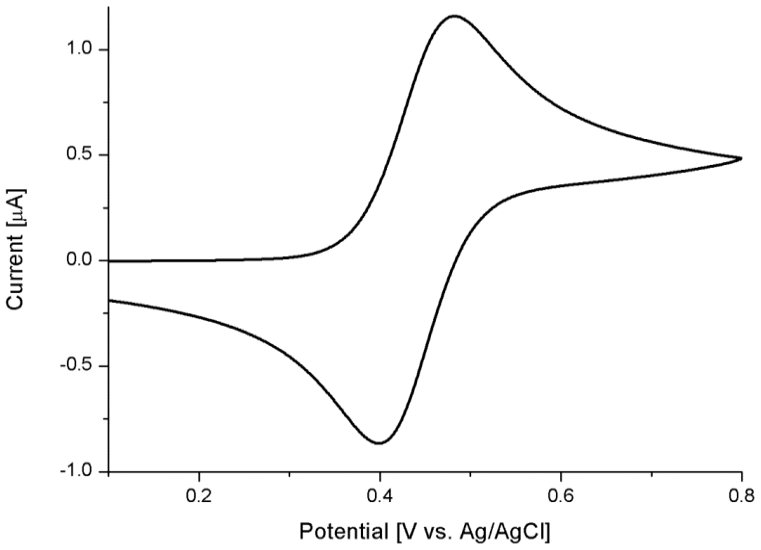

Figure 3.5. Cyclic voltammogram recorded at a bare NEE in a 5 mM KNO_3 and 0.1 mM FA^+ solution. Scan rate 50 mV s^{-1}.

For the preparation of the nanobiosensors, NEEs with the best reversibility parameters (that are those with a peak-to-peak separation between 60 and 75 mV, half-peak potential of about 0.44 and peak current ratio of about 1) were used.

3. 1. 3. Experimental measurement of the geometric area

The geometric area of the NEE can be calculated by analysing the scan rate dependence of the CVs (see **Figure 3.6** and **Figure 3.7**).

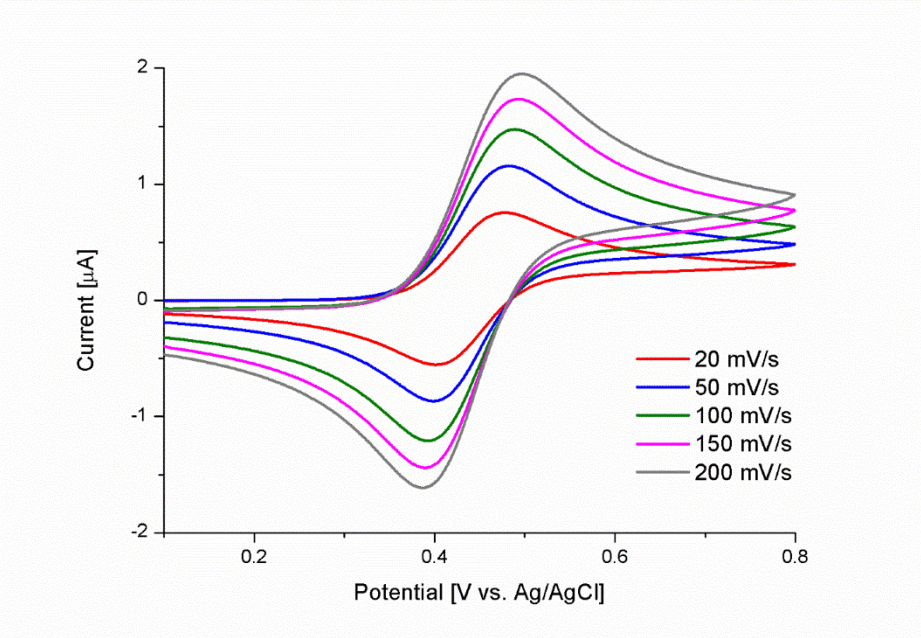

Figure 3.6. Cyclic voltammograms recorded at a bare Au-NEE in 5 mM KNO_3 solution containing 0.1 mM $FAPF_6$ at different scan rates (20, 50, 100, 150 and 200 mV s^{-1}).

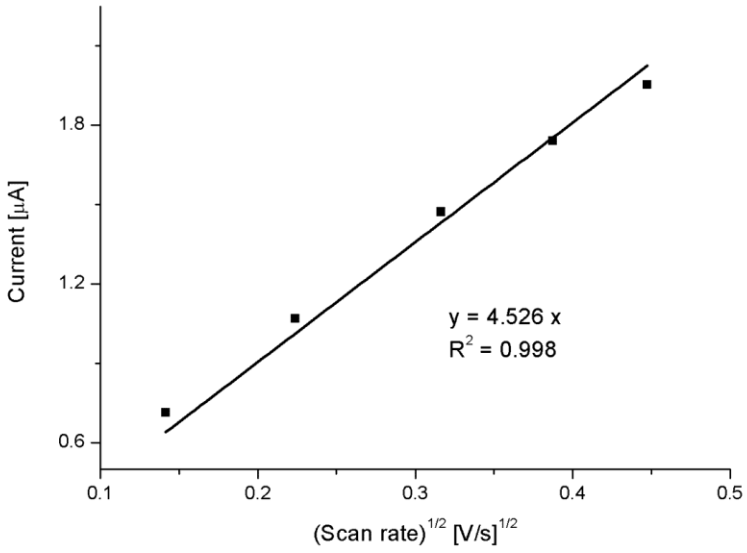

Figure 3.7. Plot of the dependence of faradaic peak current on square root of scan rate.

The evidence that the faradaic peak current (i_p) depends linearly on $\nu^{1/2}$, indicates that the NEE operates in the total overlap response regime, and consequently i_p obeys the Randles-Sevcik equation (**Equation 3.6**):

$$i_p = 2.69 \cdot 10^5 \cdot n^{3/2} \cdot A_{geom} \cdot D^{1/2} \cdot C^* \cdot \nu^{1/2} \qquad (\mathbf{3.6})$$

where:

- i_p is the faradaic peak current [A];
- n is the number of transferred electron, that for the $FAPF_6$ is one;
- A_{geom} is the geometric area [cm^2];
- D is the diffusion coefficient of the $FAPF_6$, that is $(4\pm1)\cdot10^{-6}$ cm^2 s^{-1} [103];
- C^* is $FAPF_6$ bulk concentration [mol cm^{-3}];
- $\boldsymbol{\nu}$ is the scan rate [V s^{-1}].

Knowing the slope value from plot in Figure 3.7, it is possible to calculate the value of the experimental geometric area of the NEE from **Equation 3.7**:

$$A_{geom} = \frac{slope}{2.69 \cdot 10^5 \cdot n^{3/2} \cdot D^{1/2} \cdot C^*} = 0.084\ cm^2 \qquad (\mathbf{3.7})$$

The theoretical geometric area is equal to the area of the hole punched in the insulating layer of monokote, that has a diameter of 3 mm (**Equation 3.8**).

$$A_{geom} = \pi(0.15\ cm)^2 = 0.071\ cm^2 \qquad (\mathbf{3.8})$$

Taking into account the uncertainty in the D value used for the calculation, the experimental and theoretical values result in satisfactory agreement.

From the above A_{geom} and A_{act} values we can calculate the fractional electrode area (f), according to **Equation 3.9**.

$$f = \frac{A_{act}}{A_{geom}} = \frac{5.94 \cdot 10^{-4}}{0.084} = 7.071 \cdot 10^{-3} \qquad (\mathbf{3.9})$$

3. 1. 4. Characterization by SEM imaging

To image the surface of the NEE after removal of the Au surface layer, scanning electron microscopy (SEM) can be used, since it allows to evaluate if the pores of the polycarbonate membrane have been filled by gold, so obtaining a good ensemble of nanowire electrodes surrounded by PC.

Figure 3.8 shows a SEM image of part of the surface of a NEE, in which is possible to distinguish the polycarbonate membrane (dark) from the metallic gold nanowires (white spots and lines). The bright spots correspond to the heads of the gold nanowires, whereas the fading lines represent the gold nanowires grown in the pores; it is possible to image the nanowires grown inside the membrane because of the partial transparency of the polycarbonate under the electron beam [152]. It is observed that the nanowires are oriented with different angular distribution as a consequence of the different orientation of the pores in the track-etch PC membranes (due to the industrial tracking process).

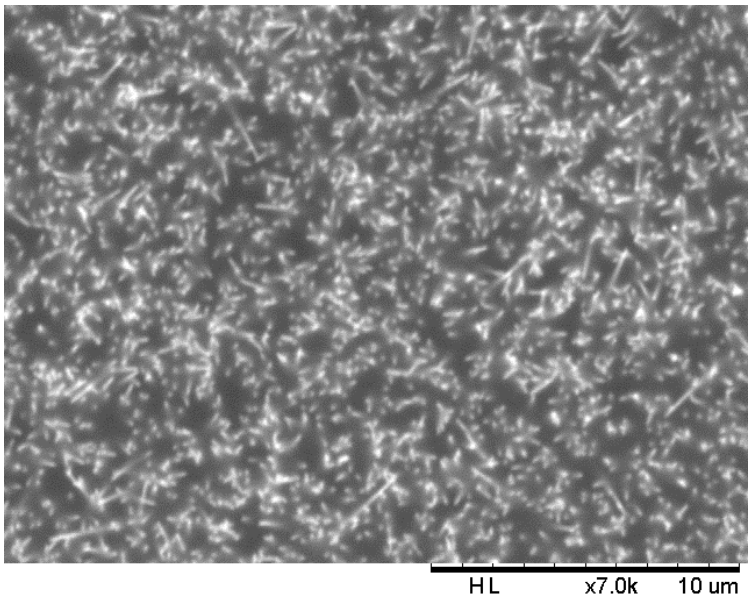

Figure 3.8. SEM image of a section of NEE.

The average diameter of the Au nanodisks of the NEE estimated by the SEM is 40±10 nm. This value is close to average nominal diameter of the pores of the

track-etch polycarbonate membrane used for the gold electroless deposition reported by the manufacturer (30 nm). Since the density of Au nanoelectrodes in the NEE is about $6 \cdot 10^8$ per cm^2, if we suppose that each nanopore of the polycarbonate membrane is filled with gold, a NEE with a geometric area of 0.084 cm^2 contains about 50 million nanoelectrodes.

3. 2. Thermal curing of NEEs

The solution creeping into the junctions between the conductive nanoelectrode elements and the polycarbonate host membrane is undesirable because it increases the double layer charging current [113,157].

Menon and Martin demonstrated that heating the NEEs above the glass transition temperature of the polycarbonate (about 150°C), the PC membrane shrinks, with the consequent sealing between the gold nanowires and the pore wall of the insulator [103].

On this basis, we tested the effect of thermal curing on the electrochemical properties of our NEEs. In particular, we examined the effect of the time of the heating treatment on the double-layer capacitive current and on the faradaic current. To this aim, the same NEE has been heat-treated at 153°C for different time frames: 15, 30, 45, 60 and 75 minutes.

Figure 3.9 shows the overlay of the CVs recorded at a bare NEE in pure supporting electrolyte solution after different heating time, whereas **Figure 3.10** reports the plot of the capacitive current as function of the heating time. It is evident that the capacitive current drastically decreases when increasing the heating time from 15 to 30 minutes, whereas heat-treatment for more than 30 minutes does not cause any further significant decrease.

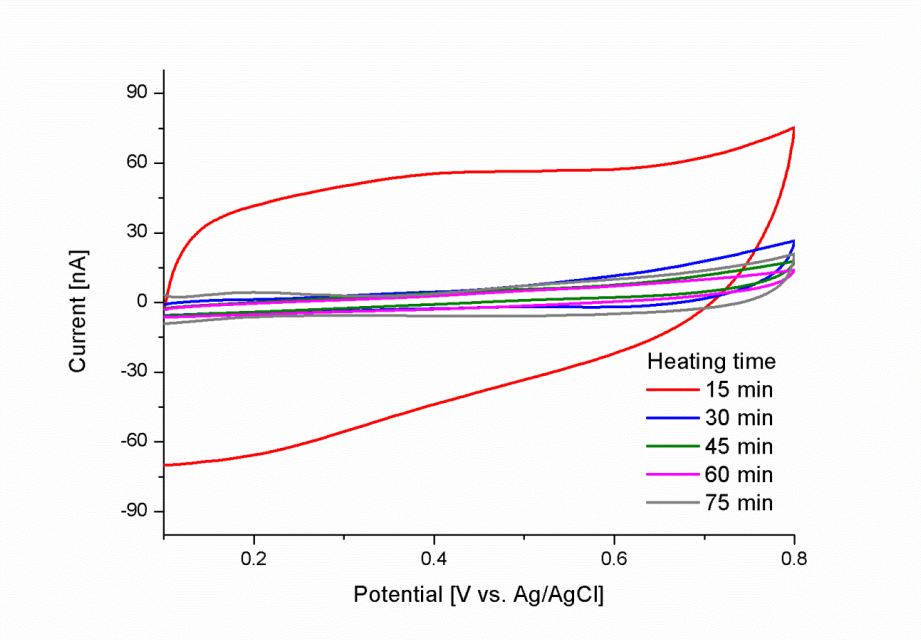

Figure 3.9. Cyclic voltammograms recorded at a bare NEE in 5 mM KNO_3 after thermal treatment at 153°C for different time frames (15, 30, 45, 60 and 75 minutes). Scan rate 50 mV s^{-1}.

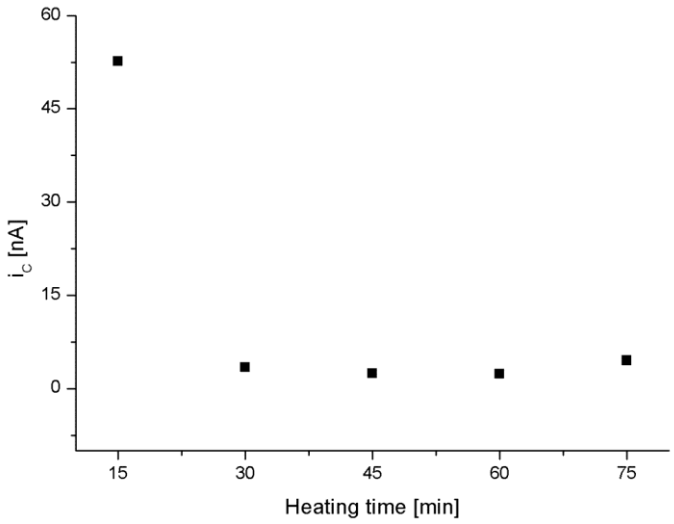

Figure 3.10. Plot of the capacitive current as function of the heating time.

It is worth noting that heat-treating the NEE for more than one hour causes an increase of the capacitive current (see **Figure 3.10**), probably related to a damage of the NEE surface.

Figure 3.11 shows the CVs recorded at a bare NEE in a supporting electrolyte solution containing FA^+ after different heating time. The faradaic peak current slightly decreases increasing the heating-time from 15 to 45 minutes, whereas after 45 minutes of heating treatment, i_f drastically decreases.

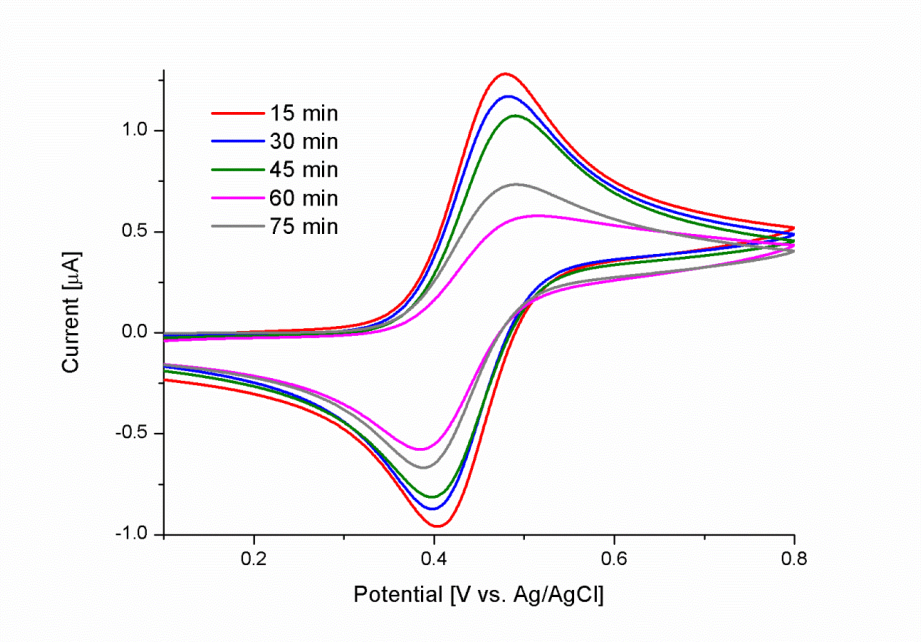

Figure 3.11. Overlay of the CVs recorded at a bare NEE in 5 mM KNO_3 and 0.1 mM FA^+ after different heating time (15, 30, 45, 60 and 75 minutes) at 153°C. Scan rate 50 mV s^{-1}.

Table 3.1 reports the values of the capacitive current and of the faradaic anodic peak current recorded at a bare NEE after heat-treatment at 153°C for different time frames, as well as the faradaic-to-capacitive current ratio.

Table 3.1. Capacitive and faradaic current values and faradaic-to-capacitive current ratio at a NEE heat-treated for different time frames. All the measurement had been taken as triplicate, and are reported as average value ± standard deviation.

Heating time [min]	Capacitive current [nA]	Faradaic current [µA]	i_f/i_c
15	52.675 ± 0.8	1.220 ± 0.007	23.167
30	3.440 ± 0.4	1.130 ± 0.02	328.472
45	2.421 ± 0.3	1.074 ± 0.007	443.417

Heating time [min]	Capacitive current [nA]	Faradaic current [µA]	i_f/i_c
60	2.374 ± 0.9	0.539 ± 0.02	227.121
75	4.492 ± 0.5	0.739 ± 0.01	164.633

On the basis of the obtained results, the more convenient heating time, which gives the higher faradaic-to-capacitive current ratio, is between 30 and 45 minutes.

3. 3. NEE-based immunosensor for IgG anti-tTG

.

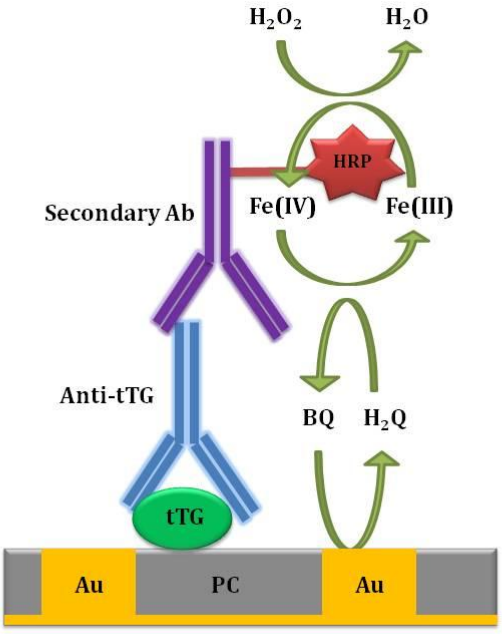

Figure 3.12. Schematic illustration of the immunosensor architecture for the detection of IgG anti-tTG and the associated enzymatic and electrochemical process. After immobilization of the capture antigen (tissue transglutaminase) on the electrode surface, the obtained sensor is incubated with anti-tissue transglutaminase (in standardized serum samples). The detection of the antigen-antibody complex is achieved by incubating the sensor with secondary antibodies anti-IgG labelled with HRP. After adding hydrogen peroxide (the substrate) and hydroquinone as suitable redox mediator, an enzymatic reaction occurs, enabling the detection of the analyte by cyclic voltammetric measurements. Components are not in scale.

The scheme of the immunosensor developed for the detection of the IgG isotype of anti-tTG is reported in **Figure 3.12**. Relevant components are indicated in the caption. The detailed description of the preparation of the sensor is in the Experimental Section.

3. 3. 1. Voltammetric behaviour of hydroquinone at NEEs

A redox mediator suitable to exchange electrons between the nanoelectrode surface and HRP label is hydroquinone [145,158-161]. For this reason, at first we examined the CV behaviour of this redox mediator, as described below.

The cyclic voltammetric behaviour of hydroquinone at a gold NEE has been studied by Habtamu [151]: NEEs in the presence of hydroquinone show an electrochemical behaviour similar to the one observed at chemically modified macroelectrodes [159,162], since NEEs behave as electrode with partially blocked surface [103,104,163]. The solid line in **Figure 3.13** shows the cyclic voltammetric behaviour of 1 mM hydroquinone at a bare NEE.

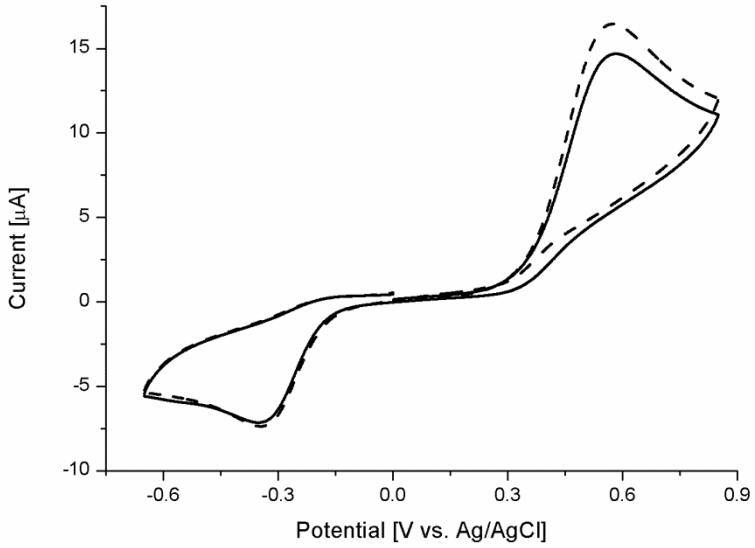

Figure 3.13. Cyclic voltammograms recorded at a bare NEE in 50 mM PB (pH 7.4) containing 1 mM hydroquinone before (solid line) and after (dashed line) addiction of 1.5 mM H_2O_2. Scan rate 50 mV s^{-1}.

The CV is characterized by two well defined peaks, one detected in the anodic and the other in the cathodic portion of scan. The peak-to-peak separation is rather large, being equal to 0.93 V. The comparison with previous studies [158-161,162,164-167] together with the above evidences allow us to attribute the signals to the two electrons/two protons electrochemical oxidation of hydroquinone (H_2Q) to benzoquinone (BQ) (see **Figure 3.14**), which occurs under quasi-reversible conditions. The wide peak-to-peak separation is due to the quasi-reversible character of the electron transfer as well as to the role of the deprotonation (oxidation)/protonation (reduction) reactions associated to the electron transfer.

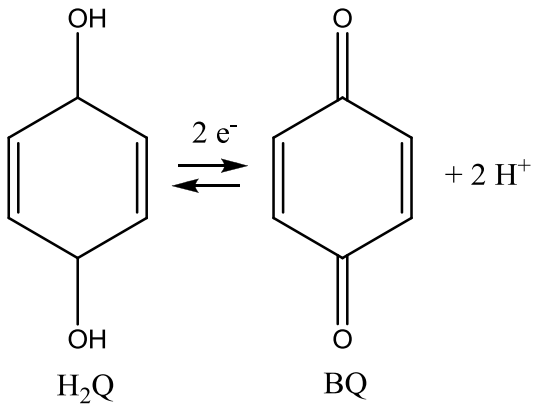

Figure 3.14. Oxidation of hydroquinone to benzoquinone.

Since the electrochemical process involves exchanges of protons, the peak potential will depend also on the pH of the electrolyte [165]: in order to keep the pH constant, all the electrochemical measurements are carried out in buffer solution (pH 7.4).

The dashed line CV in **Figure 3.13**, recorded in the presence of 1.5 mM H_2O_2, confirms that the presence of hydrogen peroxide does not significantly alter the cyclic voltammetric pattern of hydroquinone, that indicates that H_2O_2 does no react directly with hydroquinone [161].

3. 3. 2. Detection of IgG anti-tTG antibodies

Figure 3.15 compares the cyclic voltammograms recorded at a bare NEE (dashed line) and at the same NEE after the treatment (solid line) with the procedure described in the Experimental Section (incubation with tTG, BSA, serum sample with concentration of 1.44 u mL^{-1} and IgG secondary antibody-HRP labelled) in a 50 mM PB solution containing 1 mM H_2Q (note that the latter CVs are recorded in the absence of H_2O_2). The cyclic voltammetric behaviour of hydroquinone after the functionalization is comparable to the one observed before the functionalization, apart a broadening of the peak. This confirms that the attachment of biomolecules does not interfere significantly with the electrochemical behaviour of hydroquinone. This suggests that the biomolecules are bound mainly on the polycarbonate membrane of the NEE, and not on the gold nanoelectrodes. Indeed, the functionalization procedure dose not hinder significantly the electron transfer between the redox mediator and the electrode surface [102,150].

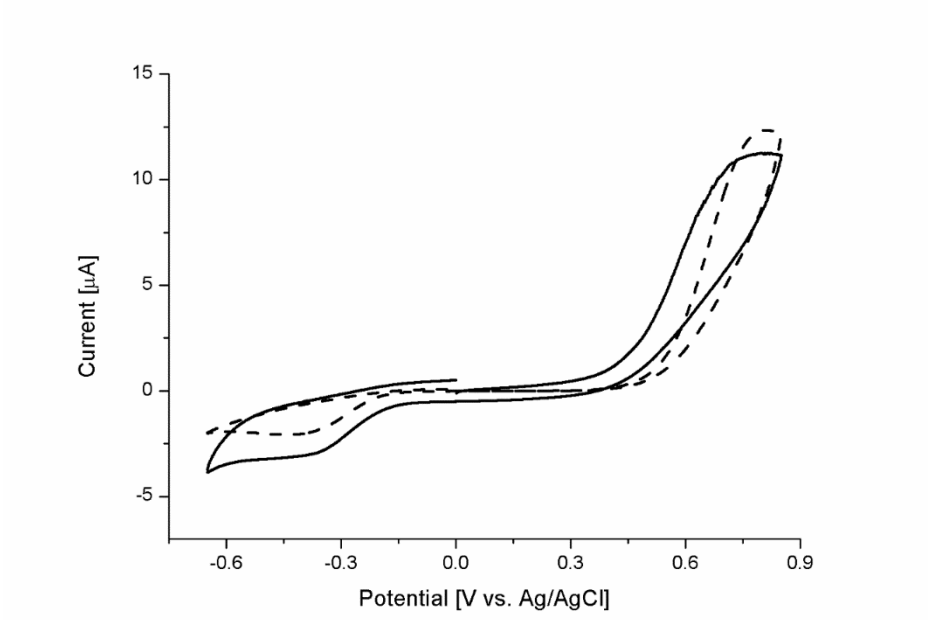

Figure 3.15. Cyclic voltammograms recorded at a bare NEE (dashed line) and at the same NEE after the complete functionalization procedure (solid line) in 50 mM PB containing 1 mM hydroquinone. Scan rate 50 mV s^{-1}.

Figure 3.16 compares the cyclic voltammograms recorded at a tTG-NEE after incubation with anti-tTG (1.44 u mL^{-1}) and anti IgG-HRP in 1 mM hydroquinone in 50 mM PB in the absence (dashed line) and in the presence (solid line) of 1.5 mM hydrogen peroxide. It is evident that in the presence of hydrogen peroxide the anodic peak at 0.75 V almost completely disappears whereas the cathodic peak at -0.4 V increases.

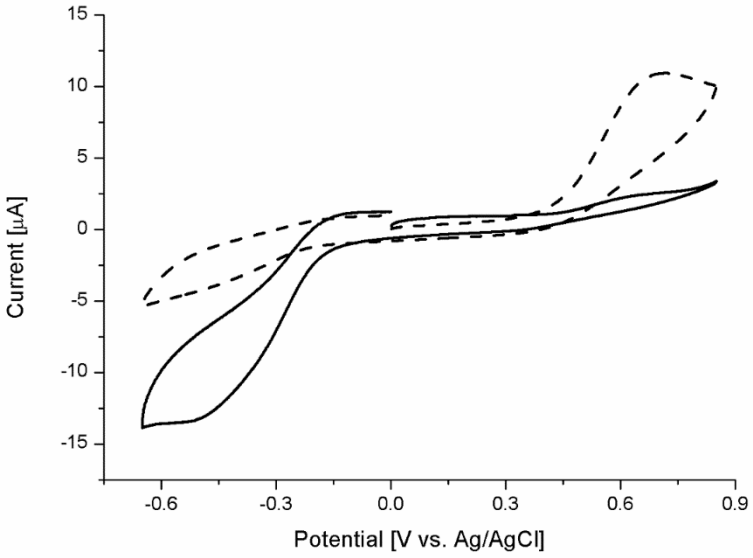

Figure 3.16. Cyclic voltammograms recorded at a NEE after the complete functionalization procedure in 50 mM PB containing 1 mM hydroquinone in the absence (dashed line) and in the presence of 1.5 mM hydrogen peroxide (solid line). Scan rate 50 mV s^{-1}.

The increase of the reduction peak and the disappearance of the re-oxidation peak agree with the occurrence of an electrocatalytic process mediated by the horseradish peroxidise. The process involves three different steps.

$$HRP(Fe^{3+}) + H_2O_2 \rightarrow HRP(Fe^{4+}=0) + H_2O \quad \textbf{(i)}$$

$$HRP(Fe^{4+}=O) + H_2Q \rightarrow HRP(Fe^{3+}) + BQ + H_2O \quad \textbf{(ii)}$$

$$BQ + 2\,H^+ + 2\,e^- \rightarrow H_2Q \quad \textbf{(iii)}$$

where:

- HRP(Fe^{3+}) is the reduced form of the HRP;
- HRP(Fe^{4+}=0) is the oxidized form of HRP (ferryloxy-HRP).

The horseradish peroxidase converts hydrogen peroxide (substrate) to water, with the contemporary oxidation of its Fe^{3+} active center to ferryloxy Fe^{4+}=O [160,161,168] (**reaction i**).

The ferryloxy-HRP specie is chemically reduced to regenerate the original form of the enzyme by the hydroquinone, which is concomitantly oxidized to benzoquinone with the formation of water (**reaction ii**). This is the reason for the disappearance of the anodic peak: the hydroquinone is oxidized to benzoquinone no more electrochemically, but chemically as a consequence of the presence of HPR and its substrate, so that BQ concentration is locally increased.

Benzoquinone is indeed electrochemically reduced back to H_2Q at the surface of the electrode (**reaction iii**): this reflects in the increase of the cathodic current (recorded at about -0.5 V).

The combination of these three reaction gives a complete electrocatalytic cycle.

The formation of benzoquinone is a consequence of the enzymatic reaction driven by the horseradish peroxidase in the presence of its substrate (where the enzyme concentration depends on the quantity of the captured IgG anti-tissue transglutaminase). Therefore, the increase of the cathodic peak is expected to finally scale with the amount of IgG anti-tTG present in the serum sample, which binds the anti IgG-HRP.

This holds when the enzyme substrate (H_2O_2) concentration and the redox mediator (H_2Q) are in excess, in order to have a catalytic process limited by the concentration of the enzyme (horseradish peroxidase).

3. 3. 3. Evaluation of aspecific bindings

Figure 3.17 reports the cyclic voltammograms recorded at a tTG-NEE blocked with 1% BSA and incubated with anti IgG-HRP in H_2Q solution before (dashed line) and after (solid line) the addition of hydrogen peroxide. It is worth stressing that this test was performed in the absence of anti-tTG. Since the voltammetric pattern after the addition of the enzyme substrate does not significantly change (there is no decrease of the anodic peak current neither the appearance of an electrocatalytic peak during the reverse scan), therefore the blocking step with 1% BSA effectively prevents the aspecific binding of the secondary antibody on the surface of the NEE.

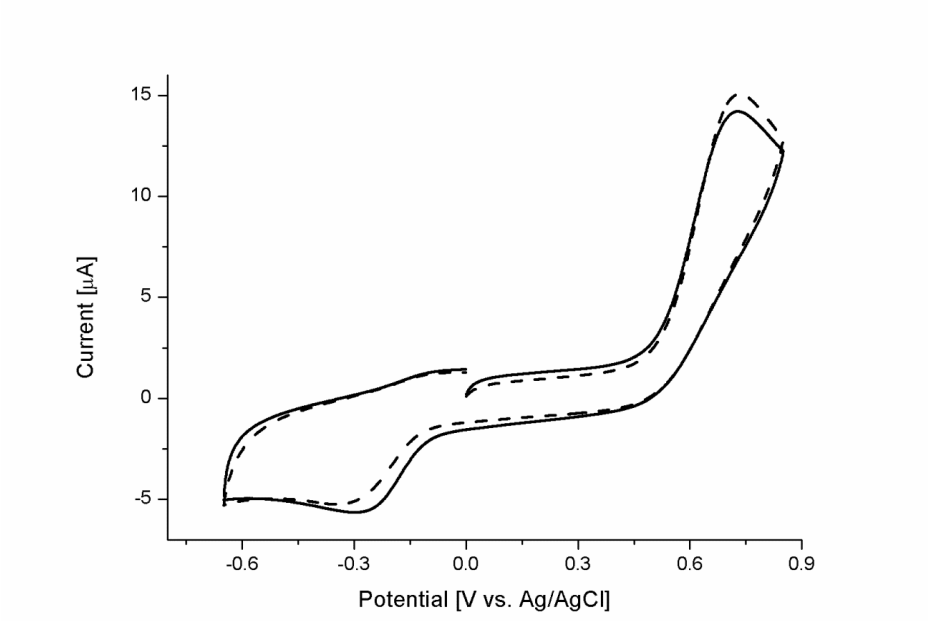

Figure 3.17. CVs recorded at a NEE functionalized with tTG, 1% BSA and anti IgG-HRP in 50 mM PB (pH 7.4) containing 1 mM H_2Q before (dashed line) and after the addition of 1.5 mM H_2O_2 (solid line). Scan rate 50 mV s^{-1}.

3. 3. 4. Quantitative analysis of IgG anti-tTG

In this work, a calibration curve was developed using human standardized serum samples supplied by IRCCS Materno Infantile Burlo Garofolo (Trieste, Italy). These samples contain known concentration of anti-tTG (both in the IgG and IgA isotypes), determined by fluorescent enzyme immunoassay (FEIA) in Burlo Garofolo. Our experiments were performed by functionalizing different NEEs with tTG, BSA, human standardized serum sample and anti IgG-HRP, as described in Experimental Section. Different concentrations of the target analyte (anti-tTG) were obtained by suitable dilution of the standardized sample in PBS. This procedure was adapted because no standard for human anti-tTG is commercially available. Measurements were performed in triplicate at each of the seven dilution of the standardized serum sample.

Figure 3.18 shows the dependence of the electrocatalytic current increment at the immunonosensor on the concentration of IgG anti-tTG in the standardized serum sample in the concentration range between 0.72 and 28.8 u mL^{-1}.

The electrocatalytic increment (i_{net}) was calculated as the absolute value of the difference between the cathodic peak current of hydroquinone in the absence of H_2O_2 and of the electrocatalytic current in the presence of 1.5 mM H_2O_2 at a potential of -0.5 V (**Equation 3.10**):

$$i_{net} = \left| i(H_2Q) - i(H_2Q)_{\,with\ H_2O_2} \right| \qquad \textbf{(3.10)}$$

where:

- $i(H_2Q)$ is the cathodic peak current of H_2Q in the absence of H_2O_2;
- $i(H_2Q)_{\,with\ H_2O_2}$ is the cathodic peak current of H_2Q in the presence of H_2O_2.

The value of the current increment measured at -0.5 V scales linearly with the concentration of IgG anti-tTG in the 0.72 - 7.2 u mL^{-1} range. For concentration > 7 u mL^{-1} (in particular, 7.2, 14.4 and 28.8 u mL^{-1}) the plot acquires an asymptotic profile. This means that it is no possible to quantify the analyte concentration by this plot for anti-tTG $\gtrsim$ 7 u mL^{-1}.

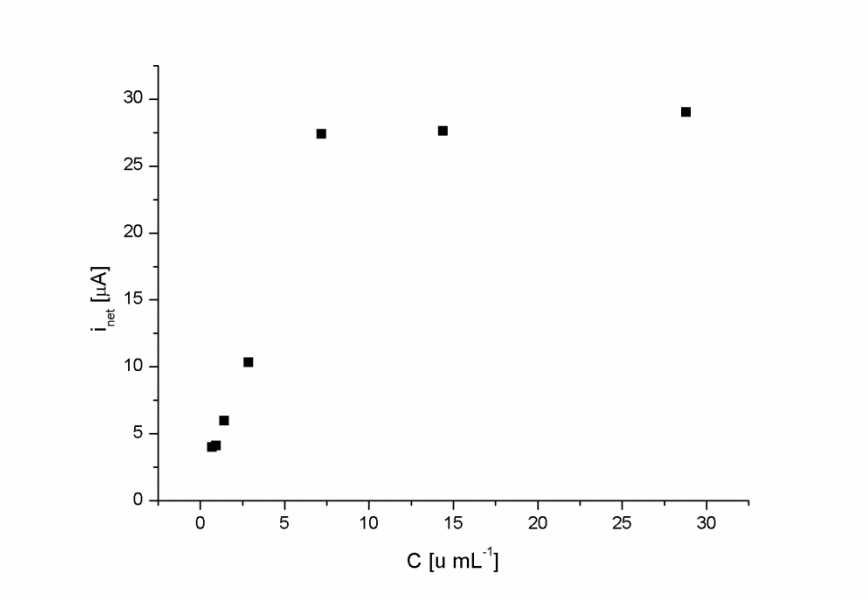

Figure 3.18. Plot of the electrocatalytic current increment at the immunosensor versus the concentration of IgG anti-tTG present in a standardized serum sample (concentration of 0.72, 0.96, 1.44, 2.88, 7.2, 14.4, 28.8 u mL^{-1}).

Linear calibration plot is in **Figure 3.19** (correlation coefficient R^2 = 0.995). The short error bars for each point of the calibration plot indicate that the proposed method is characterized by a good reproducibility. Note that for the development of the calibration curve, omogeneous NEEs with quite identical voltammetric parameters were employed.

The relative standard deviation (RDS) (n=6) for a concentration of 2.88 u mL^{-1} IgG anti-tTG results 9.4%. The detection limit (DL) results 0.70 u mL^{-1}, the quantification limit (QL) 2.3 u mL^{-1}, calculated using **Equation 3.11** and **Equation 3.12**, respectively [169].

$$DL = 3\frac{SD}{m} \quad (\mathbf{3.11})$$

$$QL = 10\frac{SD}{m} \quad (\mathbf{3.12})$$

where:

- SD is the standard deviation of the y intercept of the linear regression;
- m is the slope of the linear calibration plot (sensitivity).

The wide linear range, the low detection limit and the good reproducibility obtained with the proposed electrochemical immunosensor denote it as an useful tool for the detection in the serum sample of IgG anti-tissue transglutaminase, an effective biomarker of the celiac disease.

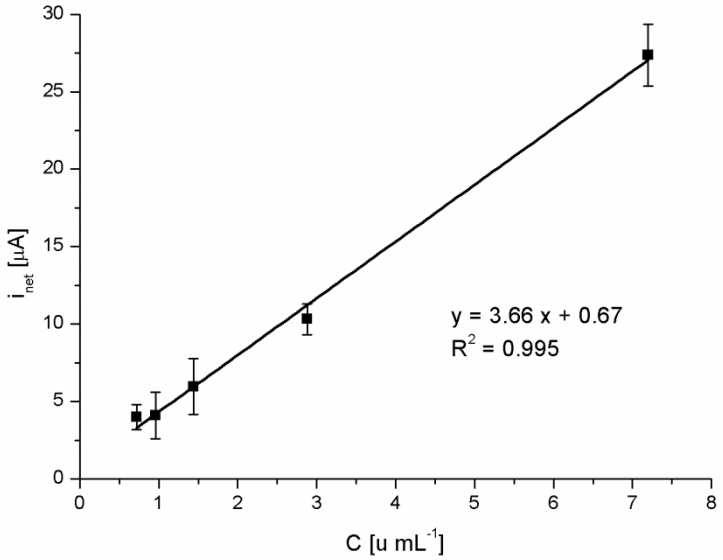

Figure 3.19. Linear calibration plot of the immounosensor for the detection of IgG anti-tissue transglutaminase (current increment versus IgG anti-tTG concentration). Error bars show standard deviation of triplicate measurements (n=3).

3. 4. NEE-based immunosensor for IgA anti-tTG

The scheme of the immunosensor developed for the detection of the IgA isotype of anti-tTG is represented in **Figure 3.20**. Relevant components are indicated in the caption. The detailed description of the preparation of the sensor can be found in the Experimental Section.

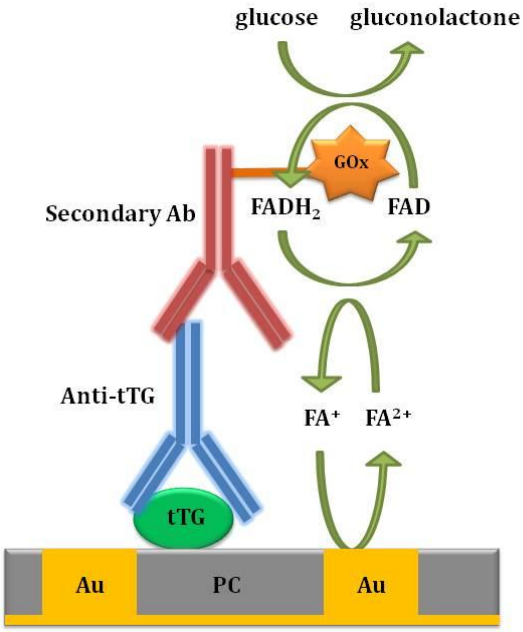

Figure 3.20. Schematic illustration of the immunosensor architecture for the detection of IgA anti-tTG and the associated enzymatic and electrochemical process. After immobilization of the capture antigen (tissue transglutaminase) on the electrode surface, the obtained sensor is incubated with anti-tissue transglutaminase (in standardized serum samples). The detection of the antigen-antibody complex is achieved by incubating the sensor with secondary antibodies anti-IgA labelled with GOx. After adding glucose (the enzyme substrate) and FA^+ as suitable redox mediator, an enzymatic reaction occurs, enabling the detection of the analyte by cyclic voltammetric measurements. Components are not in scale.

The immunosensor for the detection of the IgA anti-tTG is similar to the one used for the detection of IgG anti-tTG, with the main difference of using a secondary antibody suitable to detect the IgA form of the target analyte. To this aim, a

secondary antibody against immunoglobulin IgA labelled with glucose oxidase was chosen.

The electrochemical behaviour of glucose oxidase has already been studied at NEEs; in particular, GOx was used to detect glucose [151] and as label for the detection of the hybridization of DNA [149]. In both cases, (ferrocenylmethyl)trimethylammonium (FA^+) resulted to be an efficient redox mediator to shuttle electrons between the glucose oxidase redox active site and the gold nanoelectrodes. Therefore, in this work, FA^+ was chosen as suitable redox mediator for the electrochemical detection of IgA anti-tTG.

The electrochemical behaviour of FA^+ at bare NEEs has been already presented in Paragraph 3. 1. 2. Here, at first, we examined the possible effect of the presence of glucose on the CVs. Preliminary experiments, shown in **Figure 3.21**, confirmed that, at bare NEEs, the presence of the sugar does not influence at all the cyclic voltammetric behaviour of FA^+, so confirming that glucose does no directly react with FA^+.

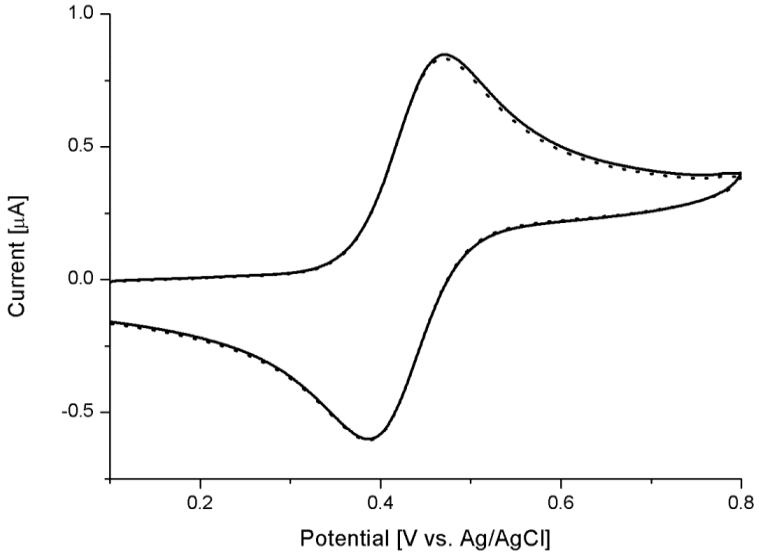

Figure 3.21. Cyclic voltammograms recorded at a bare NEE in 10 mM PBS containing 0.1 mM FA^+ before (dashed line) and after (solid line) addiction of 0.1 M glucose. Scan rate 50 mV s^{-1}.

3. 4. 1. Detection of IgA anti-tTG antibodies

Figure 3.22 shows the cyclic voltammograms recorded at a NEE before (dashed line) and after the complete functionalization with tTG, BSA, anti-tTG and anti IgA-GOx (solid line) in 0.1 mM FA^+. As for the case of the IgG immunosensor, the functionalization of the NEEs with biomolecules does not interfere with the total overlap diffusive regime which characterizes the FA^+ at non-functionalized NEEs [103,170]: in fact, the cyclic voltammetric pattern typical of a reversible one-electron oxidation of FA^+ is maintained almost unchanged, with only minor changes. This further confirms that the immobilization of the biomolecules occurs mainly on the polycarbonate membrane of the NEE, and not on the gold nanoelectrodes, and even if it occurs on the nanoelectrodes, it does not hinder significantly the electron transfer at the gold nanoelectrodes.

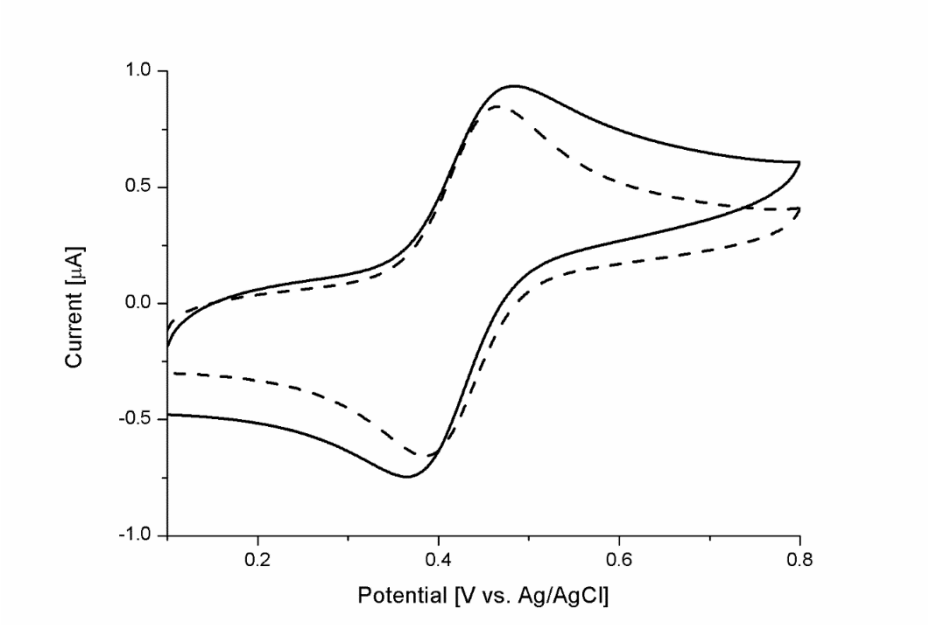

Figure 3.22. Cyclic voltammograms recorded at the same NEE before (dashed line) and after the complete functionalization procedure for the preparation of the IgA anti-tTG immunosensor with a IgA anti-tTG concentration of 123.5 u mL^{-1} (solid line) in 10 mM PBS containing 0.1 mM FA^+. Scan rate 50 mV s^{-1}.

Figure 3.23 shows the effect of the addition of 0.1 M glucose in 0.1 mM FA^+ solution on the voltammetric pattern recorded at a IgA-NEE.

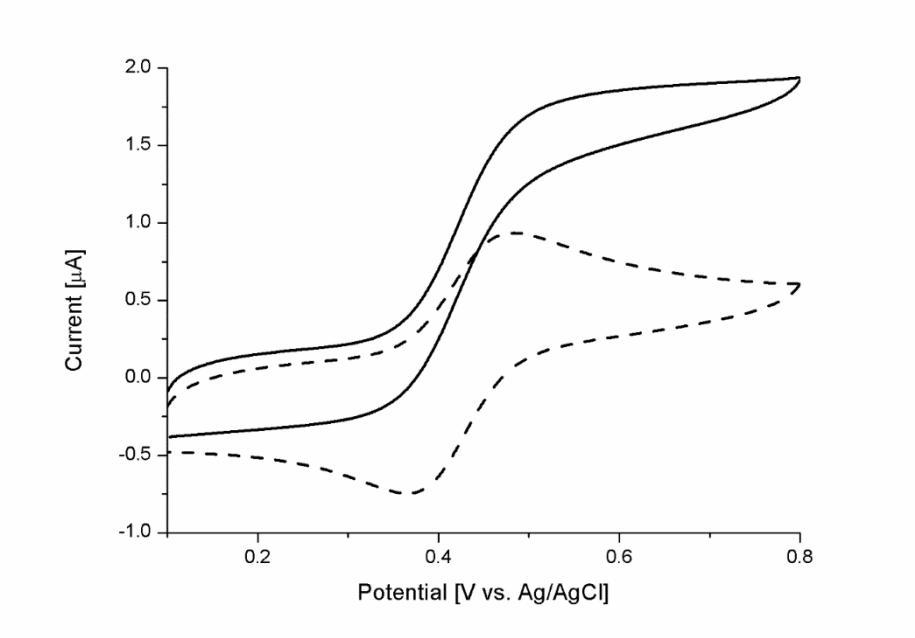

Figure 3.23. Cyclic voltammograms recorded at a NEE functionalized with tTG/BSA/IgA anti-tTG (123.5 u mL^{-1})/anti IgA-GOx in the absence (dashed line) and in the presence of glucose 0.1 M (solid line) in a 10 mM PBS (pH 7.4) solution containing 0.1 mM FA^{+}. Scan rate 50 mV s^{-1}.

It is evident that when glucose (the enzyme substrate) is added to the solution containing the redox mediator, the voltammetric pattern changes drammatically: the oxidation peak abruptly increases, while the reduction peak disappears, giving a sigmoidal CV pattern typical of an electrocatalytic process [171-174]. This agrees with the occurrence of the following electrocatalytic cycle.

$$FA^{+} \rightarrow FA^{2+} + e^{-} \quad \textbf{(i)}$$

$$GOx(FAD) + \text{D-glucose} \rightarrow GOx(FADH_2) + \text{D-glucono-1,5-lactone} \quad \textbf{(ii)}$$

$$GOx(FADH_2) + 2FA^{2+} \rightarrow GOx(FAD) + 2FA^{+} \quad \textbf{(iii)}$$

The redox mediator is oxidized at the electrode surface (**reaction i**). The glucose oxidase catalyses the oxidation of its substrate (D-glucose) to D-glucono-1,5-lactone, while its active centre is reduced from FAD to $FADH_2$ (**reaction ii**). The reduced form of the active centre of the enzyme is re-oxidized by reaction with the oxidized form of the redox mediator (**reaction iii**). Finally, the oxidized form of the redox mediator is regenerated at the electrode surface (**reaction i**).

As a consequence of the glucose oxidation catalysed by glucose oxidase, the redox mediator is no more electrochemically, but chemically reduced by the GOx($FADH_2$): this reflects in the disappearance of the cathodic peak current while the continuous local regeneration of FA^+ causes the increase of the anodic current. Note that the latter increment is further enhanced because per each molecule of reduced form of the enzyme two molecules of FA^+ are generated and subsequently oxidized at the electrode surface. Finally, the observation of a well-defined sigmoidal shape indicates the occurrence of the antigen-antibody recognition event, followed by the specific binding of the secondary antibody labelled with glucose oxidase.

The electrocatalytic current increment (i_{net}) is now defined as difference between the anodic peak currents of FA^+ in the presence (i_{cat}) and the absence (i_p) of glucose (**Equation 3.13**).

$$i_{net} = i_{cat} - i_p \qquad (\mathbf{3.13})$$

where:

- i_{cat} is the anodic peak current of FA^+ in the presence of glucose;
- i_p is the anodic peak current of FA^+ in the absence of glucose.

3. 4. 2. Study of the glucose oxidase kinetic

In order to study the kinetic of the glucose oxidase used as label enzyme in the proposed biosensor, different CVs were recorded at IgA-NEE in the presence of increasing glucose concentration. Data in **Figure 3.24** show that the sigmoidal character of the CV becomes progressively prevalent increasing the glucose concentration. In particular, the cathodic peak current completely disappears for glucose concentration > 10 mM, while for concentration > 100 mM the peak current does not further increase.

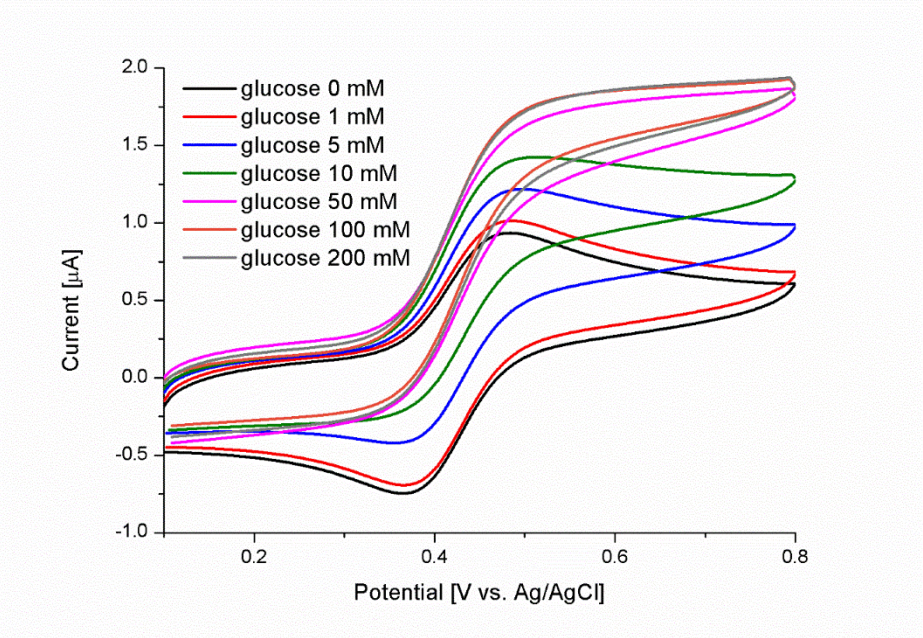

Figure 3.24. Cyclic voltammograms recorded at a NEE functionalized with tTG/BSA/IgA anti-tTG (123.5 u/mL)/anti IgA-GOx in a 10 mM PBS solution containing 0.1 mM FA^{+} at different glucose concentration (0, 1, 5, 10, 50, 100 and 200 mM). Scan rate 50 mV s^{-1}.

Figure 3.25 shows the plot of i_{net} as function of the glucose concentration.

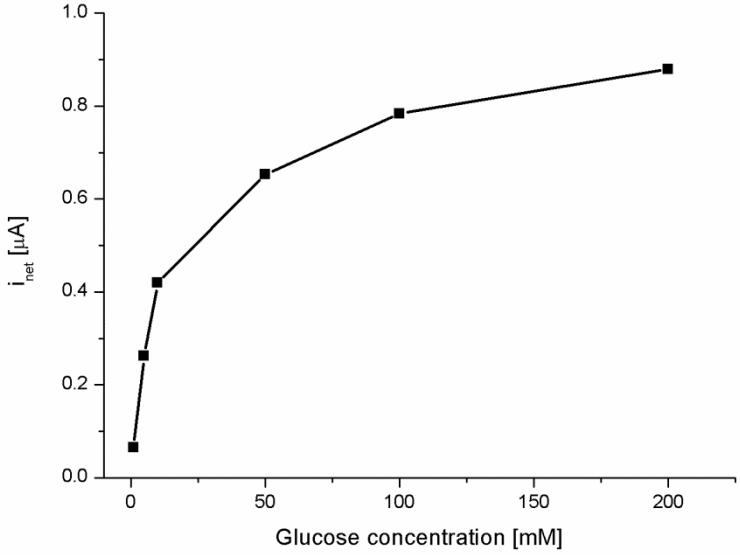

Figure 3.25. Plot of the enzyme catalysed current as function of the glucose concentration.

The current increment progressively increases with the glucose concentration, tending asymptotically to a limit value.

Indeed, the plot in **Figure 3.25** presents the features typical of a Michaelis-Menten enzyme kinetics (see **Equation 1.4** in the Introduction).

The kinetics of the enzymatic reaction catalysed by glucose oxidase determines indeed the rate of chemical reduction of FA^{2+} to FA^{+}, which is finally responsible for the electrocatalytic current increase. Therefore, under kinetic control, the electrocatalytic current increment i_{net} is directly related to the rate of the enzymatic reaction [175]. Consequently, an equation similar to the Michaelis-Menten can be applied to model the electrocatalytic response (**Equation 3.14**).

$$i_{net} = \frac{i_{max}\,[S]}{K_m + [S]} \qquad \textbf{(3.14)}$$

where:

- i_{net} is the electrocatalytic current increment;
- i_{max} is the maximum electrocatalytic current increment;
- [S] is the glucose concentration;
- K_m is the Michaelis-Menten constant that quantifies the enzyme's affinity for its substrate.

Figure 3.26 reports the plot of the reciprocal of the current increment versus the reciprocal of the glucose concentration (Lineweaver-Burk plot). The trend is linear, and it is algebraically expressed by **Equation 3.15**.

$$\frac{1}{i_{net}} = \frac{K_m + [S]}{i_{max}\,[S]} = \frac{K_m}{i_{max}} \cdot \frac{1}{[S]} + \frac{1}{i_{max}} \qquad \textbf{(3.15)}$$

The intercept of the straight line with the abscissa axis should be equal to $-1/K_m$ (**Equation 3.16**), so the glucose oxidase Michaelis-Menten constant can be estimated, and results 13 mM.

$$If \ \frac{1}{i_{net}} = 0 \ \Rightarrow \ \frac{1}{[S]} = -\frac{1}{K_m} \qquad \textbf{(3.16)}$$

This value is close to the ones reported in the literature [176-178], indicating that the glucose oxidase used as enzyme label in the proposed immunosensor is characterized by a high enzymatic activity.

On the other hand, the intercept with the ordinate axis is equal to $1/i_{max}$, so the maximum enzymatic catalyzed current increment can be estimated, and result equal to 0.93 μA.

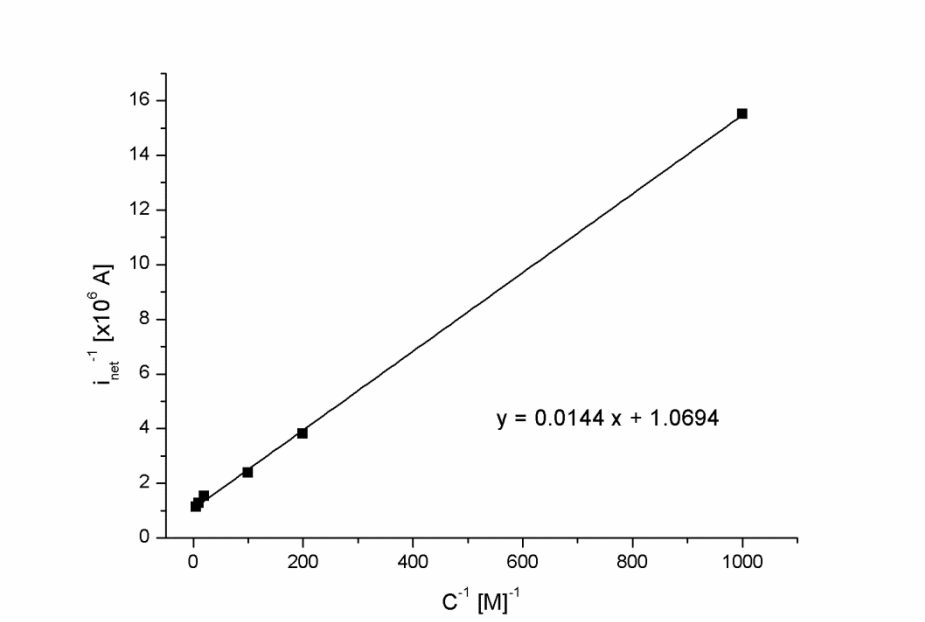

Figure 3.26. Double reciprocal plot.

Figure 3.27 shows the cyclic voltammograms recorded at different scan rates with a IgA-NEE in a 0.1 mM FA^+, 0.1 M glucose solution.

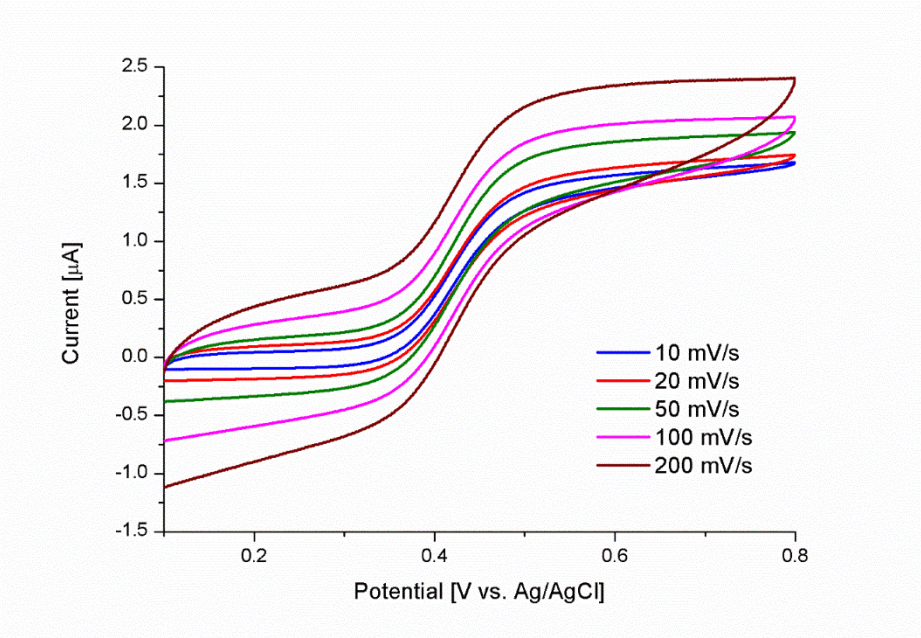

Figure 3.27. CVs recorded at a NEE functionalized with tTG/BSA/IgA anti-tTG (123.5 u mL^{-1})/anti IgA-GOx in 10 mM PBS containing 0.1 mM FA^+ and 0.1 M glucose at different scan rates (10, 20, 50, 100 and 200 mV s^{-1}).

The values of the plateau current measured at different scan rates corrected for the relevant background current are listed in **Table 3.2**.

Table 3.2. Average values of the maximum current recorded at a IgA-NEE in a 10 mM PBS solution containing 0.1 mM FA^+ and 0.1 M glucose at different scan rates (10, 20, 50, 100 and 200 mV s^{-1}).

Scan rate [mV s^{-1}]	**Average plateau current ± SD [µA]**
10	1.376 ± 0.010
20	1.358 ± 0.009
50	1.483 ± 0.029
100	1.429 ± 0.013
200	1.450 ± 0.010

The evidence that these values are almost independent on the scan rate confirms that, in the experimental conditions used for recording CVs of **Figure 3.27**, the process is under pure kinetic (not diffusive) control. For developing the calibration curve and performing the analysis of the serum samples, a glucose concentration of 0.1 M was therefore used.

3. 4. 3. Evaluation of aspecific bindings

Since the polycarbonate membrane of the NEE presents great affinity toward biomolecules, it is important to completely block the surface of the electrode before performing the incubation step with the serum sample in order to avoid the aspecific attachment of interfering biomolecules which could be present in the serum sample, and of the anti IgA-GOx.

Different experiments were conducted in order to evaluate the best way to block the polycarbonate membrane, minimizing aspecific bindings.

Figure 3.28 A shows the CVs recorded in FA^+ solution at a bare NEE (dotted line) and at the tTG-NEE incubated with anti IgA-GOx, but in the absence of anti-tTG, before (dashed line) and after the addition of glucose (solid line). It is quite evident that when glucose is added into the electrolyte solution, a catalytic effect is observed notwithstanding the absence of the target analyte. This indicates the occurrence of some aspecific absorptions of the anti IgA-GOx secondary antibody on the NEE.

Experiments aimed to test the effect of adding a blocking step indicate that incubation of the tTG-NEE with 1% BSA is only partially effective to this aim (**Figure 3.28 B**), while 3% BSA shows to be more efficient to completely block the polycarbonate membrane (**Figure 3.28 C**).

Table 3.3 reports the values of the current increment measured with the three different tTG-NEEs described above (unblocked, or blocked with 1% or 3% BSA).

Table 3.3. Values of the current increments recorded at the NEEs functionalized respectively with tTG/anti IgA-GOx, tTG/1%BSA/anti IgA-GOx and tTG/3%BSA/anti IgA-GOx, data from **Figure 3.28 A, B C**.

	Current increment [µA]
no blocking	0.6280
BSA 1%	0.1629
BSA 3%	0.0310

On the basis of the obtained results, in order to prevent aspecific bindings, 3% BSA was used for performing the blocking of the tTG-NEE before the incubation with the serum samples both for the development of the IgA anti-tTG calibration curve either for performing the quantitative analysis of the target analyte in the standardized serum samples.

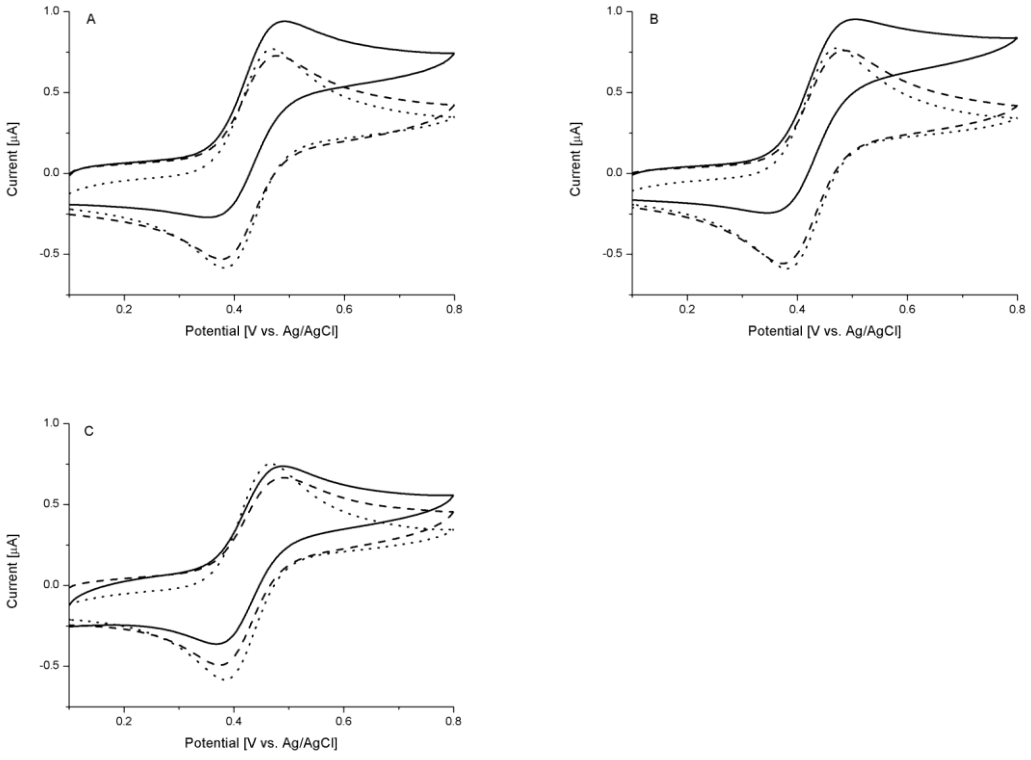

Figure 3.28. CVs recorded at a bare NEE (dotted line) and at the same NEE functionalized with 20 µL of 20 µg mL^{-1} tTG and 20 µL of 20 µg mL^{-1} anti IgA-GOx in a 10 mM PBS containing 0.1 mM FA^{+} before (dashed line) and after the addition of glucose 0.1 M (solid line). A. No blocking step. B. Blocking with 1% BSA. C. Blocking with 3% BSA.

3. 4. 4. Optimization of the incubation time with anti IgA-GOx

Different tTG-NEEs were incubated with serum sample containing 0.12 u mL^{-1} anti-tTG. These electrodes were then incubated with anti IgA-GOx, but using different incubation times. **Table 3.4** reports the values of the catalytic current increments recorded at these NEEs in the presence of 0.1 M glucose and 0.1 mM FA^{+}, as a function of the incubation time.

Table 3.4. Values of the current increments recorded at the NEEs incubated with anti IgA-GOx for different time frames.

Incubation time with anti IgA-GOx [min]	Current increment [μA]
60	0.1266
45	0.1245
30	0.1294
15	0.1001

Figure 3.29 shows the plot of the current increment as function of the incubation time with anti IgA-GOx.

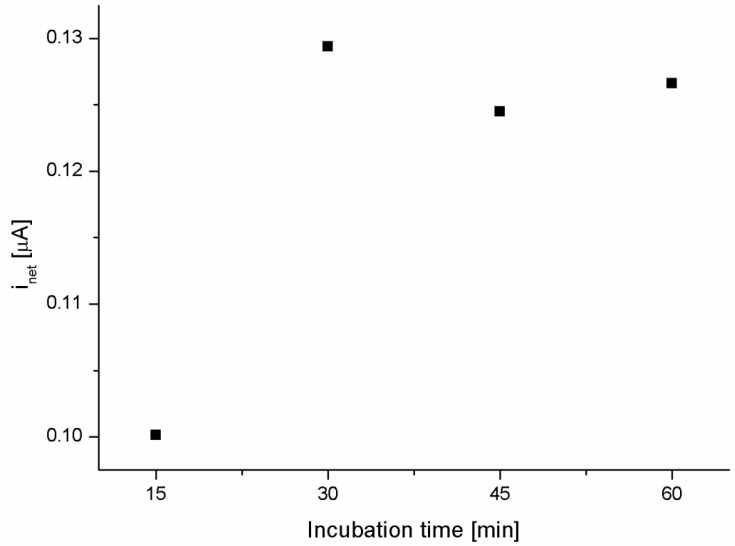

Figure 3.29. Plot of the current increment as function of incubation time of anti IgA-GOx.

It is evident that the current increment does not considerably change decreasing the time of incubation with anti IgA-GOx. Obtained results indicate an incubation time with the secondary antibody of 30 minutes as the best compromise between a good sensitivity and a reasonable time length of the incubation (in the ELISA test the incubation with the goat-anti human secondary Ab is usually left to occur for 30 minutes [179]).

3. 4. 6. Quantitative analysis of IgA anti-tTG

Following a procedure similar to the one used for the developing of the IgG anti-tTG calibration curve, a curve for the quantification of the IgA anti tissue transglutaminase was developed, incubating different tTG-NEEs (blocked with 3% BSA) with anti-tTG and goat anti-human IgA secondary antibody. In particular, different concentrations of IgA anti-tissue transglutaminase were used, diluting a standardized serum sample with a known concentration of the target analyte in PBS (the same standardized serum sample used for the development of the IgG anti-tTG calibration curve). Measurements in triplicate were performed at each of the nine dilution of the standardized serum sample.

Figure 3.30 reports the plot of the electrocatalytic current increment at the immunonosensor versus the concentration of IgA anti-tTG in the standardized serum sample (in the concentration range between 0.12 and 123.5 u mL^{-1}).
The electrocatalytic increment (i_{net}) was calculated as the difference between the anodic peak current of FA^+ in the absence and in the presence of 0.1 M glucose according to **Equation 3.13**. The value of the current increment scales linearly with the concentration of IgA anti-tTG in the 0.25 and 8.54 u mL^{-1} range. For concentration above 8.54 u mL^{-1} the plot acquires a asymptotic profile, and it is no possible to quantify the analyte since the signal is constant and no more depending on the analyte concentration.

Figure 3.31 is a zoom-in of the initial linear portion of the calibration plot (correlation coefficient R^2 = 0.988). The short error bars of the calibration plot suggest that the proposed method is characterized by a good reproducibility. Note

that for the development of the calibration curve omogeneous NEEs with quite identical voltammetric parameters were employed.

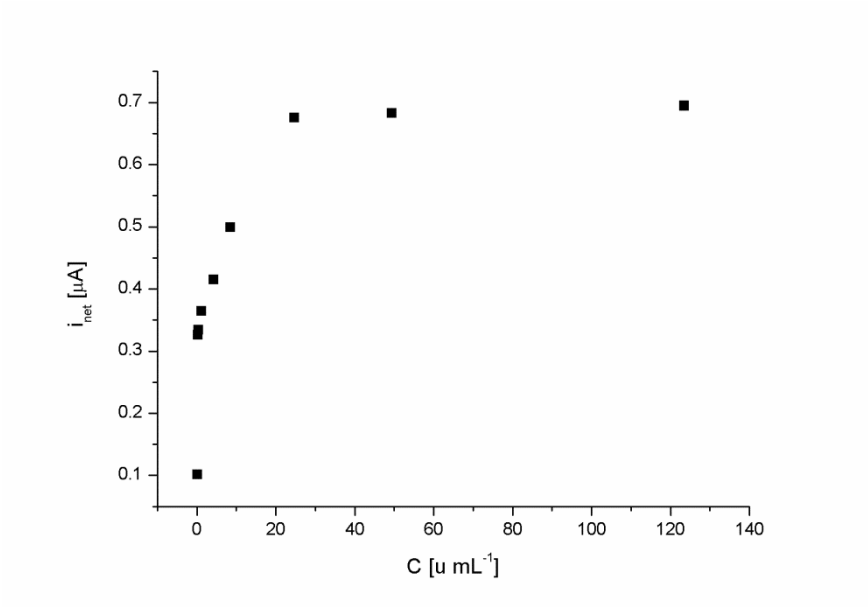

Figure 3.30. Plot of the electrocatalytic current increment at the immunosensor versus the concentration of IgA anti-tTG present in the standardized serum sample (concentration of 0.12, 0.25, 0.50, 1.23, 4.27, 8.54, 24.7, 49.4 and 123.5 u mL^{-1}).

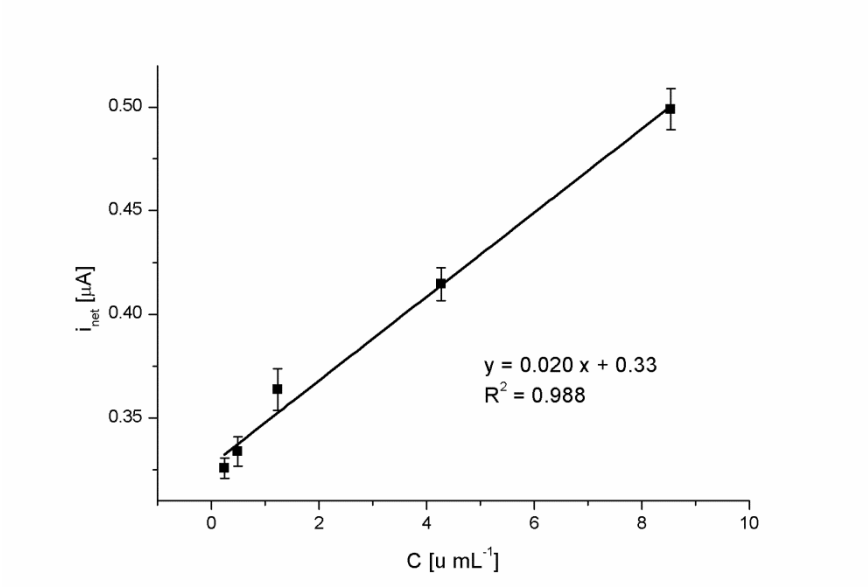

Figure 3.31. Linear calibration plot of the immounosensor for the detection of IgA anti-tissue transglutaminase (current increment versus IgA anti-tTG concentration). Error bars show standard deviation of triplicate measurements (n=3).

The relative standard deviation (RDS) (n=6) for a concentration of 1.23 u mL^{-1} IgA anti-tTG results 11.5%. The detection limit and the quantification limit (0.72 and 2.40 u mL^{-1} respectively) were calculated using **Equation 3.11** and **Equation 3.12**.

It is interesting to note that the calculated detection limit is slightly higher than the concentrations of the first points of the calibration plot. Indeed, as shown in **Figure 3.32**, even a low concentration such as 0.25 u mL^{-1} produces a detectable electrocatalytic current increment. This discrepancy could be due to an overestimation of DL by the use of **Equation 3.11** or to a small effect related to some aspecific response (see **Figure 3.28**).

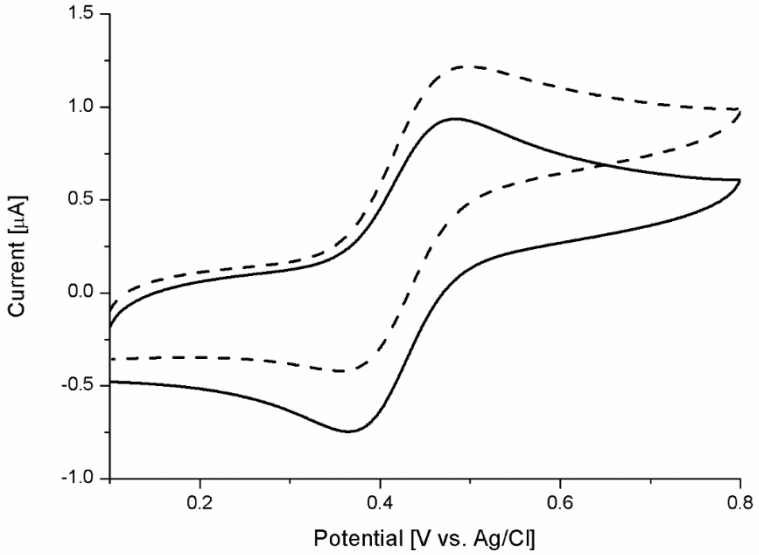

Figure 3.32. CVs recorded at a IgA-NEE functionalized with a IgA anti-tTG concentration of 0.25 u mL^{-1} in 10 mM PBS containing 0.1 mM FA^{+} in the absence (solid line) and in the presence of glucose 0.1 M (dashed line).

Considering the wide linear range, the low detection limit and the good reproducibility obtained with the proposed electrochemical immunosensor, this can be successfully used to detect and quantify the level of IgA anti-tissue transglutaminase in serum samples.

3. 5. Quantitative analysis of IgG and IgA anti-tTG in human serum samples

To establish the feasibility of the proposed immunosensors for clinical applications, we performed experiments aimed to quantify the level of both the IgG and IgA isotypes of anti-tissue transglutaminase in four human standardized serum samples, after proper dilution, using different tTG-NEEs. The quantification of the signal was carried out by interpolation of the electrocatalytic current increment with the calibration plot reported in **Figure 3.19** and **Figure 3.31**, respectively.

Table 3.5 compares the concentrations of IgG and IgA anti-tTG determined using IgG-NEEs and IgA-NEEs respectively and by clinical fluoroenzyme immunoassay (FEIA).

Table 3.5. Average concentrations (n=3) of IgG and IgA anti-tTG determined in standardized serum samples with the proposed electrochemical immunosensors (IgG-NEEs and IgA-NEEs) and the clinical fluoroenzyme immunoassay (FEIA).

Standardized serum sample	**IgG anti-tTG [u mL^{-1}]**		**IgA anti-tTG [u mL^{-1}]**	
	FEIA	IgG-NEE	FEIA	IgA-NEE
10801	44	35	13	25
10832	31	73	39	30
10858	11	56	52	75
10823	93	112	3770	2574

Figure 3.33 shows the correlation of the concentration of IgG and IgA isotypes of anti-tTG determined using the IgG-NEEs and IgA-NEEs (in Figure 3.33 A and Figure 3.33 B, respectively) with the concentration determined by the FEIA method.

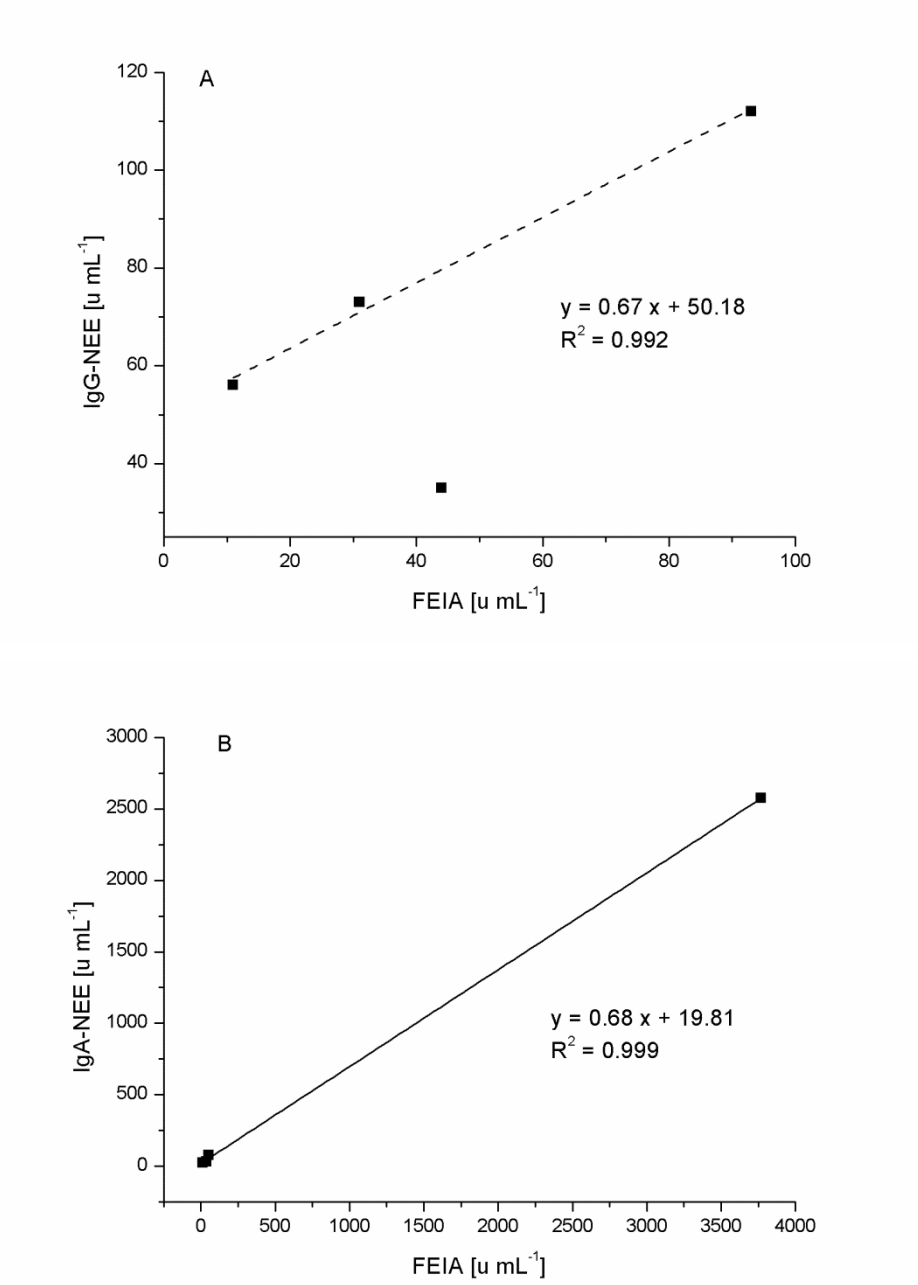

Figure 3.33. Correlation between the anti-tTG concentration determined using NEE-based immunosensors and by FEIA. A. IgG isotype. B. IgA isotype. Note that for the linear fitting of IgG data, sample 10801 has been excluded.

For the IgG isotype, a quite satisfactory agreement between the IgG-NEE results and FEIA data is observed, apart for sample 10801. A much better agreement is obtained for IgA data. The discrepancy observed for the former case can be due to some aspecific binding, suggesting the necessity to improve the blocking step.

Further measurements, conducted using serum samples of healthy individuals, do not reveal any electrocatalytic signal at the NEE-based immunosensors.

On the basis of the presented results, we can affirm that both the biosensors that exploit the nanoensemble electrodes can be considered selective and sensitive tools for the detection and quantification of anti-tissue transglutaminase, and show positive prospects of application, however with more reliable results for the IgA anti-tTG isotype. Further studies are necessary to evaluate the effective clinical applicability of the proposed biosensors and to improve the detection of the IgG isotype.

Chapter 4
Conclusions

In this work, NEE-based immunosensors were developed for the voltammetric detection of both the IgG and IgA isotypes of anti-tissue transglutaminase as reliable serological biomarker for the celiac disease, by combining the specificity of the antibody–antigen interaction with the electrochemical capabilities of NEEs.

Nanoelectrode ensembles demonstrated to be a useful detection platform for two reasons. They are suitable since capable to immobilize relatively large amounts of the capture antigen (tissue transglutaminase), maintaining its antigenicity, without any preliminary modification of the electrode surface, simply exploiting the affinity of polycarbonate for biomolecules. This allows to avoid time-wasting and reagent-consuming procedures of pretreatment. Moreover, after the functionalization for the biosensor preparation, the electron transfer to the nanoelectrode elements is not hindered, allowing us to exploit the advantageous high signal-to-noise ratio typical of NEEs. As a consequence, very low detection limits were achieved; this feature is fundamental for the anti-tTG analysis in complex matrices such as serum samples, and for all cases where high dilution is necessary, e. g. to minimize interferences by other biomolecules.

This work demonstrates that the selective detection of the IgG or IgA isotype is possible by using tTG-NEE platforms finally incubated with a proper secondary antibody, against immunoglobulin IgG and immunoglobulin IgA respectively. The two antibodies are labelled with different enzymes, so allowing one to distinguish the analytical response for the two different anti-tTG isotypes.

The proposed NEE-based immunosensors are able to detect both the anti-tTG isotypes in human standardized serum samples with a wide calibration linear range (0.72-7.2 u mL^{-1} for IgG isotype and 0.72-8.54 u mL^{-1} for IgA isotype), providing low detection limits (0.70 u mL^{-1} for IgG and 0.72 u mL^{-1} for IgA), with a good reproducibility. The sensitivity (slope of the calibration curve) of both the immunosensors is high, in particular the one for the detection of the IgG isotype is higher than the one for the IgA isotype (3.66 μA u^{-1} mL and 0.020 μA u^{-1} mL respectively).

The presented method allows the quantification of anti-tTG in standardized serum samples, with satisfactory agreement with the outcome obtained using the clinical FEIA method, and the discrimination between positive and negative serum controls. The obtained results indicate the proposed biosensor as a potentially trustful analytical screening tool for the serological diagnosis of celiac disease; this is confirmed for IgA anti-tTG while for the IgG isotype further studies are necessary to improve the analytical process.

Further future work should be focused on the analytical validation of these promising electrochemical biosensor by processing a higher number of samples coming from celiac patients as well as control samples, in order to evaluate the clinical sensitivity and specificity of the method.

It can be noted that by our approach, for the detection of the IgG isotype, a cathodic signal is obtained, whereas for the detection of the IgA isotype an anodic one, each being detected in a different potential range. In principle, it would be possible to develop a single immunosensor able to detect simultaneously both the isotypes of anti-tTG by functionalization with two different secondary antibodies labelled with suitable enzymes.

Acknowledgements

I gratefully acknowledge my supervisor Prof. Paolo Ugo for giving me the opportunity to work on this interesting research project, and for providing me stimulation and motivation during the entire graduation internship.

I would like also to thank all the members of the group of electrochemical sensors of Ca' Foscari, in particular Dr. Henok Baye Habtamu, for teaching me how to perform the experiments in the laboratory and for giving me many useful suggestions.

I am grateful to Prof. Tarcisio Not and Dr. Luigina De Leo (IRCCS Materno Infantile Burlo Garofolo, Trieste) for the supplying of the serum samples.

References

[1] J. West, R.F. Logan, P.G. Hill, et al., *Gut* 2003, **52**, 960.

[2] M. Maki, K. Mustalahti, J. Kokkonen, et al., *N Engl. J. Med.* 2003, **348**, 2517.

[3] G. Tatar, R. Elsurer, H. Simsek, et al., *Dig. Dis. Sci.* 2004, **49**, 1479.

[4] A. Fasano, I. Berti, T. Gerarduzzi, et al., *Arch. Intern. Med.* 2003, **163**, 286.

[5] P.J. Bingley, A.J. Williams, A.J. Norcross, et al., *BMJ* 2004, **328**, 322.

[6] P. H. R. Green, C. Cellier, *N. Eng.l J. Med.* 2007, **357**, 1731.

[7] A. Di Sabatino, G. R. Corazza, *Lancet* 2009, **373**, 1480.

[8] A. Fasano, C. Catassi, *Gastroenterol.* 2001, **120**, 636.

[9] F. Panetta, G. Torre, F. Colistro, F. Ferretti, A. Daniele, A. Diamanti, *Acta Paediatrica* 2011, **100**, 728.

[10] M.F. Kagnoff, *J. Clin. Invest.* 2007, **117**, 41.

[11] A. Di Sabatino, A. Vanoli, P. Giuffrida, O. Luinetti, E. Solcia, G. R. Corazza, *Autoimmun. Rev.* 2012, **11**, 746.

[12] K. Kaukinen, J. Partanen, M. Maki, P.Collin, *Am J Gastroenterol.* 2002, **97**, 695.

[13] L.M. Sollid, *Nat. Rev. Immunol.* 2002, **2**, 647.

[14] B.M. Mohamed, C. Feighery, J. Kelly, et al., Dig. Dis. Sci. 2006, **51**, 1862.

[15] A. Ivarsson, O. Hernell, H. Stenlund, L.A. Persson, *Am. J. Clin. Nutr.* 2002, **75**, 914.

[16] B. Shahbazkhani, R. Malekzadeh, M. Sotoudeh, et al., *J. Gastroenterol. Hepatol.* 2003, **15**, 475.

[17] A. Sood, V. Midha, N. Sood, V. Malhotra, *Indian J. Gastroenterol.* 2003, **22**, 124.

[18] J.C. Gomez, G.S. Selvaggio, M. Viola, et al., *Am. J. Gastroenterol.* 2001, **96**, 2700.

[19] C. Catassi, I.M. Ratsch, L. Gandolfi, et al., *Lancet* 1999, **354**, 647.

[20] J.F. Ludvigsson, K. Michaelsson, A. Ekbom, S.M. Montgomery, *Aliment. Pharmacol. Ther.* 2007, **25,** 273.

[21] M.R. Jafri, C.W. Nordstrom, J.A. Murray JA, et al., *Dig. Dis. Sci.* 2008, **53**, 964.

[22] A. Ventura, G. Magazzu, L. Greco, *Gastroenterol.* 1999, **117**, 297.

[23] D. Bai, P. Brar, S. Holleran, R. Ramakrishnan, P.H. Green, *Scand. J. Gastroenterol.* 2005, **40**, 183.

[24] M. Viljamaa, K. Kaukinen, H. Huhtala, S. Kyronpalo, M. Rasmussen, P. Collin, *Scand. J. Gastroenterol.* 2005, **40**, 437.

[25] J.A. Murray, A. Rubio-Tapia, C.T. Van Dyke, et al., *Clin. Gastroenterol. Hepatol.* 2008, **6**, 186.

[26] G.R. Corazza, A. Di Sario, L. Cecchetti, et al., *Gastroenterol.* 1995, **109,** 122.

[27] H. Hin, G. Bird, P. Fisher, N. Mahy, D. Jewell, *BMJ* 1999, **318**, 164.

[28] I.R. Korponay-Szabo, K. Szabados, J. Pusztai, et al., *BMJ* 2007, **335**, 1244.

[29] G. Oberhuber, G. Granditsch, H. Vogelsang, *Eur. J. Gastroenterol. Hepatol.* 1999, **11**, 1185.

[30] G.R. Corazza, V. Villanacci, C. Zambelli, et al., *Clin. Gastroenterol. Hepatol.* 2007, **5**, 838.

[31] C. Lagerqvist, I.Dahlbom, T. Hansson, E. Jidell, P. Juto, P. Olce´n, et al., *J. Pediatr. Gastr. Nutr.* 2008, **47**, 428.

[32] I.D. Hill, M.H. Dirks, G.S. Liptak, R.B. Colletti, A. Fasano, S. Guandalini, et al., *J. Pediatr. Gastr. Nutr.* 2005, **40**, 1.

[33] E. Fabiani, C. Catassi*, Eur. J. Gastroen. Hepat.* 2001, **13**, 659.

[34] C. Sategna-Guidetti, R. Pulitano, S. Grosso, G. Ferfoglia, *J. Clin. Gastroenterol.* 1993, **17**, 123.

[35] A. Tursi, G. Brandimarte, G.M. Giorgetti, *J. Clin. Gastroenterol.* 2003, **36**, 219.

[36] R.C. Wong, R.J. Wilson, R.H. Steele, G. Radford-Smith, S. Adelstein, *J. Clin. Pathol.* 2002, **55**, 488.

[37] A. Rostom, C. Dube, A. Cranney, et al. *Gastroenterol.* 2005, **128**, Suppl 1:S38.

[38] A. Lenhardt, A. Plebani, F. Marchetti, et al., *Dig. Liver. Dis.* 2004, **36**, 730.

[39] S. K. Lee, W. Lo, L. Memeo, H. Rotterdam, P.H. Green, *Gastrointest. Endosc.* 2003, **57**, 187.

[40] K. Vahedi, F. Mascart, J.Y. Mary, et al., *Am. J. Gastroenterol.* 2003, **98**, 1079.

[41] M.M. Pietzak, *Gastroenterol.* 2005, **128**, 135.

[42] P.J. Kumar, J. Walker-Smith, P. Milla, G. Harris, J. Colyer, R. Halliday, *Arch. Dis. Child.* 1988, **63**, 916.

[43] C. O'Leary, P. Wieneke, M. Healy, C. Cronin, P. O'Regan, F. Shanahan, *Am. J. Gastroenterol.* 2004, **99**, 2437.

[44] K.E. Lundin, E.M. Nilsen, H.G. Scott, et al. *Gut* 2003, **52**, 1649.

[45] H. Arentz-Hansen, B. Fleckenstein, O. Molberg, et al., *PLoS Med* 2004, **1,** e1.

[46] M. Siegel, M.T. Bethune, J. Gass, et al., *Chem. Biol.* 2006, **13**, 649.

[47] D. Stepniak, L. Spaenij-Dekking, C. Mitea, et al., *Am. J. Physiol. Gastrointest. Liver Physiol.* 2006, **291**, G621.

[48] G. Corrao, G.R. Corazza, V. Bagnardi, et al., *Lancet* 2001, **358**, 356.

[49] U. Peters, J. Askling, G. Gridley, A. Ekbom, M. Linet, *Arch. Intern. Med.* 2003, **163**, 1566.

[50] P.H. Green, A.T. Fleischauer, G. Bhagat, R. Goyal, B. Jabri, A.I. Neugut, *Am. J. Med.* 2003, **115**, 191.

[51] C. Cellier, E. Delabesse, C. Helmer, et al., *Lancet* 2000, **356**, 203.

[52] S.D. Rampertab, K.A: Forde, P.H. Green, *Gut* 2003, **52**, 1211.

[53] J.S. Trier, *N. Engl. J. Med.* 1991, **325**, 1709.

[54] A. Al-toma, O.J. Visser, H.M. van Roessel, et al., *Blood* 2007, **109**, 2243.

[55] C. S. Greenberg, P.J. Birckbichler, R.H. Rice, *FASEB J* 1991, **5**, 3071.

[56] D. Aeschlimann, M. Paulsson, *Thromb. Haemost.* 1994, **71**, 402.

[57] M. Griffin, R. Casadio, C.M. Bergamini, *Biochem. J.* 2002, **368**, 377.

[58] H.F. Upchurch, E. Conway, Jr M.K. Patterson, M.D. Maxwell, *J. Cell. Physiol.* 1991, **149**, 375.

[59] M. Lesort, K. Attanavanich, J. Zhang, G.V. Johnson, *J. Biol. Chem.* 1998, **273**, 11991.

[60] J. Martinez, D.G. Chalupowicz, R.K. Roush, A. Sheth, C. Barsigian, *Biochemistry* 1994, **33**, 2538.

[61] J.E. Folk, *Adv. Enzymol. Relat. Areas Mol. Biol.* 1983, **54**, 1.

[62] L. Lorand, R.M. Graham, *Nat. Rev. Mol. Cell. Biol.* 2003, **4**, 140.

[63] L. Fesus, Z. Szondy, *FEBS Lett.* 2005, **579**, 3297.

[64] K.E. Achyuthan, C.S. Greenberg, *J. Biol. Chem.* 1987, **262**, 1901.

[65] E.A. Verderio, T. Johnson, M. Griffin, *Amino Acids* 2004, **26**, 387.

[66] S. Kojima, K. Nara, D.B. Rifkin, *J. Cell. Biol.* 1993, **121**, 439.

[67] C.A. Aoki, A.T. Borchers, M. Li, R.A. Flavell, C.L. Bowlus, A.A. Ansari, et al., *Autoimmun. Rev.* 2005, **4**, 450.

[68] R.N. Barnes, P.J. Bungay, B.M. Elliott, P.L. Walton, M. Griffin, *Carcinogenesis* 1985, **6**, 459.

[69] S.E. Bruce, I. Bjarnason, T.J. Peters, *Clin. Sci*. 1985, **68**, 573.

[70] G. D'Argenio, I. Sorrentini, C. Ciacci, S. Spagnuolo, R. Ventriglia, A. de Chiara, et al., *Gut* 1989, **30**, 950.

[71] R. Ciccocioppo, A. Di Sabatino, G.R. Corazza, *Clin. Exp. Immunol.* 2005, **140**, 408.

[72] W. Dieterich, T. Ehnis, M. Bauer, P. Donner, U. Volta, E.O. Riecken, et al., *Nat. Med.* 1997, **3**, 797.

[73] F. Biagi, H.J. Ellis, J.Y. Yiannakou, G. Brusco, G.L. Swift, P.M. Smith, et al., *Am. J. Gastroenterol.* 1999, **94**, 2187.

[74] O. Molberg, S.N. McAdam, R. Körner, H. Quarsten, C. Kristiansen, L. Madsen, et al., *Nat. Med.* 1998, **4**, 713.

[75] C.Y. Kim, H. Quarsten, E. Bergseng, C. Khosla, L.M. Sollid, *Proc. Natl. Acad. Sci. USA* 2004, **101**, 4175.

[76] S. Dorum, M.O. Arntzen, S.W. Qiao, A. Holm, C.J. Koehler, B. Thiede, et al., *PLoS One* 2010, **5**, e14056.

[77] S. Martucci, G.R. Corazza, *Gastroenterol.* 2002, **122**, 2072.

[78] W. Vader, Y. Kooy, P. Van Veelen, A. De Ru, D. Harris, W. Benckhuijsen, et al., *Gastroenterol.* 2002, **122**, 1729.

[79] J.A. Abrams, P. Brar, B. Diamond, H. Rotterdam, P.H. Green, *Clin. Gastroenterol. Hepatol.* 2006, **4**, 726.

[80] M.V. Barone, I. Caputo, M.T. Ribecco, M. Maglio, R. Marzari, D. Sblattero, et al., *Gastroenterol.* 2007, **132**, 1245.

[81] M. Siegel, C. Khosla, *Pharmacol. Ther.* 2007, **115**, 232.

[82] L.M. Sollid, C. Khosla. *Nat. Clin. Pract. Gastroenterol. Hepatol.* 2005, **2**, 140.

[83] A. Lerner, *Autoimmun. Rev.* 2010, **9**, 144.

[84] O. Molberg, S. McAdam, K.E. Lundin, C. Kristiansen, H. Arentz-Hansen, K. Kett, et al., *Eur. J. Immunol.* 2001, **31**, 1317.

[85] L. Maiuri, C. Ciacci, I. Ricciardelli, L. Vacca, V. Raia, A. Rispo, et al., *Gastroenterol.* 2005, **129**, 1400.

[86] V. De Laurenzi, G. Melino, *Mol. Cell. Biol.* 2001, **21**, 148.

[87] J.M. Wodzinska, *Mini Rev. Med. Chem.* 2005, **5**, 279.

[88] K. Choi, M. Siegel, J.L. Piper, L. Yuan, E. Cho, P. Strnad, et al., *Chem Biol* 2005, **12**, 469.

[89] Antibody isotyping guide, http://www.ebioscience.com.

[90] A. Manz, N. Pamme, D. Iossifidis, *Bioanalytical chemistry*, Imperial College Press, 2004, pp. 109-130.

[91] A. J. Cunningham, *Introduction to bioanalytical sensors*, Wiley-Interscience Publication, 1998.

[92] J. Wang, *Analytical electrochemistry*, third edition, Wiley-VCH, 2006.

[93] D. N. Gray, M.H. Keyes, B. Watson, *Anal. Chem.* 1977, **49**, 1067A.

[94] H. H. Weetall, *Anal. Chem* 1974, **46**, 602A.

[95] M. Aizawa, A. Moricka, S. Suzuki, *Anal. Chim. Acta* 1980, **115**, 61.

[96] P. Skladal, *Electroanalysis* 1997, **9**, 737.

[97] I. Rosen, J. Rishpon, *J. Electroanal. Chem*. 1989, **258**, 27.

[98] R. K. Kobos, *Trends Anal. Chem*. 1987, **6**, 6.

[99] S. Kaku, S. Nakanishi, K. Horiguchi, *Anal. Chim. Acta* 1989, **225**, 283.

[100] A. Warinske, A. Benkert, F.W. Scheller, *Fres. J. Anal. Chem.* 2000, **366**, 622.

[101] M. Ongaro, P. Ugo, *Anal. Bioanal. Chem.* 2013, **405,** 3715.

[102] S. Pozzi Mucelli, M. Zamuner, M. Tormen, G. Stanta, P. Ugo, *Biosens. Bioelectron.* 2008, **23**, 1900.

[103] V.P. Menon, C.R. Martin, *Anal. Chem.*, 1995, **67**, 1920.

[104] P. Ugo, L.M. Moretto, S. Bellomi, V.P. Menon, C.R. Martin, *Anal. Chem.* 1996, **68**, 4160.

[105] L.M. Moretto, N. Pepe, P. Ugo, *Talanta* 2004, **62**, 1055.

[106] F.C. Pereira, L.M. Moretto, M. De Leo, M.V. Boldrin Zanoni, P. Ugo, *Anal. Chim. Acta* 2006, **575**, 16.

[107] R. Gasparac, B.J. Taft, M.A. Lapierre-Devlin, A.D. Lazareck, J.M. Xu, S.O. Kelley, *J. Am. Chem. Soc.* 2004, **126**, 12270.

[108] K. Krishnamoorthy, C.G. Zoski, *Anal. Chem.* 2005, **77**, 5068.

[109] M. De Leo, A. Kuhn, P. Ugo, *Electroanalysis* 2007, **19**, 227.

[110] L.X. Cao, P.S. Yan, K. Sun, D.W. Kirk, *Electroanalysis* 2009, **21**, 1183.

[111] C.G. Zoski, N. Yang, P. He, L. Bernardini, M. Koudelka-Hep, *Anal. Chem.* 2007, **79**, 1474.

[112] L. Soleymani, Z. Fang, E.H. Sargent, S.O. Kelley, *Nat. Nanotechnol.* 2009, **4**, 844.

[113] R.M. Penner, C.R. Martin, *Anal. Chem.* 1987, **59**, 2625.

[114] C.R. Martin, In: Bard AJ, Rubinstein, *Electroanalytical Chemistry*, Marcel Dekker Inc., New York, 1999.

[115] P. Ugo, L. M. Moretto in *Handbook of electrochemistry* (Ed.: C.G. Zosky), Elsevier, Amsterdam, 2007, pp. 661-706.

[116] J. C. Hulteen, V. P. Menon, C. R. Martin, *J. Chem. Soc. Faraday Trans.* 1996, **92**, 4029.

[117] I. F. Cheng, L. D. Whiteley, C. R. Martin, *Anal. Chem.* 1989, **61**, 762.

[118] P. Ugo, L.M. Moretto. M. De Leo, A.D. Doherty, C. Vallese, S. Pentlavalli, *Electrochimica Acta* 2010, **55**, 2865.

[119] A. J. Bard, L. Faulkner, *Electrochemical Methods* 2000, Wiley: New York.

[120] R. Greef, R. Peat, L. M. Peter, D. Pletcher, J. Robinson, *Instrumental Methods in Electrochemistry*, Ellis Horwood Ltd.: Chichester, UK, 1985.

[121] E. Sabatani, I. Rubinstein, *J. Phys. Chem.* 1987, **91**, 6663.

[122] C. Amatore, J.M. Saveant, D. Tessier, *J. Electroanal. Chem.*, 1983, **147**, 39.

[123] J. Guo, E. Lindner, *Anal. Chem.* 2009, **81**, 130.

[124] T.J. Davies, R.G. Compton, *J. Electroanal. Chem.* 2005, **585**, 63.

[125] X-J. Huang, A.M. O'Mahony, R.G. Compton, *Small*, 2009, **7**, 776.

[126] K. Teesalu, D. Agardh, M. Panarina, M. Utt, O. Uibo, R. Uibo, *Clin. Chim. Acta* 2009, **403**, 37.

[127] D. Basso, G. Guariso, D. Bozzato, E. Rossi, M. Pescarin, P. Fogar, et al., *Clin. Chim. Acta* 2011, **412**, 1662.

[128] J.J. Baudon, C. Johanet, Y.B. Absalon, G. Morgant, S. Cabrol, J.F. Mougenot, *Arch. Pediatr. Adolesc. Med.* 2004, **158**, 584.

[129] A. Carroccio, L. Di Prima, C. Falci, C. Le Moli, M. Soresi, G. Montalto, A. Notarbartolo, *Ann. Ital. Med. Int.* 2002, **17**, 102.

[130] M.G. Clemente, M.P. Musu, F. Frau, C. Lucia, S. De Virgiliis, *J. Pediatr. Gastroenterol. Nutr.* 2002, **34**, 31.

[131] A.W. Chan, J.D. Butzner, R. McKenna, M.J. Fritzler, *Pediatrics* 2001, **107**, E8.

[132] D. Villalta, M.G. Alessio, M. Tampoia, E. Tonutti, I. Brusca, M. Bagnasco, G. Pesce, N. Bizzaro, *Ann. N. Y. Acad. Sci.* 2007, **1109**, 212.

[133] D. Villalta, M.G. Alessio, M. Tampoia, E. Tonutti, I. Brusca, M. Bagnasco, G. Pesce, S. Stella, N. Bizzaro, *Clin. Chim. Acta* 2007, **382**, 95.

[134] Ivor d. Hill, *Gastroenterol.* 2005, **128**, s25.

[135] E. Bazzigaluppi, P. Roggero, B. Parma, M.F. Brambillasca, F. Meroni, S. Morac, E. Bosi, G. Barera, *Digestive and Liver Disease* 2006, **38** , 98.

[136] J. Wang, *Biosens. Bioelectron.* 2006, **21**, 1887.

[137] J. Wang, *Chem. Rev.* 2008, **108**, 814.

[138] N.J. Ronkainen, H.B. Halsall,W.R. Heineman, *Electrochemical biosensors*, Chem. Soc. Rev. 2010, **39**, 1747.

[139] D. Martin-Yerga, M.B. Gonzalez-Garcia, A. Costa-Garcia, *Talanta* 2014, **130**, 598.

[140] C. Zhu, G. Yang, H. Li, D. Du, Y. Lin, *Anal. Chem.* 2015, **87**, 230.

[141] L. Ding, D. Du, X. Zhang, H. Ju, *Curr. Med. Chem*. *2008*, ***15***, 3160.

[142] M.M.P.S. Neves, M. B. González-García, H.P.A. Nouws, A. Costa-García, *Biosens. Bioelectron.* 2012, **31**, 95.

[143] S. Dulay, P. Lozano-Sánchez, E. Iwuoha, I. Katakis, C. K. O'Sullivan, *Biosens. Bioelectron.* 2011, **26**, 3852.

[144] L.C. Rosales-Rivera, J.L. Acero-Sánchez, P. Lozano-Sánchez, I. Katakis, C.K. O'Sullivan, *Biosens. Bioelectron.* 2011, **26**, 4471.

[145] M.I. Pividori, A. Lermo, A. Bonanni, S. Alegret, M. del Valle, *Analytical Biochemistry* 2009, **388**, 229.

[146] D. Martín-Yerga, A. Costa-García, *Bioelectrochemistry* 2015, **105**, 88.

[147] M. Giannetto, M. Mattarozzi, E. Umiltà, A. Manfredi, S. Quaglia, M. Careri, *Biosens. Bioelectron.* 2014, **62**, 325.

[148] V.C. Rucker, K.L. Havenstrite, B.A. Simmons, S.M. Sickafoose, A.E. Herr, R. Shediac, *Langmuir* 2005, **21**, 7621.

[149] M. Silvestrini, L. Fruk, P. Ugo , *Biosens. Bioelectron.* 2013, **40**, 265.

[150] F. Bottari, P. Olivieri, P. Ugo, *Biosens. Bielectron.* 2014, **52**, 403.

[151] H.B. Habtamu, *Ensembles of nanoelectrodes as electrochemical and electrochemiluminescence sensing platform for molecular diagnostics*, PhD Thesis, 2015.

[152] P. Ugo, N. Pepe, L.M. Moretto, M. Battagliarin, *J. Electroanal. Chem.* 2003, **560**, 51.

[153] M. De Leo, F.C. Pereira, L.M. Moretto, P. Scopece, S. Polizzi, P. Ugo, *Chem. Mater*. 2007, **19**, 5955.

[154] M. De Leo, A. Kuhn, P. Ugo, *Electroanal.* 2007, **19**, 227.

[155] M. Henry, C. Dupont-Gillain, P. Bertrand, *Langmuir* 2003, **19***,* 6271.

[156] A.J. Bard, l.R.Faulkner, *Electrochemical methods Fundamentals and Applications*, Second edition, John Wiley & Sons Inc., 2001.

[157] K.R. Wehmeyer, R.M. Wightman, *J. Electroanal. Chem.* 1985, **196**, 417.

[158] S. S. Ordonez, E. Fabregas, *Biosens. Bioelectron.* 2007, **22**, 965

[159] Z. Wang, Y. Yang, J. Li, J. Gong, G. Shen, R. Yu, *Talanta* 2006, **69**, 686.

[160] C. -X. Lei, S.-Q. Hu, G.-L. Shen, R.-Q. Yu, *Talanta* 2003, **59**, 981.

[161] J. Zhou, C. Campbell, A. Heller, A. J. Bard, *Anal. Chem.* 2002, **74**, 4007.

[162] C. Camacho, J. C. Matas, B. Chico, R. Cao, L. Gomez, B. K. Simpson, R. Villalonga, *Electroanalysis* 19, **2007**, 2538.

[163] B. Brunetti, P. Ugo, L.M. Moretto, C.R. Martin, *J. Electroanal. Chem.* 2000, **491**, 166.

[164] X. Ji, C. E. Banks, D. S. Silvester, A. J. Wain, R. G. Compton, *J. Phys. Chem. C* 2007, **111**, 1496.

[165] P. D. Astudillo, J. Tiburcio, F. J. Gonzalez, *J. Electroanal. Chem.* 2007, **604**, 57.

[166] Z.-M. Liu, Y. Yang, H. Wang, Y.-L. Liu, G.-L. Shen, R.-Q. Yu, *Sensors and Actuators B* 2005, **106**, 394.

[167] S. Nawar, B. Huskinson, M. Aziz, *Mater. Res. Soc. Symp. Proc.* 2013, 1491.

[168] B. V. Chikkaveeraiah, A. A. Bhirde, N. Y. Morgan, H. S. Eden, X. Chen, *ACS Nano* 2012, **6**, 6546.

[169] Holler, Skoog, Crouch, *Chimica analitica strumentale*, II edition, EdiSES, 2009.

[170] M. Silvestrini, P. Schiavuta, P. Scopece, G. Pecchielan, L.M. Moretto, P. Ugo, *Electrochimica Acta* 2011, **56**, 7718– 7724.

[171] P. Alzari, N. Anicet, C. Bourdillon, J. Moiroux, J.M. Savèant, *J. Am. Chem. Soc.* 1996, **118**, 6788.

[172] B. Ballarin, C.J. Brumlik, D.R. Lawson, W.P. Liang, L.S. Vandyke, C.R. Martin, *Anal. Chem.* 1992, **64**, 2647.

[173] A.E.C. Cass, G. Davis, G.D. Francis, H.A. Hill, W.J. Aston, I.J. Higgins, E.V. Plotkin, L.D. Scott, A.P. Turner, *Anal. Chem.* 1984, **56**, 667.

[174] H.J. Bright, M. Appleby, *J. Biol. Chem.* 1969, **244**, 3625.

[175] P.N. Bartlett, C.S. Foh, E.J. Calvo and V. Flexer, *Modelling biosensor responses in bioelectrochemistry*, P.N. Bartlett Ed., Wiley and sons, 2008, chapter 8.

[176] S.B. Bankar, M.V. Bule, R.S. Singhal, L. Ananthanarayan, *Biotechnol. Adv.* 2009, **27**, 489.

[177] I.H. Boyaci, *Biochem. Eng. J.* 2005, **25**, 55.

[178] B.E. Swoboda, V. Massey, *J. Biol. Chem.* 1965, **240**, 2209.

[179] http://www.abcam.com.